UCLA-HEP-97-001

A Simple Plausible Path from QCD to Successful Prediction of $e^+e^- \rightarrow$ Hadronization Data

SeBong Chun and Charles Buchanan

UCLA

Accepted by Physics Reports for publication in Nov.~Dec. 1997.

Contents

Abstract

We find a remarkably simple path emerging which begins with QCD and ends with rather accurate predictions of detailed hadronic production data (flavors, distributions, correlations) in electron-positron interactions, the cleanest situation in which to study such hadronization phenomena. This path involves relatively few significant parameters and many plausible physical ideas. The predictions are especially clean (only two '*natural*' parameters and no '*ad hoc*' ones) and accurate for the production of various flavored light-quark mesons, the most fundamental and elementary tests of colorfield behavior. This appears to improve our understanding of the physics of the meson formation process and forms a foundation for further development of other more complex areas (e.g., baryon production, P_T effects) which we currently predict adequately, but where we must employ a small number of *'ad hoc'* parameters. The physics of our approach resembles that of a relativistic string and, in fact, historically is a spin-off from the very successful Lund modeling. However, our model's conceptual basis represents a paradigm shift away from emphasizing intermediate stages in an event and toward an emphasis on the total transition from the e^+e^- initial state to the entire set of final state hadrons. The model's central feature is a simple *Event Weight Function* incorporating a QCD-motivated space-time area law which, on the one hand, leads with very few assumptions to predictions agreeing remarkably well with $e^+e^- \rightarrow$ *hadronization* data, and, on the other hand, can also be plausibly related to strong-coupling soft QCD and can form a *'target'* for non-perturbative calculational approaches. Our approach avoids most of the parameters employed by traditional relativistic string models.

1 Introduction

It is commonly believed that QCD is the appropriate underlying theory for the 'hadronization process', that is, how hadrons are formed. Our goals, in this paper, are (first) to develop our phenomenology as a simple and accurate description of $e^+e^- \rightarrow$ *hadronization* data, especially focused on flavored meson production, and (second) to discuss the ways in which QCD relates to this phenomenology: how QCD suggests the structure of our phenomenology, how this *'fundamental'* phenomenology forms a *'target'* for QCD calculation and approaches, and how ultimately QCD may perhaps be used to predict the parameter values of the phenomenology.

Hadronization can occur in many different arenas – hadron-hadron interactions, lepton-hadron interactions, etc. The cleanest arena in which to study it in detail is electron-positron interactions in which the electro-weak annihilation creates an almost asymptotically free initial quark-antiquark pair at very

large Q^2, with a QCD colorfield emerging between them as they separate. The system then evolves into a very soft low-Q^2 non-perturbative regime in which the hadrons are finally formed. The rates and distributions of various flavored light-quark mesons are particularly useful in such studies, since they are the simplest most fundamental probes of colorfield behavior. Fortunately the data in e^+e^- interactions from E_{CM} of 10 GeV to 91 GeV is becoming so copious and detailed that decisive comprehensive studies can be carried out.

1.1 Historical development of UCLA model

The conceptual path from QCD to accurate predictions of e^+e^- data which emerges in our approach is sketched in Fig.1. Logically, the path flows from QCD (upper left in Fig.1) to comparisons with data (lower right). Historically, however, the development was exactly the opposite: We first noted ('UCLA stage I' in Fig.1) in 1987[1] that if the *Lund Symmetric Fragmentation Function* [2,3]

$$f(z, P_{T_h}^2) = N \frac{(1-z)^a}{z} \, \mathrm{e}^{-b \left(m_h^2 + P_{T_h}^2\right)/z} \tag{1}$$

was used as a hadronic production density (i.e., with a constant normalization N for all hadrons), then the predicted rates agreed rather well with measured ones. In this phenomenological approach, the suppression of heavy hadrons arises from the factor of $exp(-bm_h^2/z)$ in the fragmentation function rather than from suppression factors such as *s/u* and *vector/all* as used, for example, in the Lund implementation. (See Appendix A for a detailed comparison of the Lund and UCLA approaches.)

After this initial phenomenological success, we then began, with some guidance from the Lund group, to develop the idea and form of the *Event Weight Function*[4] ('UCLA stage II' in Fig.1), recognizing in fact that it both (a) leads to the idea of using the *Lund Symmetric Fragmentation Function* with constant normalization as a hadronic production density as we were already doing phenomenologically, and (b) also begins to connect with QCD ideas.

1.2 Present UCLA emphasis – The Event Weight Function

We now view the central feature of our approach as this *Event Weight Function* (dW_f) which emphasizes the entire transition from the initial state all the way to the final state hadrons. The *Event Weight Function* can be written for any final state of specified hadrons – that is, if the flavor (and, therefore,

The Path From QCD to Hadronization DATA
(via The UCLA Approach)

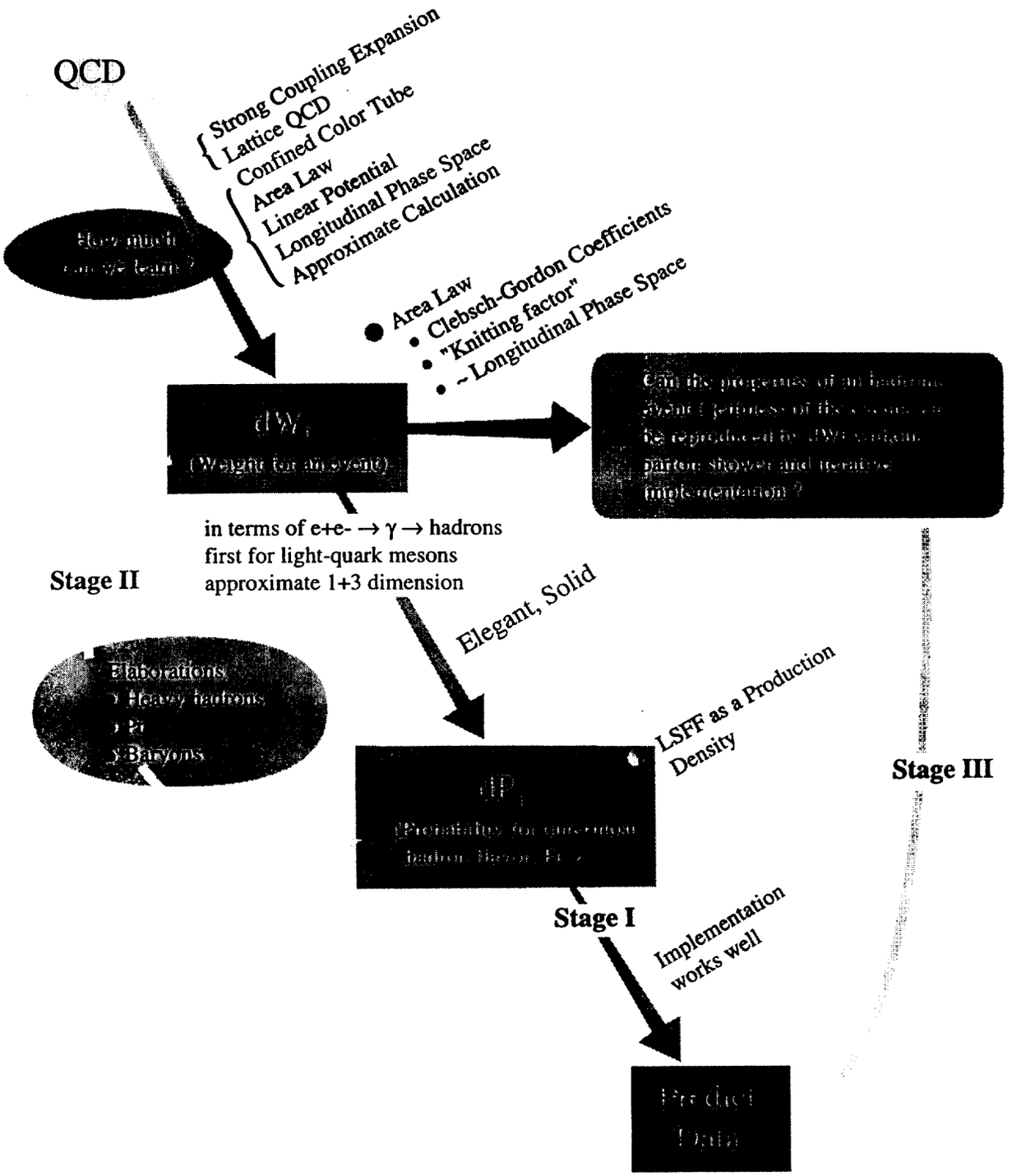

Fig. 1. The conceptual flow of the UCLA approach from QCD to the *Event Weight Function* to the *Fragmentation Function* to predictions of data. However, the historical development proceeded in roughly the opposite sequence.

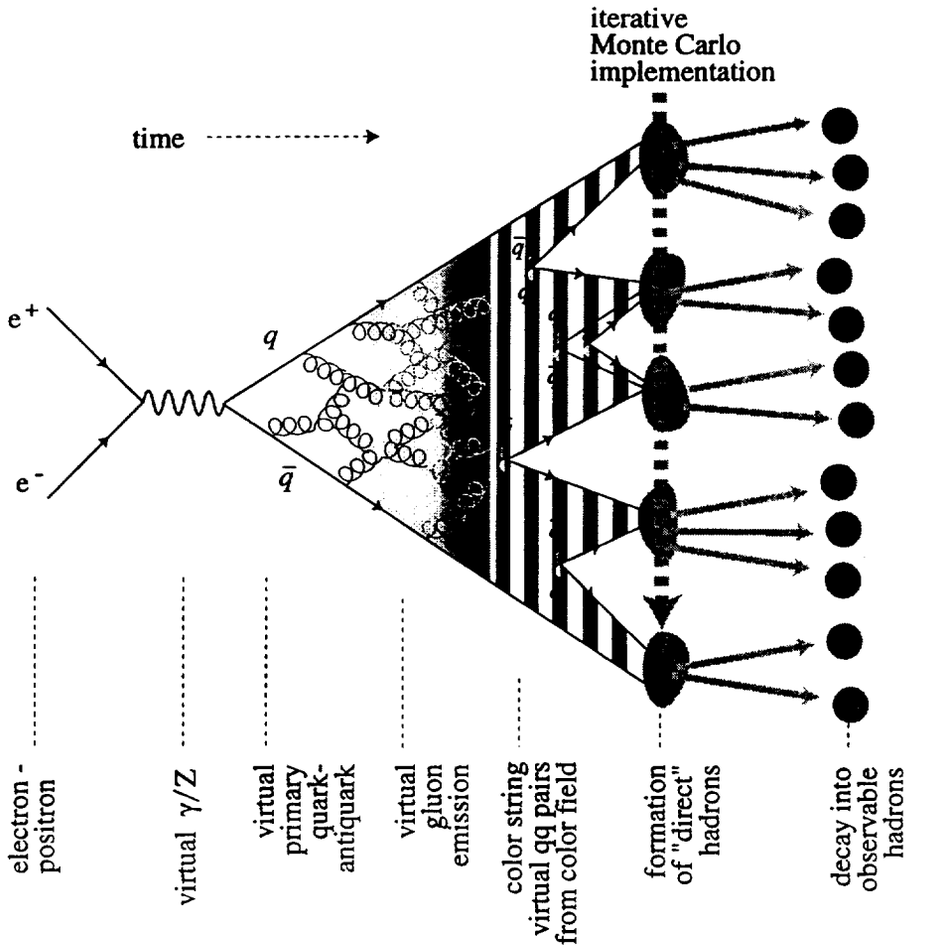

Fig. 2. Feynman-type diagram of e^+e^- annihilation into hadrons. Hot (perturbative) gluons radiated from the high-energy quark-antiquark pair get colder and colder (non-perturbative) until they collapse into a narrow tube structure about the time when virtual $q\bar{q}$ fluctuations begin to screen the colorfield and to split it into hadrons. Although implementation is done along the direction of the arrow in the picture, it must be remembered that physics happens along the time axis.

mass) and 3-momentum of each hadron is specified, then the *Event Weight Function* provides the probability of that specific event occurring relative to other possible final states.

1.3 Conceptual path from QCD to accurate predictions of light-quark mesons

Thus, we currently conceptualize the logical path (see Fig.1) as moving from QCD to the *Event Weight Function* (dW_f), to the fragmentation function (dP_1) for an 'outside-in one-hadron-at-a-time' iterative implementation, to comparisons with data. The structure of this 'logical flow' for our approach is

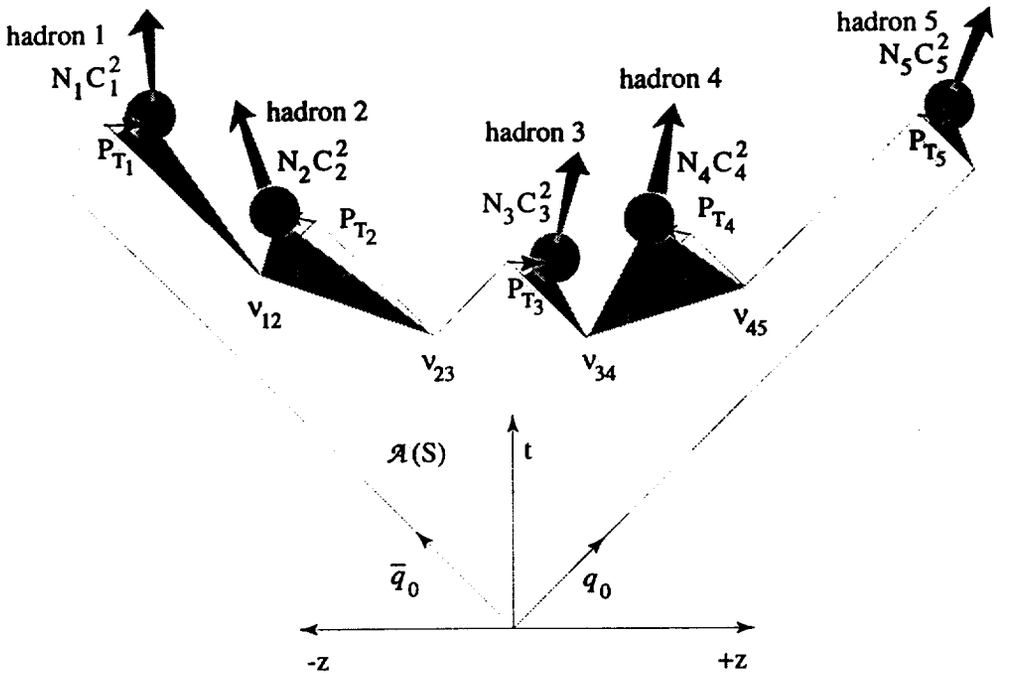

Fig. 3. Five hadrons are produced with small intrinsic P_T relative to a *"planar"* hadronic event of e^+e^- annihilation. These P_T's distort the plane of the event in such a way that the resulting area becomes slightly larger than for the planar event.

as follows:

a) QCD has two extreme regions where it can be calculated in an expansion series (see Fig.2):
   - (i) the high Q^2, high virtuality, low coupling-constant region ($g \ll 1$) just after the initial $q_0\bar{q}_0$ pair is created from the virtual photon.
   - (ii) the low Q^2, low virtuality, high coupling constant region ($g \gg 1$) at the end of the process as the hadrons are finally formed.

b) In region (i), one traditionally uses a perturbation theory expansion in *'g'*, the bare coupling constant, in terms of the number of quanta exchanged. The calculations are believed to be accurate to the order of the number of quanta exchanged (with the possible exception of not including interference effects). In practice, exact calculations are limited to two or three particles exchanged, and are often supplemented by leading-log or next-to-leading-log calculations as an approximate method of extending to several particles exchanged.

c) In region (ii), one can expand in $(1/g^2)$ on a space-time lattice with Euclidean metric and with finite lattice spacing *'a'*. Within these limitations, the calculation is exact to whatever order the expansion in $(1/g^2)$ is carried. However, to make contact with an actual physical regime, one must presume that the structure or results remain valid under two assumptions: (a) extrapolation to the continuum limit of $a = 0$, and (b)

extrapolation from the Euclidean lattice space to 'real physics' space with the Minkowskian relativistic metric.

d) The hadronization process spans from the extremes of region (i) to region (ii); this transition from very high Q^2 to very low Q^2 both contributes to the problem's interesting character and also to the difficulty of accurately calculating it.

e) In region (ii), the very important result of the first-order expansion is a space-time area law and also a perimeter law (described in Section 8) in Euclidean space-time with lattice spacing *'a'*. [Note that the region (i) weak-coupled behavior of the early system is essentially common to all events. Thus, in comparing the weights of various events, this effect essentially cancels out and one can treat the situation as if the strong-coupled area law dependence was valid throuhgout the entire space-time area of an event.]

f) We presume that this result extrapolates for our *Event Weight Function* to the continuum limit of $a = 0$ and to Minkowskian space. [Note: the fact, as shown later in our paper, that our approach works so well can be turned around to argue that these extrapolations are indeed approximately okay.]

g) From our *Event Weight Function*, we derive a fragmentation function in order to implement our ideas for comparison with data. The fragmentation function contains a factor of $\exp(-bm_h^2/z)$ arising from the *Event Weight Function* space-time area law.

h) This suppression from final state hadron mass, arising from the QCD-inspired area law in the *Event Weight Function*, is all one needs phenomenologically to fit the light-quark meson rates and distributions in e^+e^- annihilation events.

1.4 Emphasis on initial-to-final-state transition

The basis for our present approach, which centers on an *Event Weight Function* for the transition of an event-as-a-whole to the entire set of final state hadrons which are created, involves some conceptual visualization or intuitions which are somewhat different (and may seem somewhat foreign to the reader!) from our modeling's origins in which (a) the process was predominantly studied in terms of advancing forward one step at a time from one stage to another to another (i.e., from e^+e^- annihilation, to virtual γ/Z, to primary quark-antiquark, to gluon emission, to virtual quark-antiquark pairs from the colorfield, to formation of direct hadrons, to decay of some of the directly-produced hadrons into the final observed hadrons) and (b) the outside-in one-particle-at-a-time iterative fragmentation function Monte Carlo implementation strongly influenced one's conceptions. (See Fig.2.)

By contrast, we follow rather strictly the conceptualization of classical quan-

tum mechanics: (a) specify an initial state and a final state; (b) the transition rate from the initial state to the final state is controlled by a matrix element involving the transition through all the intermediate stages and is proportional to the density of final states. By recognizing that the initial stages can be calculated from ElectroWeak theory and that decay tables can be used in the last stage, our studies can be focused on transitions from an initial state of the quark and antiquark created from the virtual photon to a final state of the hadrons formed directly from the colorfield.

1.5 Physical concepts of the Event Weight Function

The *Event Weight Function* involves very simple principles: In its most general form, it involves (a) kinematics, (b) an area law[5,6] in space-time (which almost any strong-coupled theory will suggest), (c) approximately longitudinal phasespace, (d) the possibility of suppression 'penalties' in creating massive quark-antiquark pairs from the colorfield (ν_{ij}) as depicted in Fig.3, and (e) the coupling of quarks into the final state hadrons. The latter divides into: (e1) Clebsch-Gordon coefficients to describe the flavor and spin combination of a quark and antiquark as they coalesce into a meson or of three quarks into a baryon (C_i^2), and (e2)*a new concept, spatial 'knitting factors'* to describe the combinations into the spatial wave functions of the hadron to be created (N_i).

In our UCLA modeling we make the simplest possible assumptions within this general structure for the *Event Weight Function*, namely: (d) there is no appreciable suppression for creating light-quark pairs from the colorfield [namely, in Fig.3 $\nu_{ij} \simeq 1.0$ for $u\bar{u}$, $d\bar{d}$, and $s\bar{s}$ virtual pairs from the colorfield] and (e2) the spatial *'knitting factors'* for forming all hadrons are approximately the same [namely, all $N_i \simeq (75MeV)^{-2} \simeq (2.7fm)^2$]. As we will see, the suppression factor of around 0.3 usually associated with $s\bar{s}$ virtual pair creation via an 's/u' parameter value and also the suppression factor $\approx 0.3 \sim 0.6$ associated with creation of a vector meson rather than a pseudoscalar meson via a 'vector/all' parameter are replaced, in our modeling, by a suppression associated simply with the heavier mass of the actual final state hadron produced.

1.6 Testing the Event Weight Function by a fragmentation function implementation

How should we go about testing our *Event Weight Function* hypothesis against experimental data? The ideal way would be to have a computer big enough and fast enough that, for a given center-of-mass energy, a library of *Event Weight Functions* could be calculated for each possible set of final state hadrons within a grid of the flavor (mass), longitudinal momentum and transverse momentum

of each hadron produced. This, unfortunately, is not presently practical; but it is useful to remind the reader that the goal is a method to simulate this ideal. The practical technique to carry this out is to use a Monte Carlo program in which one hadron at a time is picked in such a way that an event as-a-whole is eventually constructed appropriately. The program we use is an adaptation of the relativistic string Monte Carlo JETSET7.4 written by Dr. Torbjörn Sjöstrand of Lund University, Sweden (with many thanks to him for making it available to us and aiding us in using it)[7,8]. The program uses an 'outside-in' implementation, that is, first picking the outermost hadron containing the initial quark, and then working its way inward.

1.7 Summary of the UCLA model hadronization picture

Thus, it is necessary for us, beginning with an *Event Weight Function*, to derive the fragmentation function - i.e., the probability (dP_1) - for the flavor and momentum of a first outermost hadron. (See, e.g., Fig.3.) When we perform this derivation, we find that our simple UCLA assumptions (above) for the *Event Weight Function* vertex suppression and knitting factors yield essentially the phenomenology which we originally found to be successful: namely, using the *Lund Symmetric Fragmentation Function* as a hadronic production density in the outside-in JETSET implementation framework.

The use of JETSET allows a further simplification of our treatment: Namely, we currently use JETSET's parton shower and also its recipe for moving the fragmentation implementation past a 'kink' in the relativistic string caused by a gluon emitted in the parton shower. This allows our treatment to be reduced to that of Fig.3 - the transition from a straight relativistic string between the primary quark and antiquark to the final state direct hadrons. Throughout, we have tried to be careful that the implementation always simply reflects the overall initial-to-final state conceptualization displayed in Fig.2. [There is a very interesting caveat on this which we are now exploring and which is discussed more fully in Appendix B.2, namely: The parton shower, approximately calculated by perturbative QCD, is in fact an unobserved intermediate stage and not necessarily useable as a calculable 'final state'. This raises the possibility that an area-law-dominated type of approach might in fact be developed which includes the parton shower.]

Thus, the total physics picture which emerges in our current approach for an electron-positron annihilation into hadrons (subject perhaps to the caveat of Appendix B.2) is:

A) The initial quark-antiquark pair is created by the virtual γ/Z at the (calculable) electroweak vertex.

B) As the quark and antiquark recede from each other, a colorfield emerges between them and gluon emission occurs, the first stages of which are calculable from QCD perturbation theory.

C) As the system continues to evolve, the parton shower evolves toward and then moves into a strong-coupled non-perturbative regime.

D) QCD lattice work[9] indicates that, at quark-antiquark separation $\geq 1 \sim 2$ fm, the colorfield is dominantly confined to a narrow tube of very high energy density (i.e., approximately a 'string'). Thus, the system evolves toward a tube of colorfield, kinked by the more substantial gluon emissions.

E) The JETSET7.4 Monte Carlo program[7,8] has a good approximate treatment for the parton shower and also to carry the implementation past a gluon-created kink. Thus we are allowed to focus our studies on the properties of a straight relativistic narrow colortube. (Subject possibly to the caveat of Appendix B.2.)

F) In line with the points (a)$\sim$(h) in the QCD analysis above, the strong-coupling nature of the later low Q^2 stages of the hadronization evolution suggest that we incorporate a space-time area law[5,6] in our *Event Weight Function*. Restricted transverse momentum is suggested (via the *Heisenberg Uncertainty Principle*) from the narrow finite-width colortube. The vertex suppression factors, the Clebsch-Gordon coefficients, and the *'knitting factors'* are obvious factors to introduce into a generalized *Event Weight Function* structure. Our UCLA assumptions (no appreciable $q\bar{q}$ vertex production suppression, all spatial knitting factors approximately the same) are the simplest possible assumptions within this framework; they correspond to the idea that the process is dominated by the creation of the actual final hadrons (where the virtual $q\bar{q}$ creation stage is so close to the final hadron production stage that it is in fact dominated by it).

G) In implementing this *Event Weight Function* approach in the outside-in implementation of JETSET7.4, we find that we are led into using the *Lund Symmetric Fragmentation Function* (LSFF)[2,3] as a hadronic production density, that is, with constant normalization where the normalization constant knitting factor's value is determining by probability unitarity on the fragmentation function to be $\approx (75MeV)^{-2} \simeq (2.7fm)^2$.

H) In comparing our predictions with data, we find that we predict all light-quark meson production properties (flavor, momentum distributions) from E_{CM} of 10 GeV (continuum) to 91 GeV with no significant deviations from the data using only the two natural parameter *'a'* and *'b'* of the *LSFF*. For the more complicated baryonic hadrons, the present level of agreement is encouraging, though we need one (or possibly two) *ad hoc* parameters. We also presently need an *ad hoc* parameter for P_T.

I) The success with mesons suggests that our treatment can be used as a foundation for studying more complicated phenomena such as baryon formation, P_T effects, spin-spin correlation, etc on a level more fundamental

than heretofore.

1.8 Organization of Report

In organizing this paper, we have tried to construct the body of the text for the semi-casual reader who is primarily interested in the conceptual development of our approach; thus we have systematically placed the details of our development into Appendices for the reader who wants to understand our approach in greater depth. Though we now conceptualize our approach as flowing logically from QCD to our phenomenology to data comparisons, in the structure of this paper we honor the historical approach in which the phenomenology and data comparisons were developed first and then examine the connections from QCD. Accordingly, Sections 2 $\sim$ 5 develop our phenomenology, Section 6 compares our predictions with data, Section 7 develops the crossing symmetry relation with deep inelastic scattering, and finally in Section 8 we focus on the relation between QCD and our *Event Weight Function*.

2 The Event Weight Function dW_f for Mesons

2.1 Event Weight Function *structure*

Referring to Fig.3, the *Event Weight Function* (including the possibility of suppression factors ν_{ij} for the production of virtual $q\bar{q}$ pairs in the colorfield and of different spatial knitting factors N_i) for an event with a final state f is written as:

$$
\begin{aligned}
dW_f{}^{q_0\bar{q}_0} &= \frac{N_1 C_1^2}{(2\pi)^3} dE_1 dP_{z_1} dP_{x_1} dP_{y_1} \delta\left(E_1^2 - P_1^2 - m_1^2\right) \mathrm{e}^{-\chi\left(P_{x_1}^2 + P_{y_1}^2\right)} \nu_{12} \times \ldots \\
&\times \nu_{n-1,n} \frac{N_n C_n^2}{(2\pi)^3} dE_n dP_{z_n} dP_{x_n} dP_{y_n} \delta\left(E_n^2 - P_n^2 - m_n^2\right) \mathrm{e}^{-\chi\left(P_{x_n}^2 + P_{y_n}^2\right)} \\
&\times (2\pi)^4 \delta\left(\mathbf{E} - \sum_i E_i\right) \delta\left(\mathbf{P}_z - \sum_i P_{z_i}\right) \delta\left(\mathbf{P}_x - \sum_i P_{x_i}\right) \delta\left(\mathbf{P}_y - \sum_i P_{y_i}\right) \\
&\times \mathrm{e}^{-b' \mathcal{A}_{plane}} \qquad (2)
\end{aligned}
$$

where

$$
\left(\frac{1}{2\pi}\right)^3 dE_i dP_{z_i} dP_{x_i} dP_{y_i} \delta\left(E_i^2 - P_{z_i}^2 - P_{x_i}^2 - P_{y_i}^2 - m_i^2\right) \qquad (3)
$$

is the four-dimensional phasespace for the i-th meson

$$\left(\frac{1}{2\pi}\right)^3 d^4P\delta\left(P_i^2 - m_i^2\right) = \left(\frac{1}{2\pi}\right)^3 \frac{d^3P_i}{2E_i}$$

and

$$(2\pi)^4\delta\left(\mathbf{E} - \sum_i E_i\right)\delta\left(\mathbf{P}_z - \sum_i P_{z_i}\right)\delta\left(\mathbf{P}_x - \sum_i P_{x_i}\right)\delta\left(\mathbf{P}_y - \sum_i P_{y_i}\right) \quad (4)$$

is overall four-momentum conservation, where the bold face E signifies E^{total}, etc. The factor $\exp(-b'\mathcal{A}_{plane})$ is the QCD-inspired space-time area law factor.

We include a structure to describe the probability that a quark from one virtual vertex and an anti-quark from an adjacent vertex combine to form the state function of a final meson. This involves both Clebsch-Gordon coefficients to control the flavor and spin parts (C_i^2's) and a *'knitting factor'* N_i for the spatial part of the meson's state function (see Fig.3). The factors $\exp(-\chi(P_{x_i}^2 + P_{y_i}^2))$ provide a structure for limited transverse momentum of the hadrons.

Because the JETSET implementation provides a good recipe for iterating past a gluon-induced string kink, eq(2) is written relative to a straight relativistic string.

In compact form, eq(2) can be written as

$$dW_f{}^{q_0\bar{q}_0} = \left[\prod_{i=1}^{n} \frac{N_i C_i^2}{(2\pi)^3} d^4P\delta\left(P_i^2 - m_i^2\right)\ \mathrm{e}^{-\chi P_{T_i}^2}\right]\left[\prod_{i=i}^{n-1} \nu_{i,i+1}\right]$$
$$\times(2\pi)^4\delta^4\left(\mathbf{P} - \sum_i P_i\right)\ \mathrm{e}^{-b'\mathcal{A}_{plane}} \quad (5)$$

This general form of the *Event Weight Function* structure can be used to analyze not only the assumptions in our UCLA approach, but also the structure of the Lund modeling.

2.2 Assumptions in the Event Weight Function for the UCLA model

The UCLA assumptions are:

1) The ν_{ij}'s for $u\bar{u}$, $d\bar{d}$, and $s\bar{s}$ are all ≈ 1.0, that is, there is no substantial penalty for creating any $q\bar{q}$ pair, as long as the quark mass is well below

the QCD scale of $\approx$ 1 GeV, the approximate energy stored in a string-length of the size of a hadron. [The other side of this presumption is that a $q\bar{q}$ virtual pair whose mass is substantially greater than ~1.0 GeV, e.g., $c\bar{c}$ or $b\bar{b}$, has negligible production in the colorfield.] This also recognizes that at this stage the event is very close (in time or virtuality) to the actual final state hadrons and that the virtual quark pair production from the colorfield is being 'pulled' by the configurations of allowable final state mesons, toward which QCD *'knows'* in a quantum-mechanical sense it must proceed.

2) The Clebsch-Gordon coefficients for creating mesons are remarkably simple, flowing from three aspects of our approach:

(a) Only sets of final state hadrons are allowed which correspond to local flavor conservation in creating virtual pairs in the colorfield. That is, $u\bar{u}$, $d\bar{d}$, and $s\bar{s}$ pairs can be created virtually in the colorfield, but $u\bar{d}$, $u\bar{s}$, and $d\bar{s}$ pairs cannot.

(b) Our emphasis on the total transition to the final state hadrons with no penalties for virtual $u\bar{u}$, $d\bar{d}$, or $s\bar{s}$ creation in the colorfield (with its intense energy concentration of $\approx$1 GeV/fm) means that whatever light quark-antiquark combination is needed for a particular meson is simply available from the colorfield 'for free'. For example, if a k^+ meson is part of a hypothesized *local-flavor-conservation-allowed chain*, then the $u\bar{s}$ pair needed to form the k^+ (where the u and the $\bar{s}$ come from different virtual pairs which are adjacent in rank) is simply available with no appreciable suppression penalty. The flavor coupling, then, of this 'available' $u\bar{s}$ pair into the k^+ flavor state function, whose only flavor composition is $u\bar{s}$, is simply 1.0. Note, however, for example, that a π^0 has equal terms in both $u\bar{u}$ and $d\bar{d}$ composition. Thus, if a $u\bar{u}$ mesonic combination is allowed by a hypothesized local-flavor-conservation chain, then this $u\bar{u}$'s coupling to the π^0's flavor state function would be 0.5. Similarly, the couplings which we use into either an η or into an η' have strength 0.25 from $u\bar{u}$, 0.25 from $d\bar{d}$, and 0.5 from $s\bar{s}$.

(c) The spins of the final state hadrons are presumed to be (at least, approximately) independent. Given the intense amount of spin angular momentum in the gluons of the colorfield, this would seem to be a plausible approximate assumption. Therefore, the colorfield couples in spin to a final state hadron simply with the hadron's spin degrees of freedom.

Thus, to summarize, the colorfield couples to a final state meson in flavor and spin with simply the spin-counting of the meson's spin degrees of freedom, except for neutral mesons where the additional content of the meson's flavor state function must also be coupled to by the quark-antiquark combination allowed by local flavor conservation.

3) The *'knitting factor'* N_i express the probability of a quark and its 'neighbor' anti-quark coupling into the spatial wave function of a particular

meson. The units for N_i, as can be seen from the *Event Weight Function* expression, are $(Energy)^{-2}$. [The knitting factor is conceptually somewhat akin to a mesonic decay factor in reverse]. We presume that all such knitting factors, whether the meson be a pion, kaon, η, η', ρ, ω, K^*, ϕ, etc., are all approximately the same. The unitarity normalization constraint from the probability for the outermost hadron, as we shall see in Section 3 and Appendix E.3, then establishes all $N_i \simeq (75MeV)^{-2} \simeq (2.7fm)^2$.

4) The transverse situation is described in terms of P_T of the observed hadrons. The structure used is discussed in Appendices B and C and summarized in Section 5.

In our modeling, the suppression of heavier particles arises from the mass of the final state hadron (as will be seen in Section 3), rather than from suppression factors at the virtual quark pair production level and smaller knitting factors for vector mesons, as for example Lund presumes.

2.3 Assumptions in the Lund model

The Lund model, discussed in more detail in Appendices A and B can be cast into this *Event Weight Function* form. Its assumptions are:

(1) At the virtual $q\bar{q}$ production stage, there is vertex suppression of $s\bar{s}$ production (the famous $s/u \simeq 0.3$), based on a WKB tunneling sort of argument; that is,

$$\nu_{u\bar{u}} \simeq \nu_{d\bar{d}} \simeq 1.0 \quad \text{and} \quad \nu_{s\bar{s}} \simeq 0.3$$

Also, for baryon production, the qq/q factor of ≈ 0.09 is introduced as a vertex suppression.

(2) As in our UCLA treatment, Clebsch-Gordon factors are different from 1.0 only, for example, to decide whether a $u\bar{u}$ state is to be coupled into a π^0, η, or η'.

(3) The knitting factors are used, via some detailed wave function arguments, for the *vector/all* parameters, with different suppression factors ranging from ≈ 0.3 for light quarks to ≈ 0.6 for heavy quarks. The final state phase-space spin-counting is also incorporated into the *vector/all* parameters.

(4) The Lund modeling conceptually originates the P_T structure from locally balanced non-zero transverse momenta of a virtual quark-antiquark pair as it is created from the colorfield. See Appendices A and B for more details.

(5) On the level of the *Lund Symmetric Fragmentation Function*, the Lund recipe should be followed in which the flavor (and therefore mass) and P_T of the meson are determined first and then the LSFF is used only to

determine the energy-momentum fraction z (thus avoiding the natural suppression arising from the factor $e^{-bm_H^2/z}$ in the LSFF).

3 Derivation of the *Fragmentation Function* dP_1 for the Outermost Hadron from the *Event Weight Function* dW_f

3.1 Probability and weight of an event

Quantum mechanical phenomena such as hadronization inherently involve amplitudes which, in a coherent process, are first summed and then squared in order to get a probability for the process. However, our *Event Weight Function* involves probabilities directly. This is justified as an appropriate approximation in Appendix D in which it is shown that, given a final state set of hadron flavors and momenta, then use of the area law implies that the configuration with the largest amplitude leading to that final state will almost always dominate. That is, the second largest amplitude is typically much smaller than the dominant one so that using only the probability associated with the configuration with the largest amplitude is a quite reasonable approximation.

Using this probabilistic basis, the steps from the *Event Weight Function* to the *fragmentation function* for the outermost hadron are as follows (see Appendix E for details):

- Define the *Total Weight* for all possible final state configurations at some value $S = E_{CM}^2$ by

$$g^{q_0\bar{q}_0}(S) = \sum\!\!\!\!\!\!\int_f dW_f{}^{q_0\bar{q}_0}(S) \tag{6}$$

  where $\sum\!\!\!\!\!\!\int$ sums over all possible final state flavors and multiplicities and integrates over all possible momenta.

- Then:

$$dP_f{}^{q_0\bar{q}_0}(S) \equiv \frac{dW_f{}^{q_0\bar{q}_0}(S)}{g^{q_0\bar{q}_0}(S)} \tag{7}$$

  is a properly normalized probability for an event of specified final state f such that

$$\sum\!\!\!\!\!\!\int_f dP_f{}^{q_0\bar{q}_0}(S) = 1$$

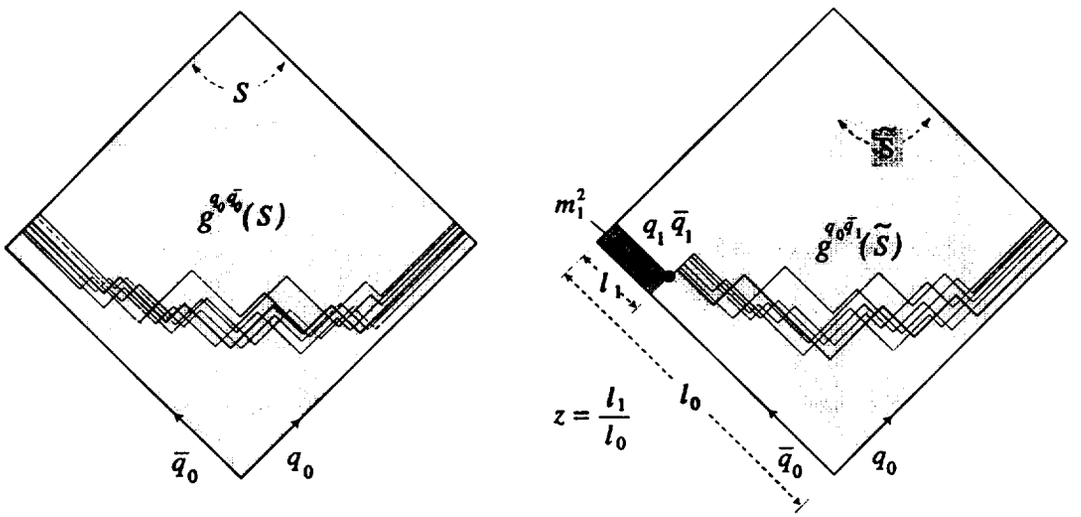

Fig. 4. The probabilty that the first hadron is produced with a specific energy-momentum and flavor can be extracted by comparing $g^{q_0\bar{q}_1}(\tilde{S})$ (an *integration/summation* of the weight function for the rest of the system) to $g^{q_0\bar{q}_0}(S)$ (an *integration/summation* of the weight function for the original system). The primary $q\bar{q}$ with kinetic energy E will stretch until all kinetic energy is converted to potential energy, i.e., $2E = \kappa d$ where κ is the string tension (presumed constant) and d is the maximum separation between the primary $q\bar{q}$. This enables one to write distance and area in terms of energy and energy-squared respectively. For example, the energy-momentum fraction of the hadron z can be written in terms of the lengths l_1 and l_0 and the mass-squared of the first hadron can be recognized as the area labeled m_1^2 in the figure.

3.2 Light-cone variables

- Integrate over the azimuthal angle of each hadron, introduce light cone variables W_+, W_-, and define

$$z_i \equiv \frac{(E_i + P_{z_i})_h}{(E + P_z)_{q_0}} \equiv \frac{W_{+_i}}{W_+} = \frac{l_1}{l_0} \tag{8}$$

  That is, z_i is the fraction of the initial quark's energy plus longitudinal momentum which the hadron carries. As is explained in the caption of Fig.4, the last step in eq(8) is due to the proportionality between the length and energy via a presumed approximately constant *string tension*. (See Appendix E.1 for details.)

- Then, eq(2) becomes:

$$dW_f{}^{q_0\bar{q}_0}(S) = \frac{N_1 C_1^2}{(4\pi)^2}\frac{dz_1}{z_1}\,\mathrm{e}^{-\chi P_{T_1}^2}\,dP_{T_1}^2\;\nu_{12} \times \ldots$$

$$\times\nu_{n-1,n}\ \frac{N_n C_n^2}{(4\pi)^2}\frac{dz_n}{z_n}\,\mathrm{e}^{-\chi P_{T_n}^2}\,dP_{T_n}^2\cdot(2\pi)^4\delta\left(1-\sum_{i=1}^{n}z_i\right)$$
$$\times\delta\left(S-\sum_{i=1}^{n}\frac{m_{T_i}^2}{z_i}\right)\delta\left(\mathbf{P}_x-\sum_{i=1}^{n}P_{x_i}\right)\delta\left(\mathbf{P}_y-\sum_{i=1}^{n}P_{y_i}\right)\ \mathrm{e}^{-b'\mathcal{A}_{plane}} \qquad (9)$$

where $m_T^2 = m^2 + P_T^2$ for the i-th hadron.

3.3 Derivation of the outermost hadron's fragmentation function

- Next, one notes that a partial weight ***integrated /summed*** over all possible flavors, multiplicities, and momenta of all particles except the first (outermost) one, normalized by the *Total Weight* g(S), yields the ***fragmentation function*** of the outermost hadron, that is, the probability of the first hadron with a specific flavor, specific energy-momentum fraction z, and specific P_T. Thus, the fragmentation function is:

$$dP_1^{q_0}\left(z_1,P_{T_1}^2,m_1^2\right)=\frac{1}{\mathrm{g}^{q_0\bar{q}_0}(S)}\frac{N_1C_1^2}{(4\pi)^2}\,\mathrm{e}^{-bm_1^2/z_1}\,\frac{dz_1}{z_1}\,\mathrm{e}^{-\chi P_{T_1}^2}\,dP_{T_1}^2\ \nu_{12}$$
$$\times\sum\!\!\!\!\!\!\int_f\ \frac{N_2C_2^2}{(4\pi)^2}\frac{dz_2}{z_2}\,\mathrm{e}^{-\chi P_{T_2}^2}\,dP_{T_2}^2\ \nu_{23}\times\ldots$$
$$\times\nu_{n-1,n}\ \frac{N_nC_n^2}{(4\pi)^2}\frac{dz_n}{z_n}\,\mathrm{e}^{-\chi P_{T_n}^2}\,dP_{T_n}^2\cdot(2\pi)^4\delta\left(1-z_1-\sum_{i=2}^{n}z_i\right)$$
$$\times\delta\left(S-\frac{m_{T_1}^2}{z_1}-\sum_{i=2}^{n}\frac{m_{T_i}^2}{z_i}\right)\ \delta\left(\mathbf{P}_x-P_{x_1}-\sum_{i=2}^{n}P_{x_i}\right)$$
$$\times\delta\left(\mathbf{P}_y-P_{y_1}-\sum_{i=2}^{n}P_{y_i}\right)\ \mathrm{e}^{-b'\tilde{\mathcal{A}}_{plane}} \qquad (10)$$

Using the variables $\tilde{S}=\left(S-m_{T_1}^2/z_1\right)(1-z_1)$ and $\tilde{z}_i=z_i/(1-z_1)$ scaled with respect to the remnant system and the identity $\delta(ax)=\frac{1}{|a|}\delta(x)$, one establishes that the part after $\sum\!\!\!\!\!\!\int$ in eq(10) is simply $\mathrm{g}^{q_1\bar{q}_0}(\tilde{S})$. (See Appendix E.1 for details.) Thus, eq(10) becomes

$$dP_1{}^{q_0}(z_1,P_{T_1}^2,m_1^2)=\frac{N_1C_1^2}{(4\pi)^2}\ \nu_{12}\ \mathrm{e}^{-bm_1^2/z_1}\,\frac{dz_1}{z_1}\ \mathrm{e}^{-\chi P_{T_1}^2}\,dP_{T_1}^2\ \frac{\mathrm{g}^{q_1\bar{q}_0}(\tilde{S})}{\mathrm{g}^{q_0\bar{q}_0}(S)} \qquad (11)$$

where $b=b'/\kappa^2$, $\kappa\simeq 1$ GeV/fm is the string tension, and m_1^2/z_1 is the part of the original area $\mathcal{A}(S)$ which is excluded from the new remaining area $\mathcal{A}(\tilde{S})\equiv\tilde{\mathcal{A}}$. (See Fig.5 for the geometrical definition.)

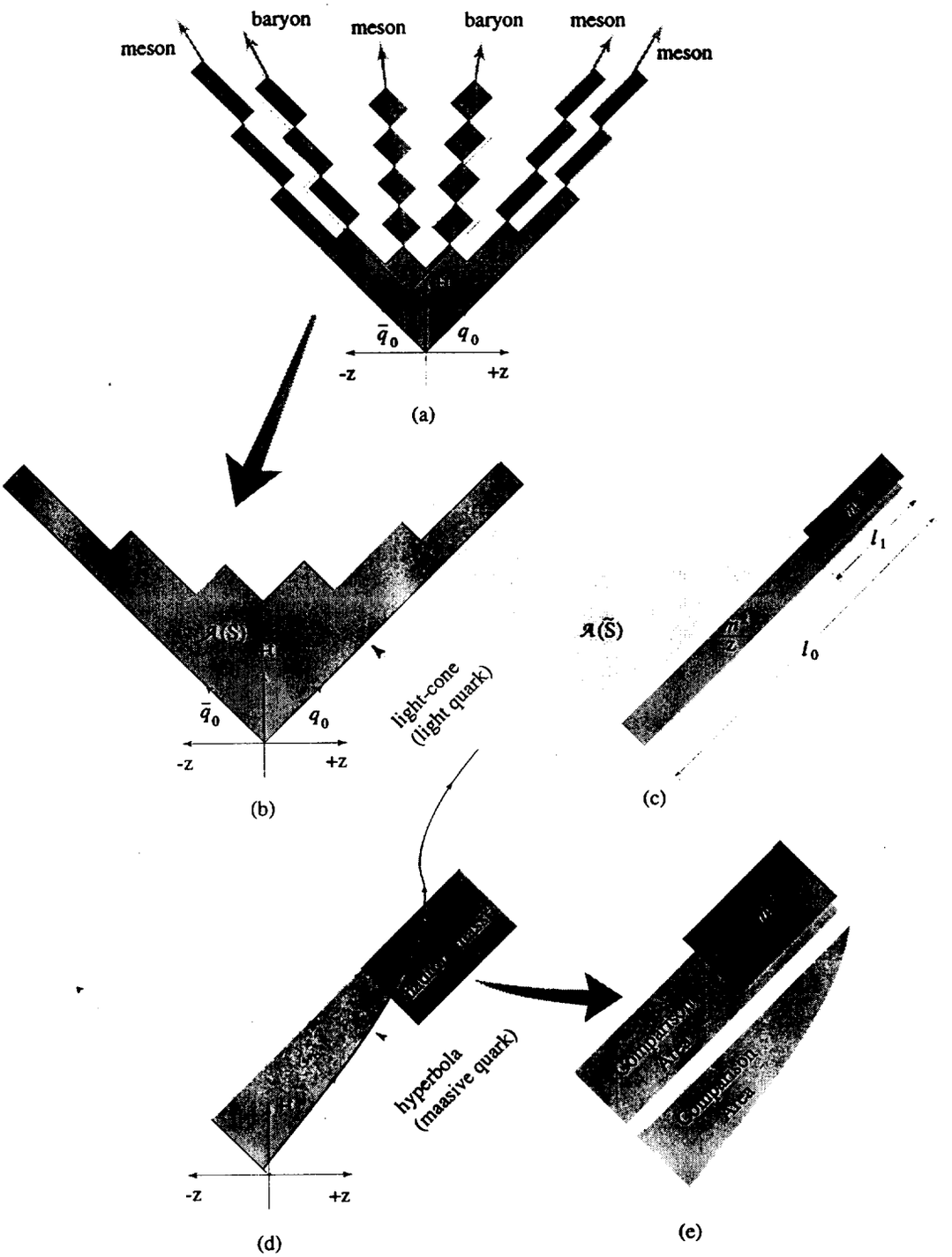

Fig. 5. Various geometrical definitions to be used in deriving the outermost hadron's fragmentation function dP_1 are displayed. A heavy initial quark travels along a hyperbola rather than a light-cone, which affects the area involved. One has to modify the definition of z in order to incorporate this change.

3.4 *Dependence of the* total weight *on* $S = E_{CM}^2$

The reason to introduce the ***Event Weight Function*** $dW_f{}^{q_0\bar{q}_0}(S)$, instead of using the probability $dP_f{}^{q_0\bar{q}_0}(S)$, is that a very useful ***Lemma*** can be proven for $g^{ij}(S)$ (see Appendix E.2 for details):

Take the natural log of both sides of eq(11). Differentiate with respect to S. Make the crucial assumption that the fragmentation function $dP_f{}^{q_0}(S)$ is, in fact, independent of S when S is large enough. (This is reminiscent of the scaling phenomenon in ***deep inelastic scattering*** that, when an electron of high enough energy probes a proton, the parton structure function is a function of the momentum fraction but not Q^2). Then, one obtains at large S

$$\frac{S}{g^{q_0\bar{q}_0}(S)}\,\frac{dg^{q_0\bar{q}_0}(S)}{dS} = \frac{\widetilde{S}}{g^{q_0\bar{q}_1}\left(\widetilde{S}\right)}\,\frac{dg^{q_0\bar{q}_1}\left(\widetilde{S}\right)}{d\widetilde{S}}$$

Separation of variables implies

$$g^{q_0\bar{q}_0}(S) = d_{q_0\bar{q}_0}S^a \quad \text{and} \quad g^{q_1\bar{q}_0}(S) = d_{q_1\bar{q}_0}S^a \tag{12}$$

where all systems have the same power 'a' of S^a, but the coefficients d_{ij} depend on the flavors of the system. (See Appendix E.2 for details.)

3.5 *Final form of* fragmentation function

Thus, finally, our fragmentation function for the outermost hadron is (as derived from dW_f ***with the one assumption that*** $dP_1{}^{q_0}(S)$ ***is independent of*** S ***at large*** S***):***

$$dP_1{}^{q_0}(z_1, P_{T_1}^2, m_1^2) = \frac{N_1C_1^2}{(4\pi)^2}\,\nu_{12}\,(1-z_1)^a\left(1-\frac{m_1^2}{Sz_1}\right)^a e^{-bm_1^2/z_1}\,\frac{dz_1}{z_1}\,e^{-\chi P_{T_1}^2}\,dP_{T_1}^2 \times \frac{d_{q_1\bar{q}_0}}{d_{q_0\bar{q}_0}} \tag{13}$$

Note that an absolute normalization

$$\frac{N_1C_1^2}{(4\pi)^2}\,\nu_{12}$$

for the fragmentation function is indicated in this derivation.

3.6 UCLA form of the fragmentation function

Eq(13), with all $\nu_{ij} \simeq 1.0$ and all N_i approximately the same, is the primary structure to be used in the outside-in iterative implementation of our UCLA modeling. However, there are several important subtleties to be mentioned in its implementation:

(1) Eq(13) contains an exponential suppression of P_T, carried over from the *Event Weight Function* of eq(2). There are questions of the structure of the argument of the exponential, of the strength parameter in this exponential, of whether P_T compensation is only global in the event or is local either on the quark-antiquark level (Lund) or on the hadron level (UCLA), and of how to incorporate whatever approach is chosen into an outside-in iterative implementation. At this stage in our work, we want simply to use some good approximate P_T treatment which works so that we can focus on the question of meson production rates. We note that if one simply replaced m_h^2 by the transverse mass squared $m_T^2 = m_h^2 + P_T^2$, this would set $\chi = b/z$ in eq(13). However, one can show that, if there are local compensation correlations between hadrons, then the subsequent P_T distributions will be narrower than the 'natural' no-compensation distributions. (See Appendix C.) In particular, in an outside-in implementation, if the P_T of one hadron is compensated for by the next n hadrons, then one can show that a factor of $n/(n-1)$ is introduced into the exponential. We find that the following works reasonably well and use it as an approximate treatment for the time being: (a) We use $n = 2$ (the most local compensation possible on the hadron level) so that the suppression factor is $exp(-2bP_T^2/z)$. (b) After one hadron's P_T is picked, the next hadron's P_T is centered at $-1/2$ of the remaining P_T imbalance. This, as will be seen, gives an adequate description of the data. We also note, however, that a different factor in $e^{-2bP_T^2/z}$ from $e^{-bm_h^2/z}$ leads to a small Left-Right symmetry violation[2].

(2) In Fig.3, we have presumed that the initial $q\bar{q}$ pair are quite light and essentially travel along the light cone. This is a good approximations for up, down, and even strange quarks. However, it is a poor approximation for charm and bottom quarks, which travel in a hyperbolic path inside the light cone. This is indicated in Fig.5(d). Focusing on area-law considerations, we presume that z_{eff} is really m_h^2/(comparison area) of Fig.5(d). This modifies the definition of the energy-momentum fraction z to be used in the exponential of eq(13), which arises from the area-law. The result is

$$z_{\text{eff}} = \frac{z}{1 - \frac{\mu^2 z}{m^2} - \frac{\mu^2 z}{m^2} \log\left(\frac{m^2}{\mu^2 z}\right)} \tag{14}$$

where μ is the current quark mass and m is the hadron mass. This has little effect on light and strange hadrons, but softens the predicted spectra for b-and c-hadrons in a manner which gives substantially better agreement with experimental spectra than otherwise.

(3) The ratio $d_{q_1\bar{q}_0}/d_{q_0\bar{q}_0}$ correctly expresses a procedure which was clearly called for in our original phenomenological approach. Consider Fig.3: Let $\bar{q}_0$ be a $\bar{u}$, where we want to focus on properly picking hadron #1 using our fragmentation function weights of eq(13). If $vertex_{12}$ is either $u\bar{u}$ or $d\bar{d}$, then hadron #1 is non-strange. However, if $vertex_{12}$ is $s\bar{s}$, then *both* hadron #1 and hadron #2 are strange and therefore heavier than otherwise and therefore provide more suppression to the event via the $exp(-bm^2/z)$ factors. In our phenomenological treatment, as we consider hadron #1, we must *'look ahead'* at hadron #2 also and incorporate the effects of the quark-antiquark flavor at vertex12 on the mass of hadron #2; that is, we include a factor of

$$\sum\!\!\!\!\!\!\int_{z,P_T}^{i} \frac{N_i C_i^2}{(4\pi)^2} \frac{(1-z)^a}{z} \left(1 - \frac{m_i^2}{Sz}\right)^a \mathrm{e}^{-b\left(m_i^2+2P_T^2\right)/z}\, dz dP_T^2$$

from each appropriate hadron #2 into the weight for each possible hadron #1. The d_{ij} factors in eq(13) explicitly summarize and require this procedure.

More precisely, eq(13) can be recast into an eigenvector problem for the d_{ij}'s with the knitting factor N related to the eigenvalue: Since some first hadron must be created, there is a probability unitarity constraint of:

$$\sum\!\!\!\!\!\!\int_{z,P_T,\ flavor} dP_1{}^{q_0}(z, P_T^2, m^2) = 1$$

where the summation over $flavor$ is for the flavor of the hadrons containing a quark q_0. Carrying out this *sum/integration* over possible hadron flavors, z's, and P_T's and generalizing to any combination of initial quark and antiquark flavors leads to a set of coupled equations:

$$d_{ij} = \sum\!\!\!\!\!\!\int_{z,P_T\ flavor} \frac{NC_{ik}^2}{(4\pi)^2} \frac{(1-z)^a}{z} \left(1 - \frac{m_{ik}^2}{Sz}\right)^a \mathrm{e}^{-b\left(m_{ik}^2+2P_T^2\right)/z}\, dz dP_T^2 \cdot d_{kj}$$

The factor quoted above which we use in the weight for hadron #1 from appropriate hadrons #2 is just the first step in an iterative solution to this eigenvector problem for the d_{ij}'s. Solving the eigenvector problem directly for our best fit values of $a = 1.65$ and $b = 1.18\ GeV^{-2}$, we find

$$d_{u\bar{u}} \simeq d_{d\bar{d}} \simeq d_{u\bar{d}} = d_{d\bar{u}}$$

$$d_{s\bar{u}} = d_{u\bar{s}} \simeq d_{s\bar{d}} = d_{d\bar{s}} \simeq 0.47\ d_{u\bar{u}}$$

$$d_{s\bar{s}} \simeq 0.47\ d_{s\bar{u}}$$

These, of course, to first order are simply the factors we have used for the hadron #2 weighting.

The solution to the eigenvalue problem also gives an intriguing new piece of information, namely, an eigenvalue for the knitting factor:

$$N \simeq 160 \sim 220 GeV^{-2} \simeq (68 \sim 80 MeV)^{-2} \simeq (2.5 \sim 2.9 \text{ fm})^2$$

The knitting factor appears to be a new and interesting concept, which may in some manner be related to the inverse of an hadronic decay constant. We note, in fact, that $N \simeq (2/f_\pi)^2$ for typical hadronic decay constants f_π of $110 \sim 160\ MeV$. The knitting factor and other spatial properties of hadronization development are discussed in a semi-classical artist's conception in Appendix F.

4 Baryon Formation

During our hadronization studies, as we have come to understand meson formation as apparently a very simple process, we have also come to view baryon formation as a much more complicated process: (1) three quarks must somehow coalesce into a baryon wave function; (2) whereas a quark and antiquark define a one-dimensional line between them in forming a meson, three quarks can have a more complex two-dimensional structure in forming a baryon; (3) one or more 'popcorn' mesons can be formed between the baryon and antibaryon; and (4) because of the multiple popcorn meson formation possible, there are many more combinations possible in the flavor chain of an event.

Recognizing this much-increased complexity for baryon formation, we extend our approach for mesons to baryon formation in as simple a manner as possible. The following approach works encouragingly well, though we currently must introduce at least one *'ad hoc'* parameter in order to reach fairly reasonable agreement with baryon rate, distribution, and correlation data. Thus, our current baryon studies have three purposes: (1) to do an adequate enough job of phenomenologically fitting baryon data so that the fit in the baryon sector doesn't produce any significant bias to our comparisons and conclusions in the meson sector; (2) to show that our UCLA approach, extrapolated to baryons, works encouragingly well; and (3) to point the way to the kind, quality, and quantity of additional data needed to bring our understanding of baryon formation close to the current level of understanding of mesons.

4.1 UCLA approach for baryon formation

Following the philosophy of our meson treatment, our approach for baryons is:

1) For any given final state of hadrons with specified flavors and three-momenta, now including baryons and antibaryons, we assign a weight via the Event Weight Function approach. For this weight function, we presume:
2) The area law approach is valid. Likewise proper kinematics for the Event Weight Function are still valid.
3) The same values of *'a'* and *'b'* are used in the fragmentation function for baryons as for mesons. (See Section 7 for possible differences of *'a'* for mesons and baryons.)
4) There is no significant suppression for creating any number of virtual $u\bar{u}$, $d\bar{d}$, and $s\bar{s}$ pairs from the colorfield, as we also assumed for mesons.
5) To knit quarks into baryons:
   - Proper Clebsch-Gordon coefficients should be used for creating baryons as well as for mesons.
   - The spatial knitting factors to form baryons are assumed to be the same as for the mesons, where the *universal* value is found to be $\approx 1/(75MeV^2)$ from data and probability conservation, as is discussed in Section 3 and Appendix E.3.

The Clebsch-Gordon coefficients for flavor and spin couplings are as simple for baryons as they are for mesons, presuming the three assumptions made in Section 2: (1) local flavor conservation in creating virtual $q\bar{q}$ pairs from the colorfield; (2) virtual $q\bar{q}$ pairs are available 'for free' from the colorfield; and (3) the spins of the final state hadrons are (at least, approximately) independent. Given these assumptions, the flavor coupling of whatever quarks are needed into the final state baryon flavor state is simply 1.0 and the spin coupling is simply the final state baryon spin degrees of freedom, i.e., 2.0 for spin 1/2 baryons and 4.0 for spin 3/2 baryons. The only difference between mesons and baryons is in the neutral sector: Mesons such as π^0, η, ρ^0, ϕ, etc. contain superpositions of different $q\bar{q}$ flavor states (i.e., $u\bar{u}$, $d\bar{d}$, and $s\bar{s}$) and therefore a given state of flavored $q\bar{q}$ (e.g., $u\bar{u}$) couples into a neutral meson flavor state with less than 1.0. By contrast, for example, every term in the Λ and Σ^0 flavor state is *uds*. Thus, the flavor coupling of quarks within the colorfield into *each* of the Λ and Σ^0 is 1.0.

In terms of area law treatment, because baryons contain three quarks, there is a new spatial degree of freedom. Whereas quark and antiquark in a meson always define a 1-dimensional line between them, the three quarks in a baryon can form a 2-dimensional spatial structure. As the three quarks propagate

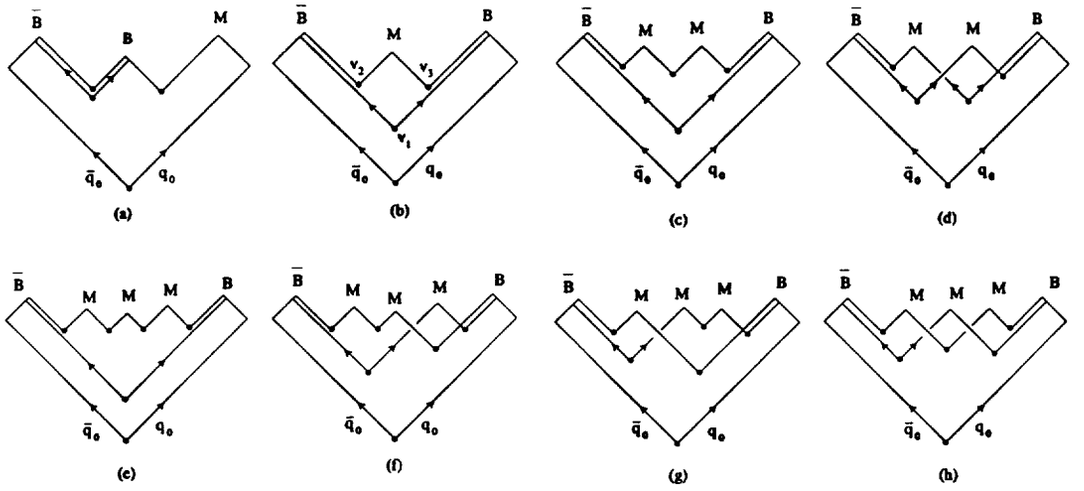

Fig. 6. (a) The baryon and anti-baryon pair are produced adjacent to each other. (b) One popcorn meson is produced between the baryon and anti-baryon. (c)(d) Two possible ways of producing two mesons between the baryon and anti-baryon. (e)-(h) Four possible ways of producing three mesons between the baryon and anti-baryon. As more popcorn mesons are produced, the number of diagrams increases rapidly.

forward in time, an area law structure can take either a 'Y' structure or a 'Δ' structure connecting them. In our current treatment, we presume that the area law for baryons can be treated in an approximate manner where the 'Y' or 'Δ' structure has been collapsed into a 1+1 dimensional structure (as for mesons).

4.2 Popcorn meson *structure*

Even within the context of our presumed 1+1 dimensional treatment for baryons, another new degree of freedom emerges: namely, events where 'popcorn' mesons are 'popped out' between the baryon and antibaryon. Fig.6 shows (a) the baryon and antibaryon are adjacent and share two virtual $q\bar{q}$ pairs; (b) there is one intermediate popcorn meson and the baryon and antibaryon share one virtual $q\bar{q}$ pair; (c) there are two popcorn mesons and the baryon and antibaryon share one virtual pair (where the 'first' virtual pair must 'live a long time' before the rest of the baryon-antibaryon formation occurs); and (d) there are two popcorn mesons in a 'crossed' diagram where the baryon and antibaryon share no virtual $q\bar{q}$ pairs; (e)-(h) various diagrams with three popcorn mesons. Hypothetically, the popcorn diagrams, with ever increasing complexity, could extent to very many popcorn mesons. Note that the popcorn diagrams introduce new baryonic degrees of freedom which are otherwise unachievable, e.g., a $\bar{p} - \Xi$ (baryon-antibaryon) pair, and thus increase the density of final states for baryon production.

We find, in fact, that the series diverges as one increases the number of popcorn mesons. Thus we must introduce a parameter to effectively cut off long popcorn chains. We are led by the fact that strong interaction theory suggests a perimeter law as well as an area law (see Section 8). In the case of popcorn diagrams, where in fact the perimeters are longer than for non-popcorn diagrams, this suggests the use of a suppression of the form $exp(-\eta \cdot m_{popcorn})$. This works well phenomenologically with $\eta \simeq 3.5/GeV$. One interesting consequence of this structure is that the possible length of popcorn chains, even though suppressed, lengthens as E_{CM} increases and thus slowly increases the density of final baryonic states as E_{CM} increases. This seems to correspond to the fact that in tuning JETSET the Lundian parameter qq/q which controls baryon production must be increased from ≈ 0.06 at $E_{CM} = 10GeV$ to $\simeq 0.10$ at 91 GeV.

5 Summary of UCLA *Event Weight Function* and Its *Fragmentation Function* Implementation

We summarize the structure used in our UCLA modeling. The *Event Weight Function* for a straight piece of relativistic string, incorporating the specific assumptions of our UCLA approach, is:

$$
\begin{aligned}
dW_f^{q_0\bar{q}_0} &= \frac{NC_1^2}{(2\pi)^3} dE_1 dP_{z_1} dP_{x_1} dP_{y_1} \delta\left(E_1^2 - P_1^2 - m_1^2\right) \mathrm{e}^{-\chi\left(P_{x_1}^2 + P_{y_1}^2\right)} \times \ldots \\
&\times \frac{NC_n^2}{(2\pi)^3} dE_n dP_{z_n} dP_{x_n} dP_{y_n} \delta\left(E_n^2 - P_n^2 - m_n^2\right) \mathrm{e}^{-\chi\left(P_{x_n}^2 + P_{y_n}^2\right)} \\
&\times (2\pi)^4 \delta\left(\mathbf{E} - \sum_i E_i\right) \delta\left(\mathbf{P}_z - \sum_i P_{z_i}\right) \delta\left(\mathbf{P}_x - \sum_i P_{x_i}\right) \delta\left(\mathbf{P}_y - \sum_i P_{y_i}\right) \\
&\times \mathrm{e}^{-b' A_{plane}}
\end{aligned}
$$

where we have

(a) set all the ν_{ij}'s (possible virtual quark-antiquark suppression factors) to 1.0, and

(b) set all the spatial knitting factors N_i (for pseudoscalar and vector couplings, etc) to be a universal factor N.

This leads to a fragmentation function of the following form to be used at each step of an outside-in one-hadron-at-a-time iterative implementation;

$$
dP_1^{q_0}(z, P_T^2, m^2) = \frac{NC_1^2}{(4\pi)^2} (1-z)^a \left(1 - \frac{m^2}{Sz}\right)^a \mathrm{e}^{-bm^2/z_{\mathrm{eff}}} \frac{dz}{z}
$$

$$\times\, e^{-\frac{n}{n-1}b\left\{(P_x-\phi_x/2)^2+(P_y-\phi_y/2)^2\right\}/z_{\rm eff}}\, dP_T^2 \;\cdot\; \frac{d_{q_1\bar{q}_0}}{d_{q_0\bar{q}_0}}$$

where:

1) we have presumed that dP_1 is independent of S at large S, which leads to

$$g^{q_i\bar{q}_j}(S) \equiv \sum\!\!\!\!\!\!\int_f dW_f{}^{q_i\bar{q}_j}(S) = d_{ij}S^a$$

2) $b = b'/\kappa^2$, where κ is the string tension ($\simeq 1\ GeV/fm$)
3) For P_T (see Appendix B and C), we have used the form

$$\chi = \frac{n}{n-1}\;\frac{b}{z_{\rm eff}}$$

The factor $n/(n-1)$ expresses the phenomenon of approximate local P_T compensation (where, as we will see from the data, $n \simeq 2$, the strongest local P_T correlation possible in this formalism). For the outside-in iterative process, we have also centered the P_T distribution at $-\phi/2$ in each of the x and y directions, where ϕ is the P_T total accumulated over the previous iterations. We note that using different factors for m^2 (*i.e.*, $-b/z$) and for P_T^2 (*i.e.*, $-2b/z$) slightly violates *left-right symmetry* for the fragmentation function [2]
4) The fact that a virtual quark with non-negligible mass travels classically in a hyperbola rather than along the light-cone leads to

$$z_{\rm eff} = \frac{z}{1 - \frac{\mu^2 z}{m^2} - \frac{\mu^2 z}{m^2}\log\left(\frac{m^2}{\mu^2 z}\right)}$$

to be used in the exponentials of the *fragmentation function*, where μ is the current quark mass and m is the mass of the hadron to be created.
5) *Unitarity* in the iterative use of the fragmentation function (some hadron must be created at each step) leads to:

$$\sum\!\!\!\!\!\!\int_{\substack{z,P_T,\\ flavor}} dP_1{}^{q_0}(z, P_T^2, m^2) = 1$$

6) In the iterative implementation, the d_{ij}'s account for the additional suppression from the mass of the next hadron (e.g., when a virtual $s\bar{s}$ pair is created in the color-string). The d_{ij}'s are the solution (using the unitarity condition of (5) above) to the eigenvector problem of the coupled linear equations (see Appendix E.3), which also determine the spatial knitting factor as $N \simeq 180 GeV^{-2} \simeq (2.7fm)^2$.
7) In producing popcorn mesons in baryon-antibaryon production, an additional factor of $\exp(-\eta m_{\rm pop})$ is included. (See Section 4.2.)

Implicit in our treatment are six other assumptions:

1) Local flavor conservation, in creating virtual quark-antiquark pairs.
2) There are no significant spin correlations between nearby hadrons.
3) There are no significant iso-spin correlations between nearby hadrons.
4) After one hadron has been created in the outside-in implementation, then the remaining system in the iterative process has the same characteristics (but based on a smaller E_{CM} system) as the initial system.
5) There are no significant interference effects. That is, we can deal with *probabilities* rather than *amplitudes*. (See Appendix D where we establish that this is a good approximation.)
6) Higher mass states (e.g., $l = 1$), which decay rapidly, are adequately approximated as pieces of relativistic string.

6 Comparisons of Predictions with Data

6.1 Structure for comparisons

Within the context of using JETSET7.4 (an outside-in iterative Monte Carlo program) to implement our approach, the comparisons of our model predictions with data and the associated tuning of parameters naturally divide into five 'sectors' which are fairly separable, though there is some 'parameter cross-talk' between the sectors: (A) the parton shower; (B) P_T effects; (C) heavy-quark hadrons (containing c- or b-quarks); (D) light-quark baryons; and (E) light-quark mesons. Our main thrust in this Report is to make sure that (A)-(D) are well-tuned so that they create negligible biases and we can study the main focus of our investigation, namely (E) the light-quark meson production rates and distributions.

Comparisons are made at e^+e^- center-of-mass energies sufficiently high for hadronization studies, where there are large data samples from more than one detector, namely 91 GeV, 29 GeV, and 10 GeV (continuum). Data used include flavored multiplicities and distributions for the light-quark meson and baryon sectors, as well as for various topological and single particle distributions for the parton shower, P_T, and heavy-quark sectors.

For multiplicities, all relevant data through Summer 1996 have been included. At 10 Gev and 29 Gev, we use the data review by E. C. Berg and C. D. Buchanan[10]; at 91 Gev, we use the 1995 data review by A. De Angelis[11], updated by publications and papers up through the ICHEP Conference at Warsaw in July 1996[12]. For the flavored distributions and for the topological and single particle distributions, a comprehensive (but not exhaustive) sample

SECTOR	PARAMETERS	VALUE
Parton Shower	Λ (QCD strength)	0.32 GeV
	Q_0 (Cuts off shower)	2.0 GeV
P_T	n (Local correlations)	2
Heavy-quark Hadrons	(None needed)	
Light-quark Baryons	η (Controls popcorn)	3.5 GeV^{-1}
Light-quark Mesons	a (Growth of g(s))	1.65
	b (related to the *string tension*)†	1.18 GeV^{-2}

Table 1
Parameters for UCLA and their tuned value. Note that this set of parameters are tuned to span 10 GeV, 29 GeV and 91 GeV.
† $b = b'/\kappa^2$ where κ and b' are the *real* and the *imaginary* part (which allows a system to decay into the final state hadrons) of the string tension respectively.

of relevant distributions gleaned from the same sources is presented.

6.2 Tuning and overall results

Our predictions have been tuned simultaneously for all three center-of-mass energies with only the one set of energy-independent parameters cited in Table 1, which lists each *sector*, the major parameters used in tuning that sector, and the best-tune values of those parameters.

Once (A)-(D) (above) are reasonably well tuned, we reach our major conclusion in sector (E): *there are no significant deviations between our predictions and data at all three center-of-mass energies for all the various flavored light-quark meson rates and distributions studied, using only the two parameters – 'a' and 'b' – natural to the light-quark meson sector.*

It is also worthy of note that: (D) our current predictions for light-quark baryons, developed following an extension of our approach used for mesons, are approximately accurate (though not as good as for light-quark mesons) using only one additional *ad hoc* parameter; (C) our predictions for spectra of heavy-quark hadrons, which are substantially influenced by the area-law approach in

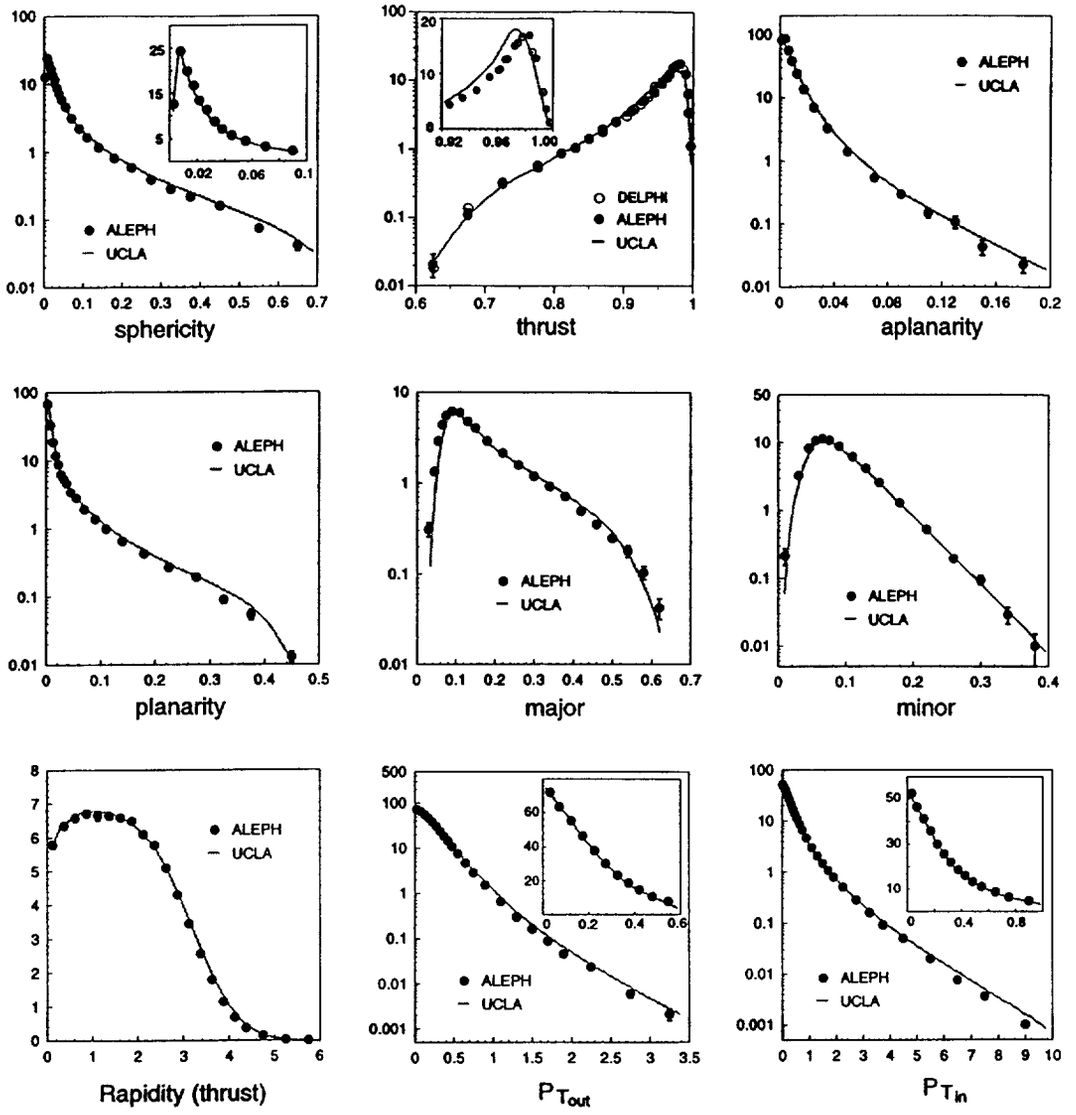

Fig. 7. UCLA predictions for various topological variables and charged particle distributions are compared to LEP experiments at $E_{CM} = 91\,GeV$.

our use of z_{eff}, are rather good and require no additional parameters; and (A,B) our predictions for the topological distributions (dependent on the JETSET parton shower treatment and using the two major parameters therein) and for the various P_T distributions (using one *ad hoc* parameter) are also rather reasonable.

It is worth noting in the comparisons that there are some deviations between our predictions and data. The important questions to bear in mind are: (1) 'Are the deviations in the other sectors significant enough to affect the light-quark meson comparisons?' and (2) 'Are the deviations in the light-quark meson sector big enough to affect our conclusions?' We feel that the answer to

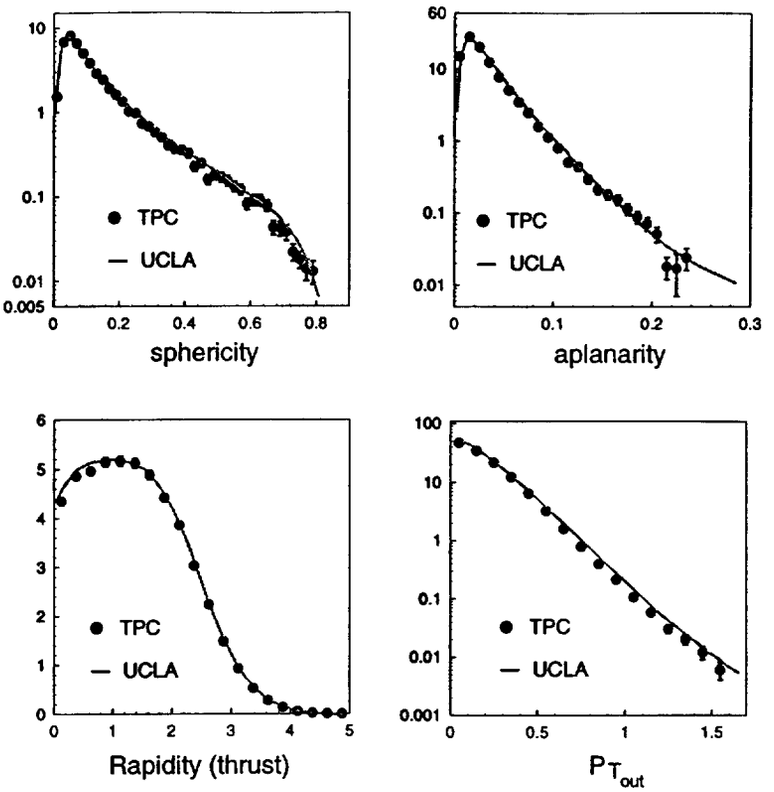

Fig. 8. UCLA predictions for various topological variables are compared to experiments at $E_{CM} = 29\,GeV$.

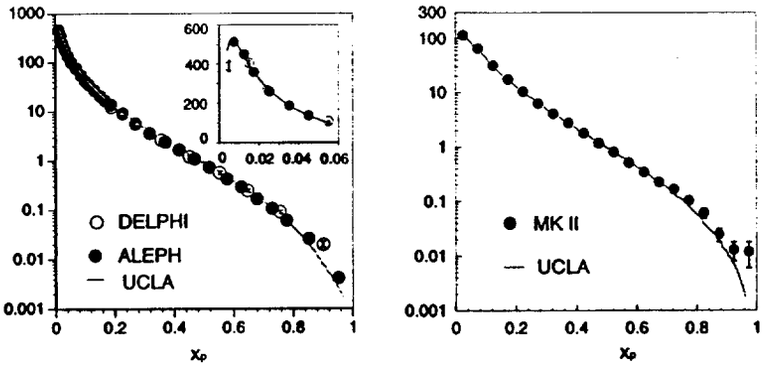

Fig. 9. UCLA predictions for $X_P = P_{hadron}/P_{beam}$ of charged particles are compared to experiments at $E_{CM} = 29,\ 91\,GeV$.

each of these questions is 'No'. We also note that there are other treatments in the JETSET7.4 program which are approximations and which therefore can affect the comparisons slightly. These include: the parton shower, the treatment during iteration to move past a gluon-created string-kink, the treatment of the final two hadrons at the end of the iteration, and the tables used to decay higher-mass hadrons into those ultimately observed in a detector. Our

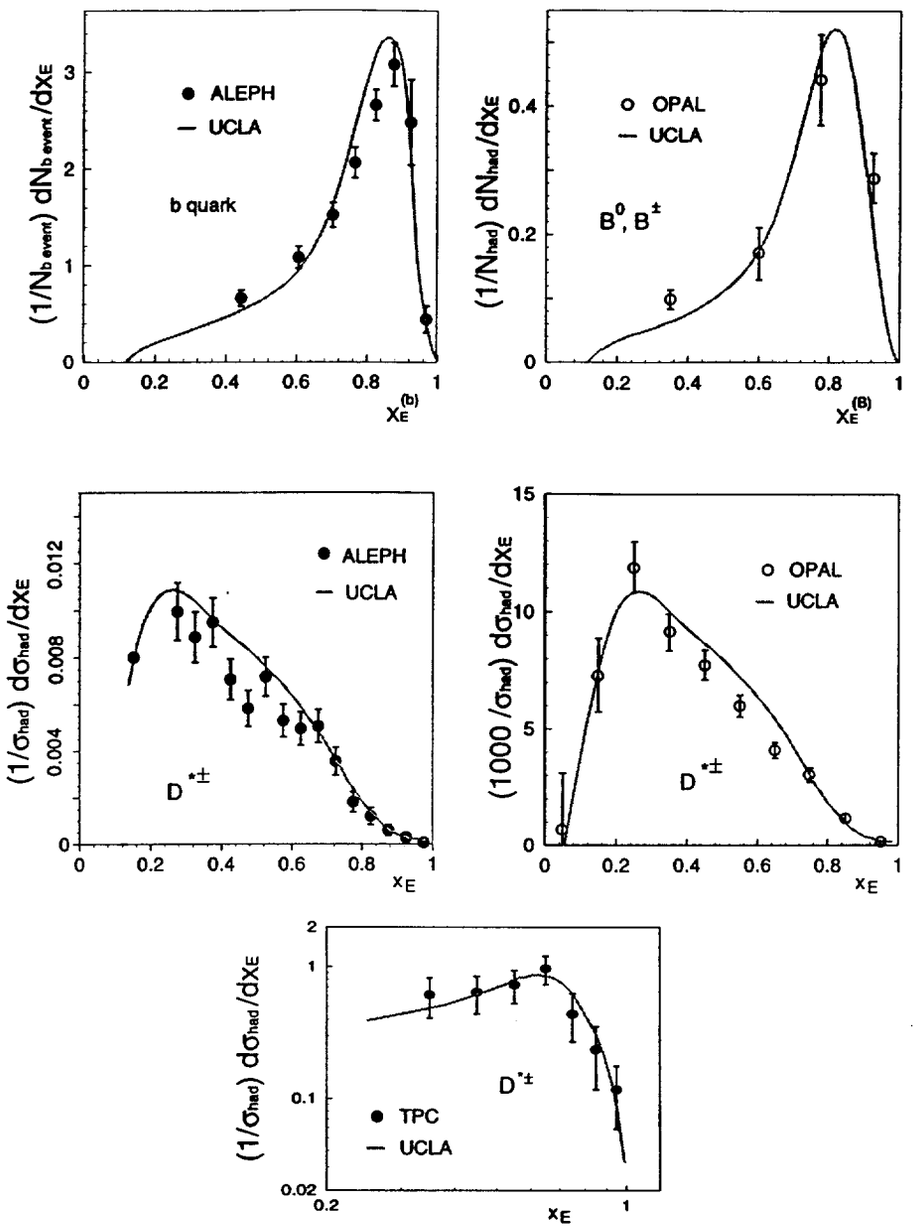

Fig. 10. UCLA predictions for the heavy-quark hadrons are compared to experiments at $E_{CM} = 29,\ 91\,GeV$.

very rough estimation is that these effects can lead to $2 \sim 10\%$ biases in the flavored multiplicities predicted.

	91 GeV			29 GeV			10 GeV		
	DATA	UCLA	$STD^{\dagger}$	DATA	UCLA	$STD^{\dagger}$	DATA	UCLA	$STD^{\dagger}$
N_{ch}	20.92 ±0.24	20.62	0.94σ	12.57 ±0.26	12.79	-0.76σ	8.48 ±0.42	7.59	2.08σ
$\pi^{\pm}$	17.06 ±0.44	16.88	0.32σ	10.60 ±0.36	10.41	0.45σ	6.53 ±0.51	6.13	0.75σ
π^0	9.39 ±0.53	9.56	-0.31σ	5.84 ±0.28	5.96	-0.40σ	3.33 ±0.26	3.55	-0.82σ
$k^{\pm}$	2.37 ±0.13	2.24	0.88σ	1.444±0.080	1.490	-0.51σ	0.897±0.058	1.001	-1.63σ
k^0	2.012±0.033	2.038	-0.38σ	1.402±0.048	1.308	1.47σ	0.899±0.049	0.854	0.80σ
η	0.95 ±0.11	0.79	1.29σ	0.593±0.075	0.484	1.31σ	0.207±0.038	0.289	-2.05σ
η'	0.22 ±0.07	0.15	1.00σ	0.260±0.103	0.105	1.49σ	0.034±0.011	0.070	-3.22σ
ρ^0	1.29 ±0.13	1.16	0.93σ	0.846±0.054	0.723	1.93σ	0.353±0.064	0.425	-1.10σ
ω^0	1.11 ±0.14	1.02	0.61σ						
$k^{*\pm}$	0.713±0.056	0.791	-1.10σ	0.641±0.062	0.518	1.69σ	0.276±0.073	0.342	-0.88σ
k^{*0}	0.759±0.041	0.736	0.38σ	0.574±0.039	0.448	2.42σ	0.299±0.029	0.280	0.56σ
ϕ^0	0.107±0.009	0.126	-1.53σ	0.084±0.010	0.080	0.33σ	0.046±0.005	0.053	-1.13σ

Table 2
UCLA predictions for the mesons at 10 GeV, 29 GeV and 91 GeV are compared to experiments.
† Decay table uncertainties are incorporated into the calculation of the number of standard deviations between the data and predictions, the column labeled *'STD'*. (See text.)

6.3 Comparisons for parton shower, P_T, and heavy-quark hadrons

6.3.1 Parton shower

We use the parton shower option of JETSET7.4. This is a recipe which incorporates leading log parton shower structure with a weighting function to allow mimicking of the matrix element calculations for the first two perturbatively-calculated gluon emissions. It employs two somewhat correlated parameters Λ controlling the QCD running strength and Q_0 controlling the low-virtuality cutoff at the end of the shower. Various 'topological' distributions, such as sphericity, thrust, aplanarity, planarity, major and minor eigenvalues of the sphericity tensor can be used to tune these parameters. A potpourri of such topological plots from 91 GeV and 29 GeV, as well as single charged particle distributions for rapidity and x_p, are displayed in Fig.7~9. The overall agreement seems quite acceptable , though there are minor discrepancies apparent at high thrust, high and low major values, and possibly high x_p.

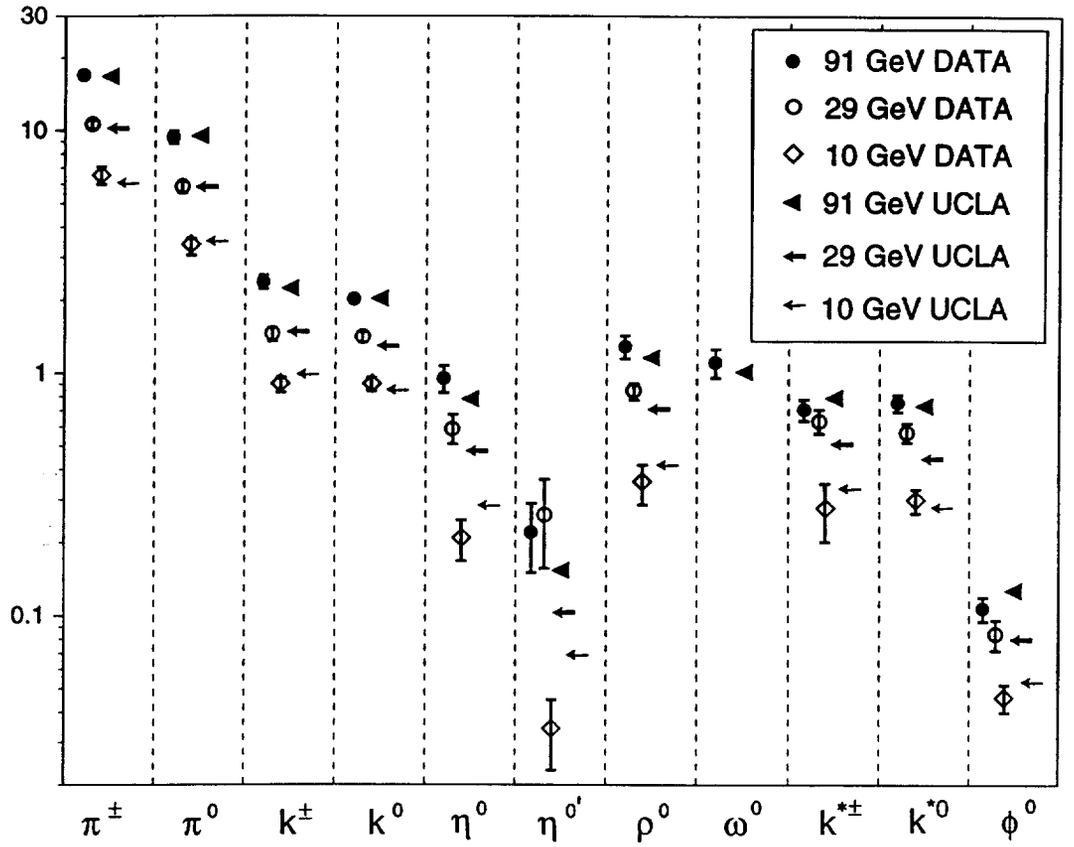

Fig. 11. Comparison of the experimental and predicted absolute production rates per event for various flavored light-quark mesons at E_{CM} = 10, 29, and 91 Gev.

6.3.2 P_T effects

If only transverse mass were involved in P_T effects, then we would use $\chi = b/z$ in eq(2) and eq(13). However, local P_T compensation between nearby hadrons, such as is discussed in Section 3 and Appendices B and C, suggests a factor greater than 'one'. We use $\chi = 2b/z$, which approximates the most local P_T correlation possible. Agreement (see Figs.7, 8) with data seem acceptably good, though our predictions might be a little high at high P_T values.

6.3.3 Spectra for heavy-quark hadrons

Our use of the area-law to derive z_{eff}, as described in Section 3, leads to considerably softer spectra for heavy-quark hadrons than would otherwise be predicted. Using this, we find reasonable agreement with the observed spectra in both peak positions and in shapes (see Fig.10). This internally-consistent treatment would seem to eliminate the need to switch to the Peterson fragmentation function[13] for the heavy-quark mesons.

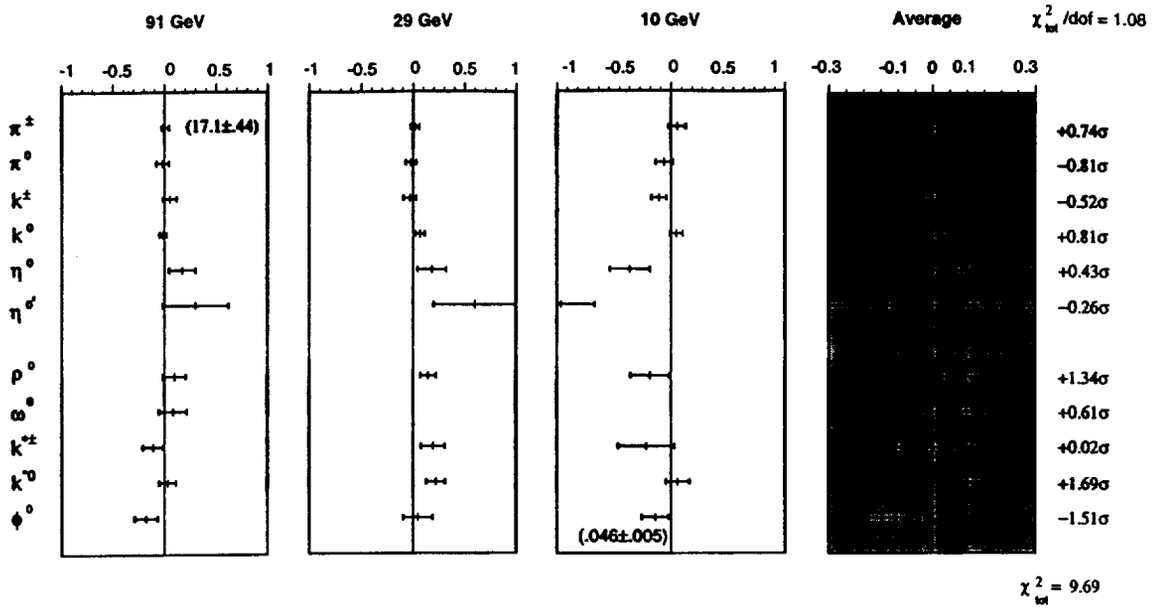

Fig. 12. The summary of experimental data vs. UCLA prediction for the mesons at E_{CM} = 10, 29, *and* 91 *GeV*. On the right, in an *expanded* scale, the comparison is shown for each flavor meson averaged over all three energies.

6.4 Comparisons for light-quark mesons

[Note: We defer the discussion of light-quark baryons, which are influenced by *'a'* and *'b'* of the fragmentation function as well as by the ad hoc *popcorn* parameter η, until after the light-quark meson discussion. Roughly speaking, the light-quark meson data are used to tune *'a'* and *'b'* and then η is used to tune to the baryon data.]

This light-quark meson sector is our most important study of *'elementary fundamental'* behavior of the colorfield. This sector is predominantly controlled by only the two 'natural' parameters of the fragmentation function for the modeling – 'a' from the growth of g(S) with S and 'b' which is related to the imaginary part of the string tension which allows the system to decay.

Our predicted multiplicities are compared with data for various pseudoscalar and vector mesons at E_{CM}=91, 29, and 10 GeV in Table 2 and in Fig.11 and 12.

Fig.11 compares the absolute magnitudes of predicted and measured multiplicities and gives an overall view of the range of rates over which prediction and experiment are compared. Fig.12 provides a finer grain comparison by suppressing the absolute rates and displaying deviations simultaneously in both percent and standard deviations. We use 'data minus prediction' to determine

the $\pm$ sign in our presentations of standard deviations.

Though the uncertainties quoted for the data in Table 2 are simply the experimental uncertainties, in the comparisons with predictions in Table 2 (the column labeled *'STD'*) and in Figs.11 and 12, we have included in quadrature estimations of the effects on the multiplicity-comparison uncertainties arising from the decay table uncertainties. [That is, if the decay table rate of a particle decaying into a relevant particle is incorrect, then the predicted rate for that relevant daughter particle will be biased. If the decay table rate is incorrect for a decay mode used experimentally to reconstruct the multiplicity for a relevant particle, then the experimental rate found will be biased. We have presumed the uncertainties in multiplicity comparisons from these decay table uncertainties to be: $\pm 2\%$ for pions; $\pm 3\%$ for kaons; $\pm 4\%$ for ρ^0 and ω^0; $\pm 6\%$ for η, η', k^0 and $k^{\pm}$; and $\pm 8\%$ for ϕ; also, $\pm 1\%$ for $N_{\rm charged}$.]

Comparing data and predictions over the range of meson multiplicities from 17.1 $\pi^{\pm}$ at 91 Gev to 0.046 ϕ's at 10 Gev (a range of ~ 400), we arrive at our Report's most important conclusion, namely: *Over this broad range, there are no deviations which seem truly significant.*

Of the 31 comparisons, the largest two deviations are: (a) We *overpredict* the η' rate at 10 GeV (measured only by the ARGUS collaboration) by 3.2 standard deviations; however, we note that, in reality, this is composed of *overpredicting* ARGUS's η multiplicity by 2.1 standard deviations and their η'/η ratio (where the η is used in reconstructing the η') by 1.1 standard deviation; also, we note that we somewhat *underpredict* the η' rates measured at 29 GeV and 91 GeV (b) We *underpredict* the vector mesons (ρ^0, $k^{*\pm}$, k^{*0}) at 29 GeV by an average of $\approx 20\%$ or 2.0 standard deviations; however, this effect does not appear at 91 GeV or 10 GeV. All 26 other comparisons are under 1.7 standard deviations; 17 (55%) are under 1.0 standard deviations. Overall, the $\chi^2/d.o.f.$ for light-quark meson multiplicities (not including $N_{\rm charged}$) is $50.7/29 = 1.75$, or an average of ~ 1.3 standard deviations per comparison.

If we presume that our model is accurate (and the deviations appear to be fairly randomly distributed), then we can treat the comparisons of the same meson at different energies as different measurements of the same quantity. Using both fractional deviations and standard deviations, these can be combined appropriately to give an overall comparison for each meson. This is displayed in the right-hand column of Fig.12, which employes an *expanded* scale, since the deviations are small. As displayed, there is very little difference between data and prediction; *each flavor is typically within* $\pm 10\%$ *and/or* ± 1.0 σ. These energy-averaged flavor comparisons have an overall $\chi^2/d.o.f. = 9.69/9 = 1.08$ or an average of ~ 1.0 standard deviation.

Fig.13$\sim$16 display sample energy and momentum distributions for various

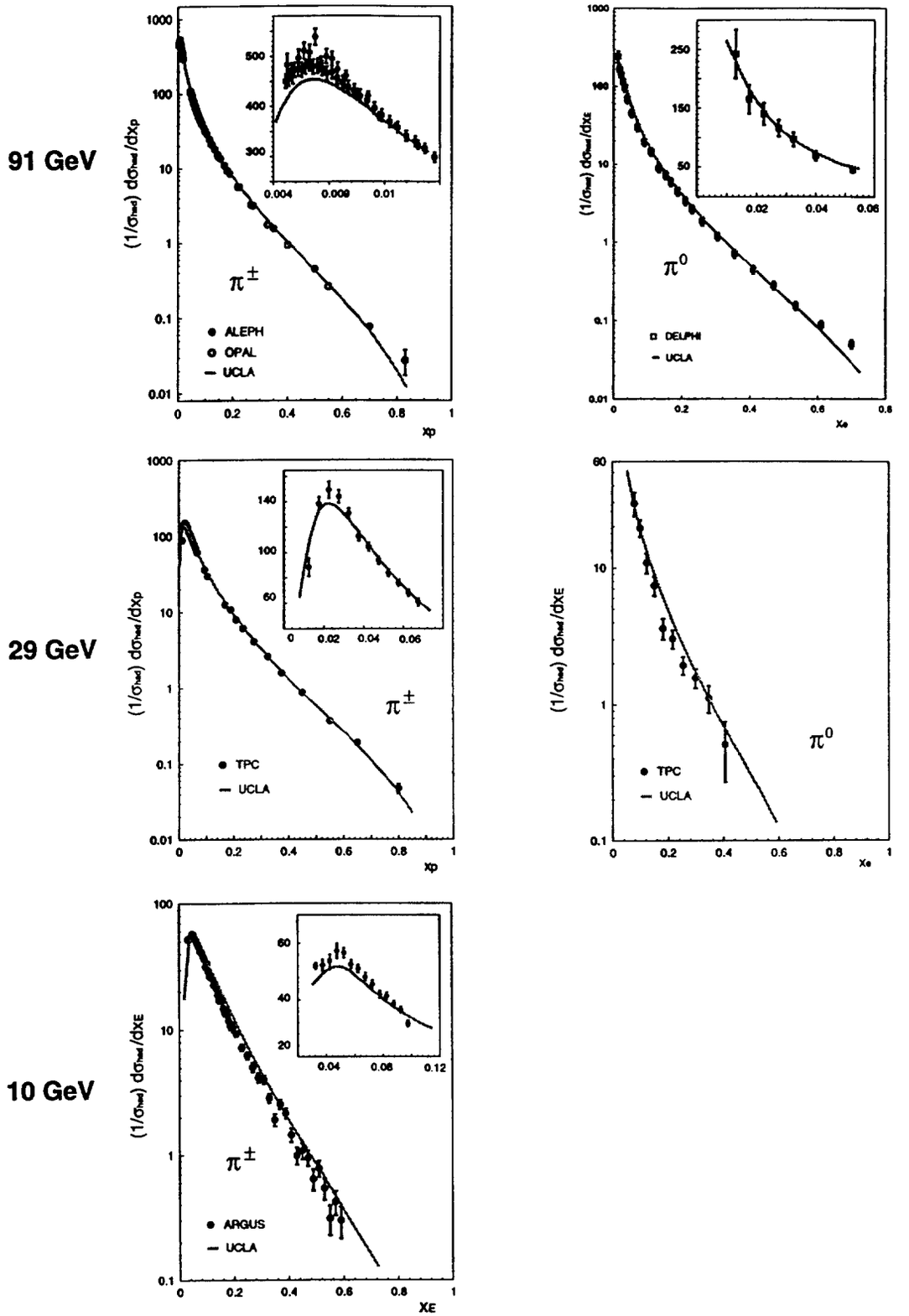

Fig. 13. UCLA predictions for π mesons are compared to experiments at $E_{CM} = 10,\ 29,\ and\ 91\,GeV$.

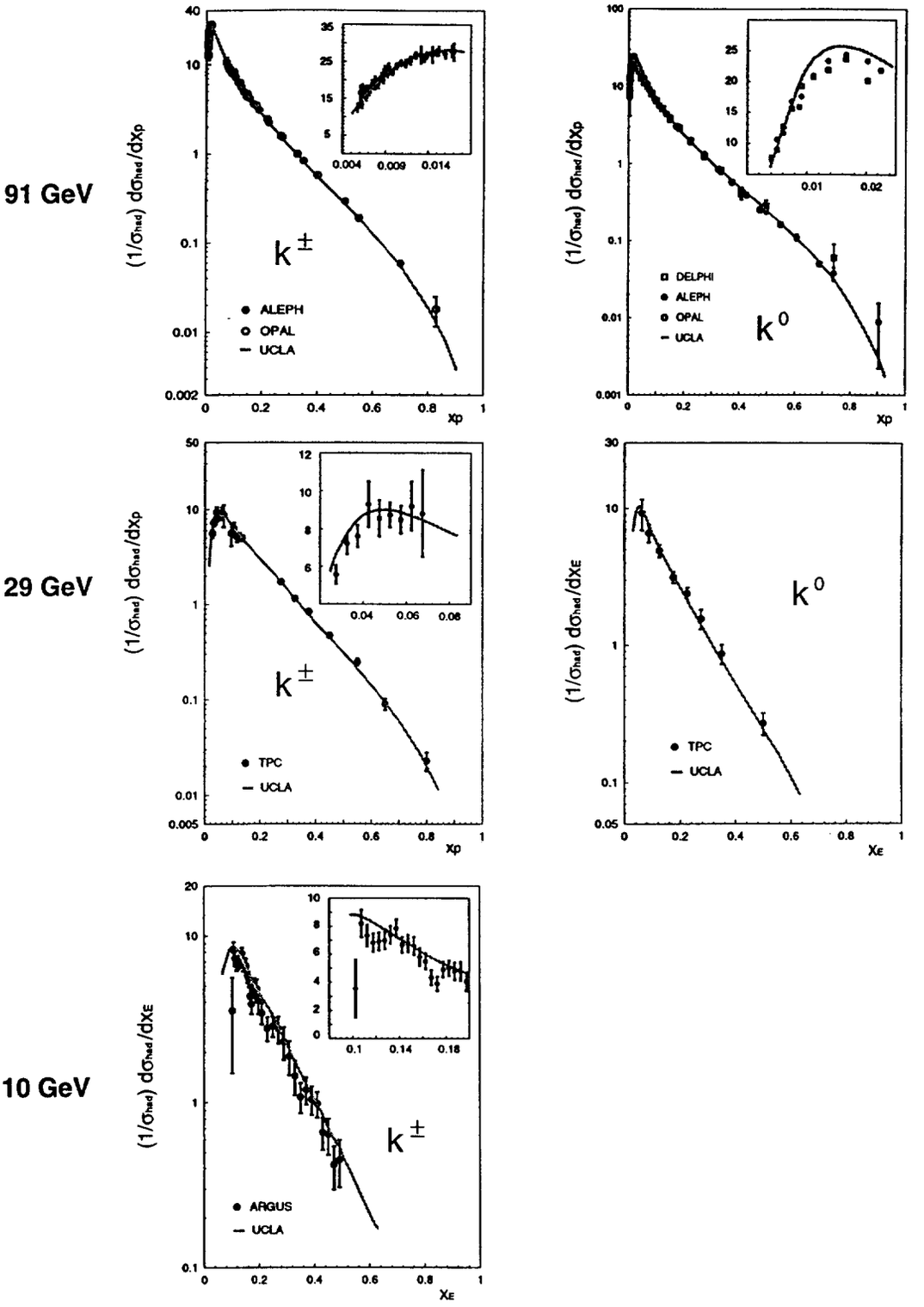

Fig. 14. UCLA predictions for k mesons are compared to experiments at $E_{CM} = 10,\ 29,$ *and* $91\,GeV$.

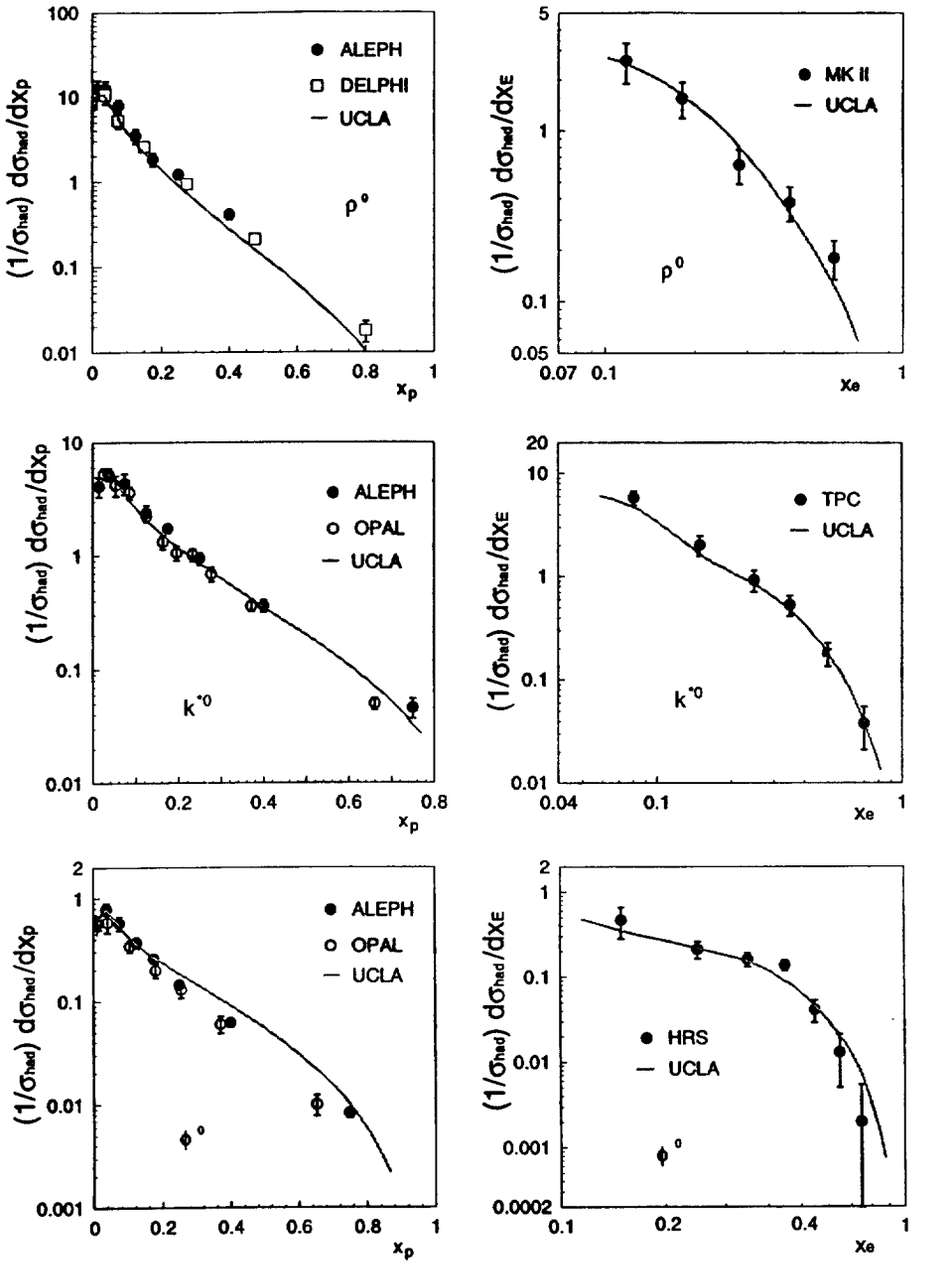

Fig. 15. UCLA predictions for various other mesons are compared to the experiments at $E_{CM} = 29$ *and* $91\,GeV$.

flavors at the three center-of-mass energies. Again, the overall agreement seems good. Possible minor concerns are: we slightly *underpredict* the data for $\pi^{\pm}$ at low momentum; we slightly *overpredict* K^0 production at low momentum at 91 GeV, but not $K^{\pm}$; we might slightly *underpredict* several of the flavors at very high momentum.

Overall, we find that our predictions for light-quark meson rates and distribu-

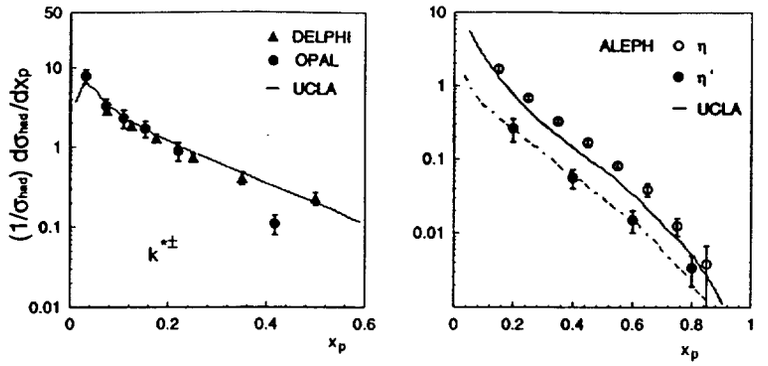

Fig. 16. UCLA predictions for $k^{*\pm}$, η and η' mesons are compared to experiments at $E_{CM} = 91\,GeV$.

tions are reasonably accurate and appear to display no significant deviations from the data over integrated multiplicity rates ranging from 17/event to .046/event (a range of ≈ 400) and over differential rates in $1/\sigma_{\rm TOT} \cdot d\sigma/dx_p$ ranging from 500 to 0.01 (a range of $\approx 50,000$).

6.5 Comparisons for light-quark baryons

Baryons are much more complicated objects than mesons and their physical dynamics are much less clear. E.g., three virtual quark-antiquark pairs must be created from the colorfield and, via some dynamics, the three quarks must knit together into a baryon; *popcorn* mesons can be formed between the baryon and antibaryon, which radically increases the number of ways in which a given set of final state hadron flavors and momenta can be achieved.

As described in Section 4, for baryon production we follow an extrapolation of our successful meson production approach in order to see whether this sort of approach makes sense for baryon production: We use our Event Weight Function (a) incorporating the area-law, (b) presuming no suppression for creating any number of $u\bar{u}$, $d\bar{d}$, or $s\bar{s}$ virtual pairs from the colorfield, (c) assuming the spatial knitting factors for baryon formation are the same as for meson formation, and (d) developing the necessary Clebsch-Gordon coupling apparatus for the flavor and spin coupling. Since we follow a Fermi Golden Rule addition of final states type of approach, the possibility of long chains of *popcorn* mesons increases the rates of baryon production. Currently, we introduce a parameter η in $\exp(-\eta\, m_{pop})$, motivated by QCD-inspired perimeter law arguments (see Section 8), to cut off these long chains.

Our goals currently in studying baryons are: (1) to show that this sort of approach has potential merit, (2) to tune the baryon sector predictions to the

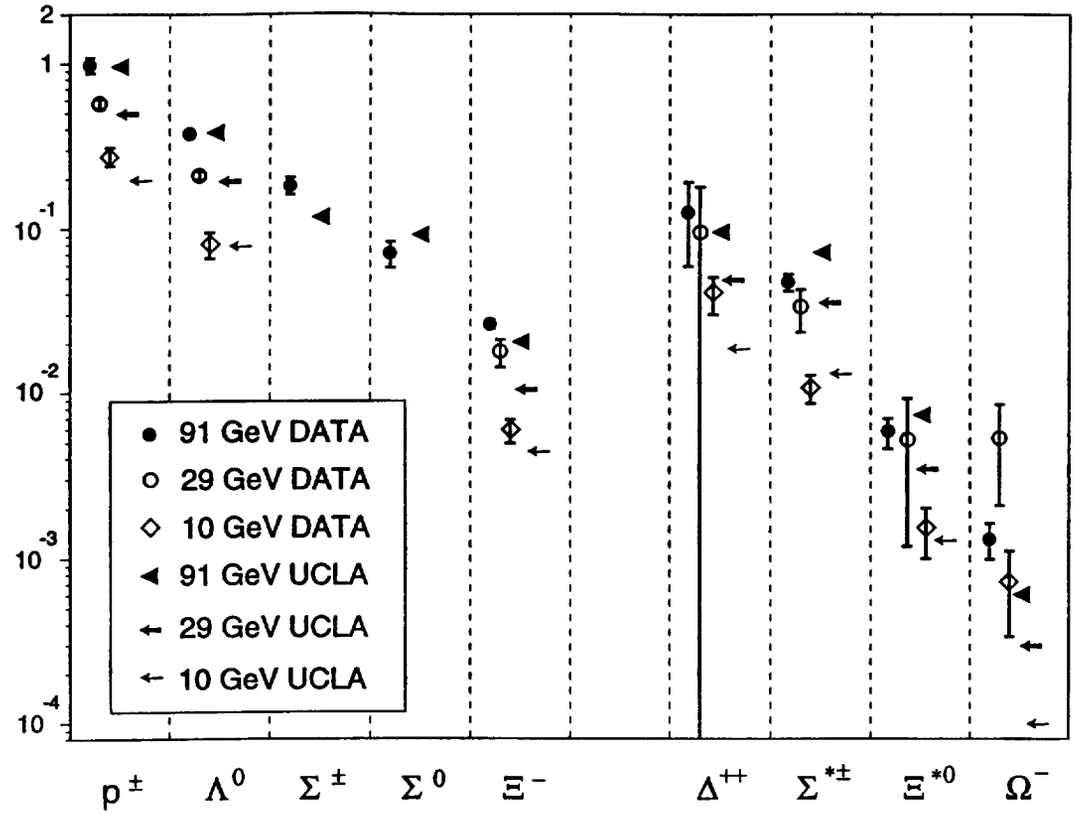

Fig. 17. Comparison of the experimental and predicted absolute production rates for various flavored baryons at E_{CM} = 10, 29, and 91 Gev.

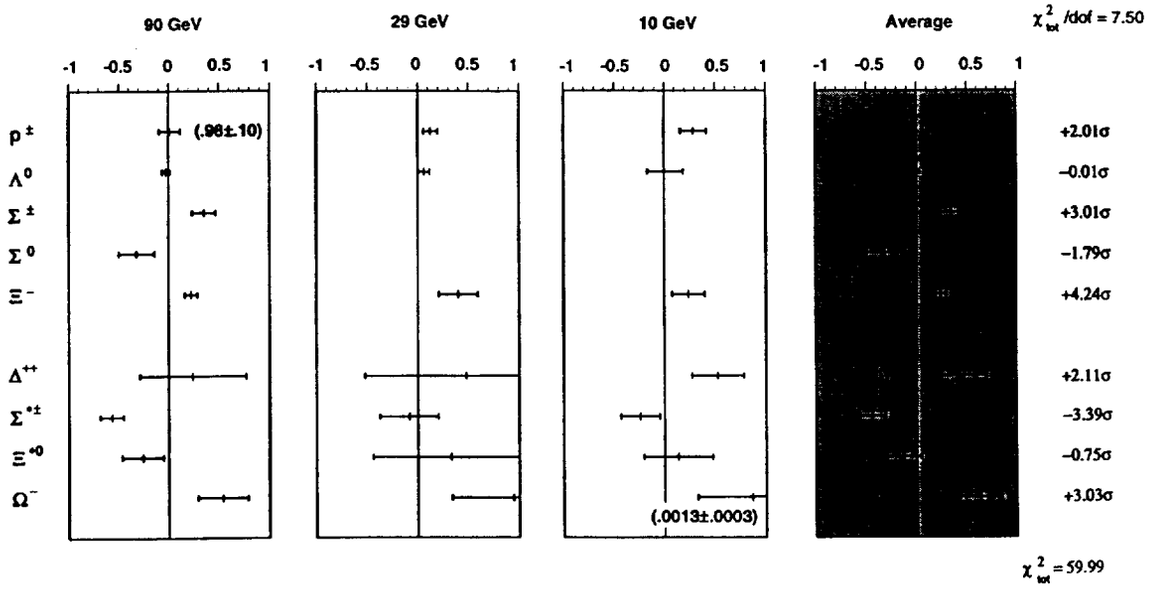

Fig. 18. The summary of UCLA prediction vs. experiments for the baryons at E_{CM} = 10, 29, *and* 91 *GeV*. On the right, the comparison is shown for each flavor baryon averaged over all three energies.

	91 GeV			29 GeV			10 GeV		
	DATA	UCLA	$STD^{\dagger}$	DATA	UCLA	$STD^{\dagger}$	DATA	UCLA	$STD^{\dagger}$
P	0.98 ±0.10	0.97	0.09σ	0.570 ±0.036	0.498	1.81σ	0.275 ±0.034	0.196	2.26σ
Λ^0	0.373 ±0.008	0.383	-0.70σ	0.209 ±0.010	0.197	1.02σ	0.080 ±0.014	0.079	0.07σ
$\Sigma^{\pm}$	0.182 ±0.019	0.119	3.01σ						
Σ^0	0.070 ±0.012	0.092	-1.79σ						
Ξ^-	0.0262±0.0010	0.0204	3.52σ	0.0176±0.0034	0.0106	2.99σ	0.0059 ±0.0009	0.0045	1.48σ
Δ^{++}	0.124 ±0.065	0.094	0.46σ	0.094 ±0.094	0.049	0.48σ	0.040 ±0.010	0.019	2.06σ
$\Sigma^{*\pm}$	0.047 ±0.005	0.074	-4.86σ	0.0330±0.0094	0.0359	-0.30σ	0.0107 ±0.0020	0.0133	-1.26σ
Ξ^{*0}	0.0058±0.0011	0.0073	-1.25σ	0.0052±0.0040	0.0035	0.42σ	0.0015 ±0.0005	0.0013	0.40σ
Ω^-	0.0013±0.0003	0.0006	2.19σ	0.0053±0.0032	0.0003	1.56σ	0.00072±0.00038	0.00010	1.62σ

Table 3
UCLA predictions for the baryons at 10 GeV, 29 GeV and 91 GeV are compared to experiments.
† The decay table uncertainties are incorporated into the calculation of the number of standard deviations between the data and predictions, the column labeled *'STD'*. (See text.)

data well enough that they won't create any biases in the meson studies, and (3) to point the way toward the kind of data needed to really understand baryon production.

We find that indeed this approach works rather well. Thus our baryon modeling, though clearly not yet as fundamental as for mesons, provides a very good platform for further developing our understanding of baryon formation on a fundamental level as significantly higher quality data becomes available.

Our baryon multiplicity comparisons are summarized in Table 3 and Figs.17 and 18, paralleling Table 2 and Figs.11 and 12 for light-quark mesons. The decay table uncertainties presumed are: ±3% for protons and lambdas; ±5% for $\Sigma^{\pm}$, Σ^0, Ξ^-, Δ^{++} and $\Sigma^{*\pm}$; and ±8% for Ξ^{*0} and Ω^-. Fig.19~20 display various single baryon distributions. Fig.21 displays the baryon-antibaryon rapidity correlation for $\Lambda\bar{\Lambda}$ pairs. Table 4 displays baryon-antibaryon, baryon-baryon, baryon-meson, and meson-meson correlation rates.

The rates vary from $\approx$ 1.0 for protons at 91 GeV to $\approx$ .001 for Ω^- at 10 GeV. Generally, the predictions follow the data fairly well. However, we seem systematically to *underpredict* the rates for Ξ^-'s and Ω^-'s and possibly protons and to *overpredict* the rates for $\Sigma^{*\pm}$. The overall $\chi^2/d.o.f$ is $87.4/22 = 3.97$,

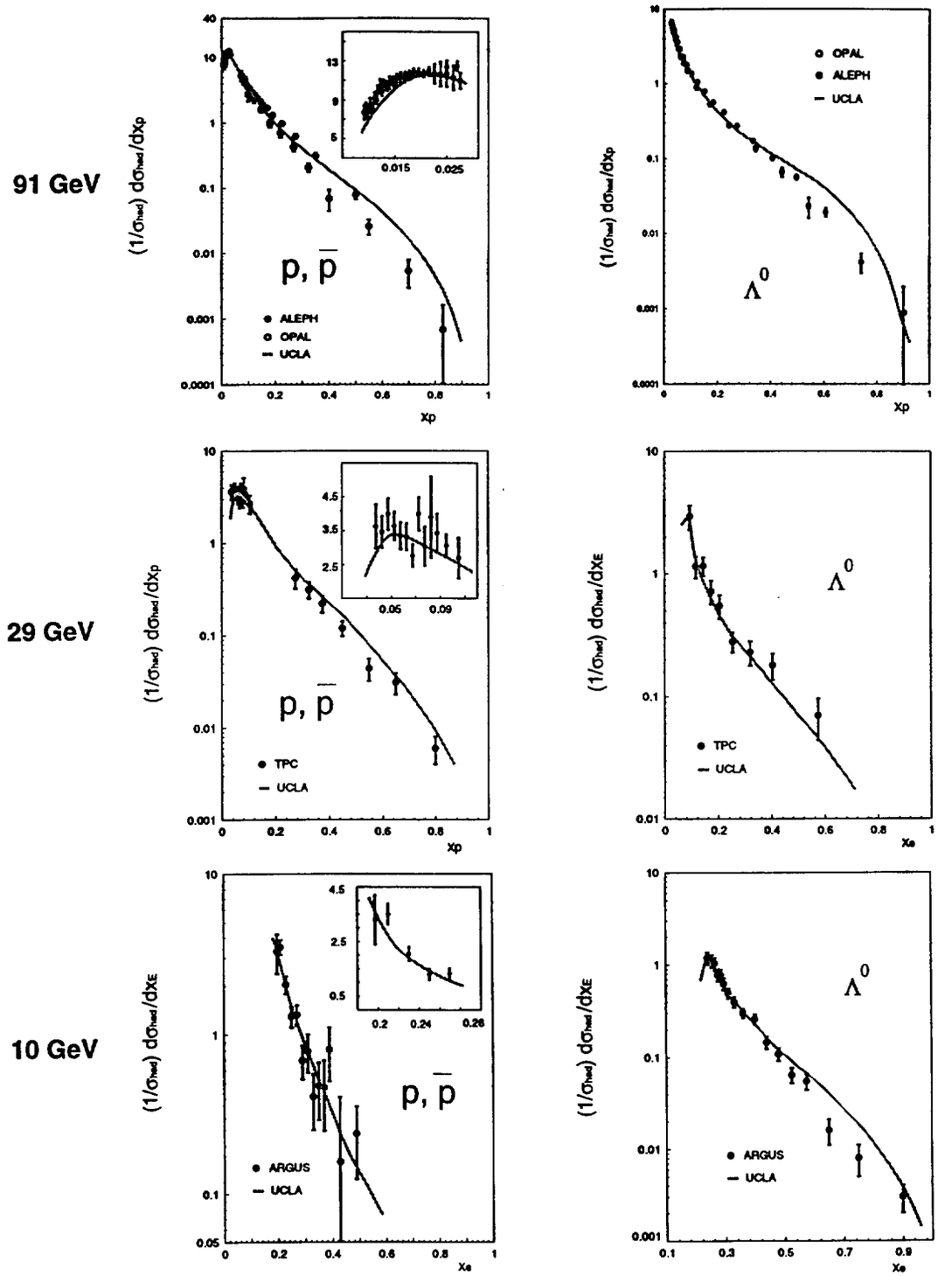

Fig. 19. UCLA predictions for protons and Λ baryons are compared to experiments at $E_{CM} = 10,\ 29,\ and\ 91\,GeV$.

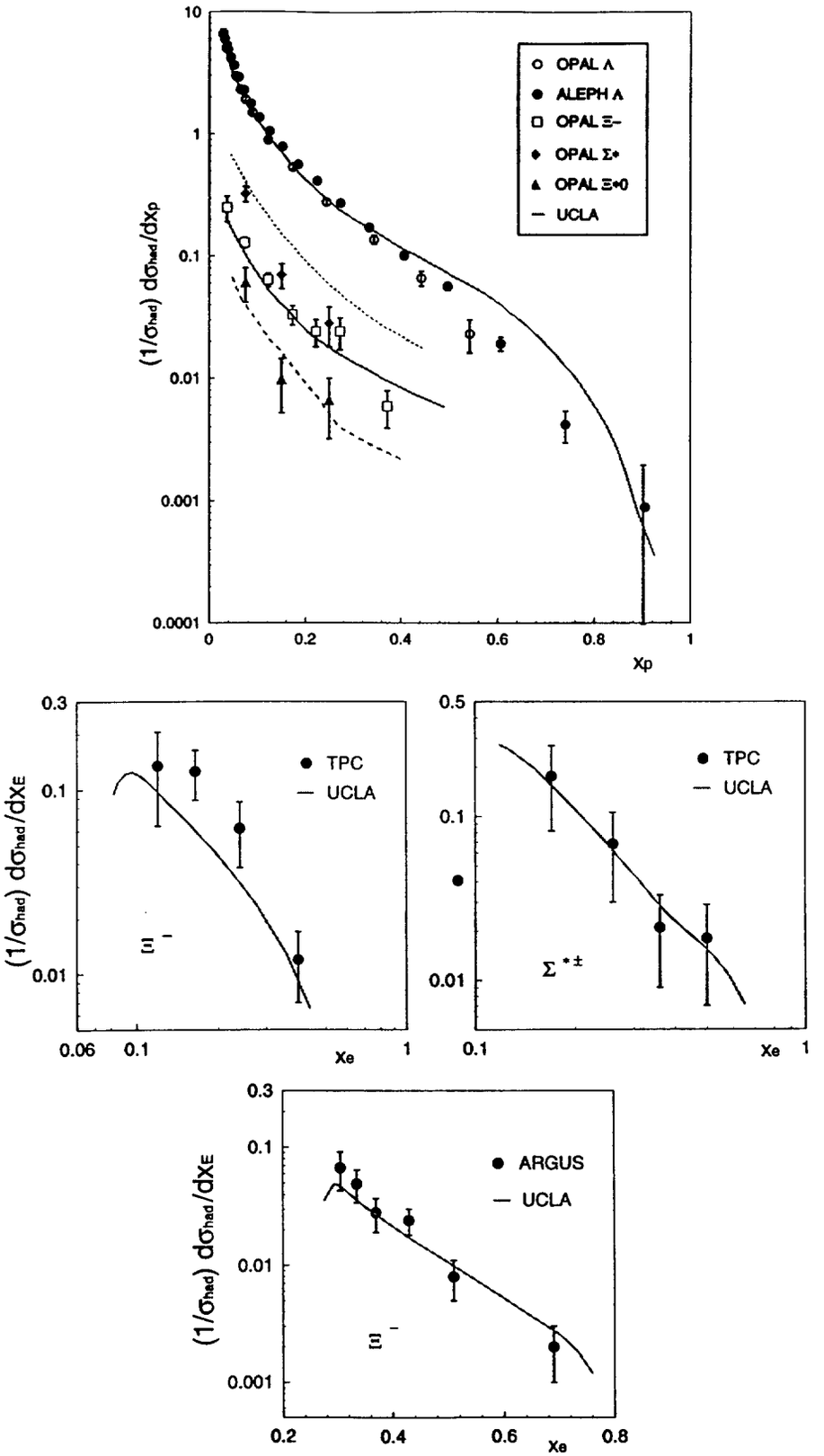

Fig. 20. UCLA predictions for various strange baryons are compared to experiments at $E_{CM} = 10,\ 29,\ and\ 91\,GeV$.

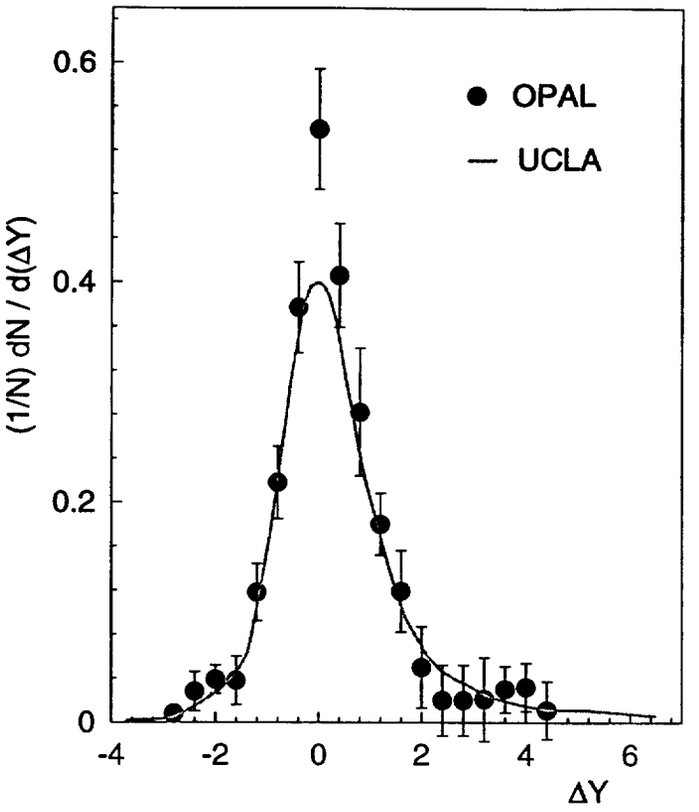

Fig. 21. UCLA prediction for the rapidity correlation of Λ and $\bar{\Lambda}$ baryon pair is compared to experiments at $E_{CM} = 91\,GeV$.

	DATA	UCLA
$\Lambda\bar{\Lambda}/evt$	0.089 $\pm$0.007	0.114
$\{(\Xi^-\bar{\Lambda} - \Xi^-\Lambda) + (\bar{\Xi}^+\Lambda - \bar{\Xi}^+\bar{\Lambda})\}/evt$	0.0096 $\pm$0.0023	0.0146
$\{\Xi^-\bar{\Xi}^+ - (\Xi^-\Xi^- + \bar{\Xi}^+\bar{\Xi}^+)\}/evt$	0.00038$\pm$0.00067	0.00128
$(\Lambda\Lambda + \bar{\Lambda}\bar{\Lambda})\,/evt$	0.0249 $\pm$0.0022	0.0272
$(\Lambda k_s^0 + \bar{\Lambda} k_s^0)\,/evt$	0.403 $\pm$0.029	0.394
$k_s^0 k_s^0/evt$	0.593 $\pm$0.036	0.628

Table 4
Baryon-antibaryon, baryon-baryon, baryon-meson and meson-meson correlation rates at Ecm=91 Gev.

or an average of $\sim$ 2.0 standard deviations. The comparisons averaged over all three energies have a $\chi^2/d.o.f$ of 59.99/8 = 7.50, or an average of $\sim$ 2.7 standard deviations.

Other intriguing deviations in baryon production include: (a) As displayed in Fig.19 and 20, we consistently *overpredict* the baryon production above $x_p \simeq 0.5$. (This phenomenon leads to the *'leading baryon suppression'* factor recently introduced into JETSET.) (b) Our predicted $\Lambda - \bar{\Lambda}$ rapidity correlation in Figure 21 is not sharp enough and too broad (e.g., suggesting somewhat too much popcorn in our Monte Carlo). However, (c) our predictions of the absolute baryon-antibaryon correlation rates (see Table 4) are too high, suggesting too little popcorn (whereas we note that our predicted baryon-baryon, baryon-meson, and meson-meson correlation rates agree adequately with the data).

To bring the understanding of baryon formation to the same, apparently fundamental, level as our current meson formation understanding will require $\approx 10^8$ e^+e^- annihilation events with good, relatively unbiased, efficiency and particle identification in order to obtain three-body baryon-meson-antibaryon rapidity correlations. This appears to be achievable only with the continuum events from one of the high luminosity B factories currently being built.

7 Crossing Symmetry with Deep Inelastic Scattering

The idea of crossing symmetry establishes an interesting relationship between hadron production in electron-positron annihilations and deep inelastic electron hadron scattering. This is illustrated in Fig.22 (a)-(f). If the diagrams are viewed with time flowing upward, then they represent electron-hadron scattering (DIS). If they are viewed with time flowing from left to right, then they represent electron-positron annihilation into hadrons (ANNIH). Fig.22 (a) (DIS) represents either elastic scattering or (ANNIH) baryon-antibaryon exclusive production. Fig.22 (b) (DIS) shows a quark within a meson struck by the virtual photon from the electron giving rise to a leading meson. Fig.22 (b) (ANNIH) represents three meson production. Fig.22 (c) (DIS) shows a baryon-antibaryon pair produced from a meson. Fig.22 (c) (ANNIH) represents production of a baryon-antibaryon pair and a meson. Fig.22 (d) (DIS) shows a leading meson and a baryon produced from a baryon. Fig.22 (d) (ANNIH) represents production of a baryon-antibaryon pair and a meson as in Fig.22 (c). Fig.22 (e) (DIS) shows a leading baryon with a non-leading meson produced from a baryon. Fig.22 (e) (ANNIH) represents baryon-antibaryon production with one popcorn meson between them. Fig.22 (f), the most complicated diagram shown, in DIS shows a leading baryon followed by two mesons. Fig.22 (f) (ANNIH) represents baryon-two popcorn mesons-antibaryon production.

In DIS, considerations on a simple parton level of different helicities of the incoming hadron in the infinite momentum frame, combined with the number

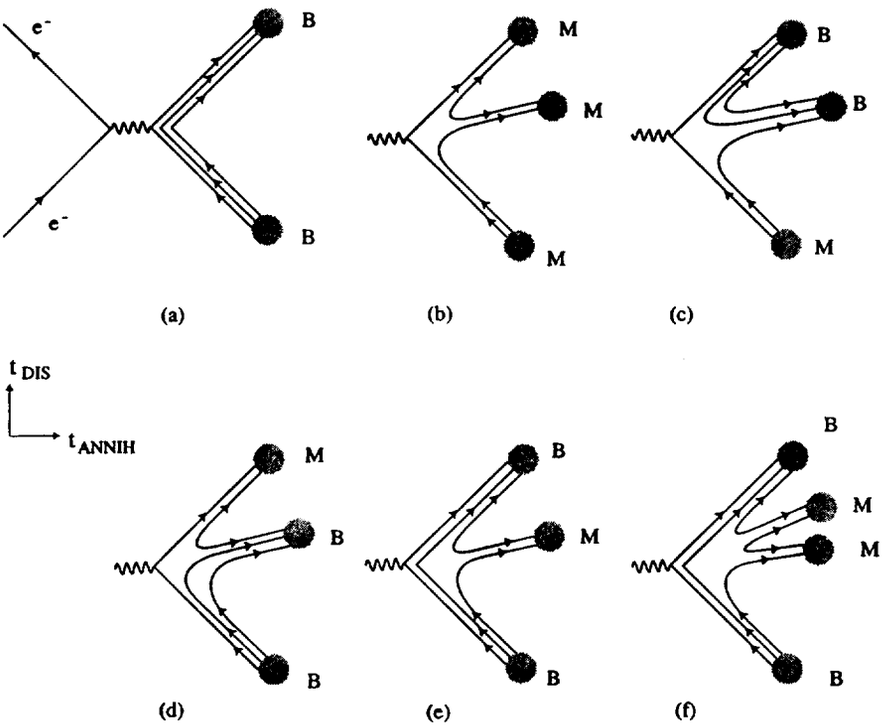

Fig. 22. Crossing symmetry between Deep Inelastic Scattering of e^- from a hadron and $e^+e^- \rightarrow hadrons$. The arrows on quark lines are for Deep Inelastic Scattering.

of spectator quarks in the incoming hadron, lead to distributions at high x of

$$(1-x)^{\alpha} \tag{15}$$

where x is the scaling variable

$$x = \frac{(E+P_z)_q}{(E+P_z)_h} \tag{16}$$

where h stands for the incoming hadron, q stands for the struck quark within the incoming hadron, and

$$\alpha = 2n_s - 1 + 2|\lambda_h - \lambda_q| \tag{17}$$

where λ_h and λ_q are the helicities of the incoming hadron and struck quark in the infinite-momentum frame respectively and n_s is the number of spectator (non-struck) quarks in the incoming hadron. This rule says that it is harder to force a struck quark to have all the parent hadron's momentum ($x \rightarrow 1$) when there are more spectator quarks and also when the struck quark has a different helicity from its parent hadron (helicity conservation). The specific exponent is a consequence of QCD[14,15].

Crossing symmetry between DIS and annihilation diagrams implies that for annihilation diagrams the same values of α will hold in distributions of

$$z = \frac{(E + P_z)_h}{(E + P_z)_q}$$

i.e., $(1 - z)^\alpha$, as $z \to 1$.

Thus α would have the following values:

(1) For a probed *proton* (DIS) or leading proton (ANNIH) $\alpha = 3$ (Fig.22 (d),(e) and (f))
(2) For a probed Δ^{++} (DIS) or leading Δ^{++} (ANNIH) $\alpha = 5$ (Fig.22 (d), (e) and (f))
(3) For any probed meson (DIS) or leading meson (ANNIH) $\alpha = 2$ (Fig.22 (b) and (c))

Note that QCD corrections would generally raise these values slightly and inclusion of *'higher twist'* terms would tend to lower the values of α[16].

Comparisons with DIS data confirm that these predicted values of α agree well[17,18] for each flavor of leading particle.

It is interesting and gratifying to note that our best-fit value for *'a'* of 1.65 is close to the naive parton-level prediction of 2.0 for leading meson production.

Since our present focus is on meson production, where all meson production would have the same value of α (or in our notation *'a'*) independent of whether the meson's spin is 0 or 1), for the time-being, we have simply used the same common value of *'a'* for both meson and baryon production, leaving for later studies whether interesting information can be learned by letting *'a'* values for baryons be greater than those for mesons. It is interesting to note that a higher value of *'a'* for leading baryons would qualitatively go in the direction to lower our predicted rates for high momentum baryons, the direction needed for better agreement with data. It is also interesting to note that eq(12) - g(S) $\propto$ S^a – expresses the idea that, as S increases, then g(S), the number of different diagrams allowed, combined with an exponential area suppression, increases at a rate comparable with S^2. Because of the many degrees of freedom associated with popcorn production, one might expect g(S) for baryon production to rise at a rate greater than for meson production.

8 Connections with QCD

When one has a successful phenomenology, there are two possible approaches toward deeper understanding: (1) Working *'backwards'* from the phenomenology with as few assumptions as possible to see what kind of a theory might justify the phenomenology, or (2) Hypothesizing a theory and then working *'forward'* to see if (or under what conditions) it leads to the phenomenology. Since QCD exists as a very strong candidate for the theory underlying hadronization, we will work primarily in the second mode to see to what extent QCD can justify our *Event Weight Function* for hadronization. [We do note, however, that virtually any strong-coupled lattice theory with a non-zero lattice spacing will lead to a space-time area law. This even includes QED, though the existence of QED's phase transition allows it to become a non-confining theory in the continuum limit.]

There are two main questions to try to answer from QCD:

- To justify the structure of the *Event Weight Function*: i.e., the space-time area law, the limited transverse phase-space, the possible vertex suppression factors, and the Clebsch-Gordon and spatial knitting factors.

- To estimate the sizes of the vertex suppression factors and knitting factors.

Ultimately, one would then hope to extend the treatment to include understanding of P_T, of baryon formation, etc.

We will discuss three tools to develop QCD related topics in the hadronization area:

1) Relativistic string theory
2) Strong coupling expansion of lattice QCD
3) Approximate Minkowskian calculations using an effective QCD lagrangian

Taken together, these approaches allow a picture to emerge which (with room for many better calculations to be done) leads from QCD to the *Event Weight Function* structure as a target and suggests that ultimately estimates of parameter sizes may be made from a QCD basis.

Lattice QCD work[9] within a Euclidean space-time metric indicates that, as a quark and antiquark separate, the color-field begins to collapse into a narrow tube-like structure – approximately a *'string'*. There is some very preliminary lattice-work indication[19] that, if virtual quark-antiquark pair production is allowed from the colorfield, then the energy density near the center of the string begins to drop – that is, the string begins to break. This, of course, is

also bolstered by the very strong intuition that as a string stretches, a string broken by a quark-antiquark pair represents a lower energy state and therefore that *the string prefers to break*. Also, there is semi-experimental corroborating evidence (see Appendix F) from the distribution of vertices in the Lundian modeling structure that the string breaks most likely when it is elongated $\approx 2 \sim 5fm$ in its center of mass system – that is just as or after the string begins to form.

8.1 Relativistic string theory

The quest to find the connection with QCD begins with the exploration for justification of the area law from a relativistic string model. Because of the striking similarity to *Wilson's lattice theory*, numerous attempts have been made to connect string theory to QCD. Indeed in 1+1-dimensional space-time, the connection between the string model and lattice QCD was made precise[20]. As will be mentioned later again, this is the rationale to expect the outcome of string theory in 1+3 dimension to hold approximately in QCD.

The classical string action, for any motion of a string, is given as

$$S = \kappa\Sigma \tag{18}$$

where Σ is an area of world sheet swept out by the string and κ is the string tension. In 1+1 dimensions, with an assumption that the probability of cutting a length of string Δx in time Δt by creating a pair of massless quarks is a universal constant $\mathcal{P}$, X. Artru and M.G. Bowler[21] obtained an area law dependence, namely the probability of having a particular string configuration is

$$e^{-\mathcal{P}\Sigma}$$

where Σ is the space-time area containing no cuts. Recognizing that e^{iS} represents a quantum mechanical amplitude for the propagation and decay of a state and combining this with eq(18), they obtained the expression for the amplitude

$$\mathcal{A}(\Sigma) \propto e^{i\kappa\Sigma}\, e^{-\frac{\mathcal{P}}{2}\Sigma} \tag{19}$$

where the string tension in the action is interpreted as a complex number

$$\xi \equiv \kappa + i\frac{\mathcal{P}}{2}$$

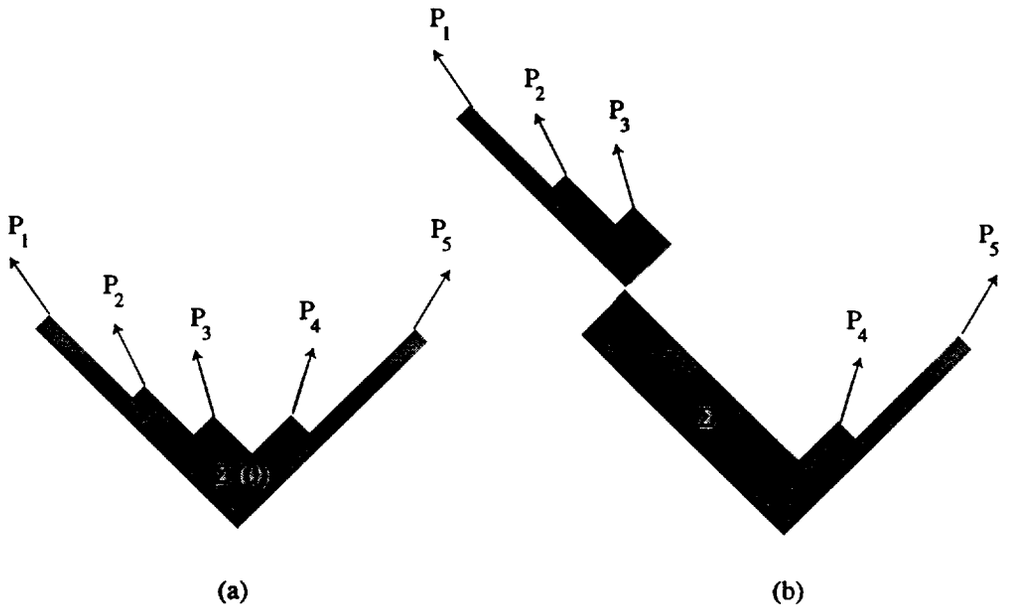

Fig. 23. (a) and (b) produce the same final state hadrons. When summed over all the histories leading to the same final state, (b) can be ignored since it involves much more area than (a).

Armed with this, they quantized the system and obtained an expression for an amplitude for n final state hadrons by a Feynman path integral approach, i.e., adding up all the possible histories of the string configuration:

$$\mathcal{A} \propto \sum_{\text{histories}} e^{i\xi\Sigma} \simeq e^{i\xi\Sigma(0)} \tag{20}$$

where in the last step, they argued by a stationary phase approximation that only the classical configurations (with space-time areas $\Sigma(0)$) give an important contribution and, further, among the classical configurations, that configurations such as Fig.23(a) are dominant in the summation compared to ones like Fig.23(b). In order to construct a probability, one needs to square the amplitude, which gives a dependence of $e^{-\mathcal{P}\Sigma(0)}$ for the probability, and integrate over the phase-space. Thus, one can motivate an area law behavior from relativistic string modeling.

8.2 Strong coupling expansion of lattice QCD

Since string theory is closely connected to lattice QCD as mentioned before, we expect that a similar structure would be observed in lattice QCD. Even if one can't expect truly quantitative results from this analytic tool due to the difficulty of extracting the behavior in the continuum limit, the strong coupling

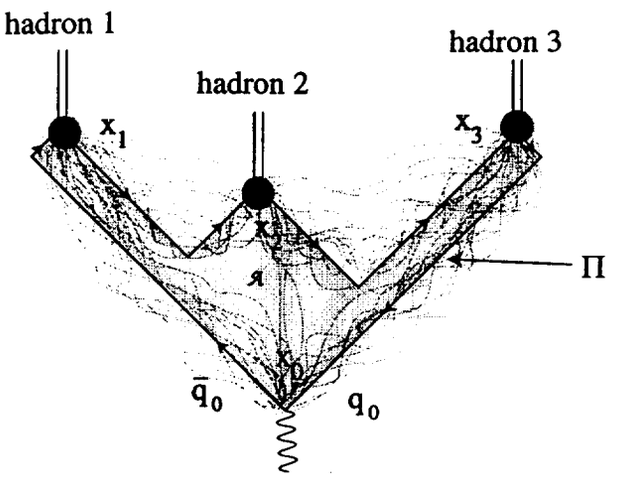

Fig. 24. The virtual photon created by the e^+e^- annihilation decays into the initial $q\bar{q}$ at x_0. Three hadrons are produced at x_1, x_2, x_3 where the solid straight lines Π depict the classical trajectories of massless fermions (quark or anti-quark) whereas gray lines depict all possible loops connecting the 4 points x_0, x_1, x_2, x_3.

expansion can provide some insights about the physics typical to the strong coupling domain which otherwise would not be possible. For this purpose, we sketch (below) the relevant results of lattice QCD without extensive derivation or justification but with appropriate references, in order to demonstrate what *lattice QCD* can suggest.

To the lowest order in QED, the cross section $e^+e^- \to f$, where f is a final state of hadrons with particular momenta and flavors can be written as

$$\sigma_{e^+e^-\to f} = \frac{8\pi^2\alpha^2}{S^3}(2\pi)^2\delta\left(P_1 + P_2 - P_f\right) l_{\mu\nu}\langle f|J^\mu(0)|0\rangle\langle f|J^\nu(0)|0\rangle^* \quad (21)$$

where

$$l_{\mu\nu} = \frac{1}{4}\sum_{\varepsilon_1,\varepsilon_2}\{\bar{v}\left(P_1,\varepsilon_1\right)\gamma_\mu u\left(P_2,\varepsilon_2\right)\}\{\bar{v}\left(P_1,\varepsilon_1\right)\gamma_\nu u\left(P_2,\varepsilon_2\right)\}^*$$

is the lepton current of an electron and

$$J^\mu \equiv \sum_q Q_q : \bar{\psi}_q\gamma^\mu\psi_q :$$

is an electromagnetic current. Q_q, ψ_q, and $\bar{\psi}_q$ are the charge of the quark and the quark and antiquark fields respectively. The matrix element $\langle f|J^\mu(0)|0\rangle$ is related to an *n-point Green's function*. For example, as displayed in Fig.24, a

4-point function, with a loose notation, can be written as

$$\langle f|J^{\mu}(0)|0\rangle \sim \langle 0|T\bar{\psi}_0\psi_0\bar{\psi}_1\psi_1\bar{\psi}_2\psi_2\bar{\psi}_3\psi_3|0\rangle \sim G\left(x_0, x_1, x_2, x_3\right) \qquad (22)$$

where indices for the quark fields 1, 2, 3 indicate the production points of hadrons and 0 indicates the origin where the virtual photon couples to the current J^{μ}.

Since, as the initial quark and anti-quark recede from each other, we expect the coupling to increase, and also since the energy of the virtual quark pairs created in the color field are smaller than the potential between the initial quark and anti-quark (a *tunneling situation*), Euclidean lattice QCD with a strong coupling expansion is rather attractive in this situation. Due to its similarity to a solid state lattice system, the expectation value of an operator is defined as the average value of the operator weighted by the Boltzman factor e^{-S} (S is the action) in lattice QCD. That is

$$\langle\vartheta\rangle = \frac{1}{Z}\int \left(dUd\bar{\psi}d\psi\right)\vartheta(U,\bar{\psi},\psi)\,e^{-S(U,\bar{\psi},\psi)} \qquad (23)$$

where

$$Z \equiv \int \left(dUd\bar{\psi}d\psi\right) e^{-S(U,\bar{\psi},\psi)} \qquad (24)$$

where U is an element of a gauge group associated with each nearest neighbor pair of lattice sites (a *link variable*). In the quantum mechanical *Hilbert space*, this is the vacuum expectation value of the corresponding time-ordered operator.

In general, there are many different ways to construct QCD action on the lattice space-time; the *Wilson action* is[22]

$$S(U,\bar{\psi},\psi) = \frac{6}{g^2}\sum_{\square}\left(1-\frac{1}{3}Tr\left(U_{\square}+U_{\square}{}^{\dagger}\right)\right) + a^3\sum_n \bar{\psi}_n(4+ma)\psi_n$$
$$-\frac{a^3}{2}\sum_{n,\mu}\bar{\psi}_n\{(1+\gamma_\mu)\,U\,(n+\hat{\mu},-\mu)\,\psi_{n+\hat{\mu}} + (1-\gamma_\mu)\,U\,(n-\hat{\mu},\mu)\,\psi_{n-\hat{\mu}}\} \qquad (25)$$

where $U_{\square}$ is the product of links connecting four nearest sites (a *'plaquette'*), μ denotes the space-time index, a is the lattice spacing, and g is the bare coupling constant. One can simplify eq(25) into

$$S = \sum_{i,j}\bar{\psi}_i K_{ij}(U)\psi_j + S_G \qquad (26)$$

with the definition of the pure gluonic part of the action

$$S_G = \frac{6}{g^2} \sum_{\square} \left(1 - \frac{1}{3} Tr \left(U_{\square} + U_{\square}^{\dagger}\right)\right) \tag{27}$$

and combining the fermion self energy and interaction part of the action by defining the matrix

$$K_{ij} \equiv (8 + 2ma)\delta_{ij} - (1 + \hat{e}_{\mu}\gamma_{\mu})U_{ij} = \frac{1}{\kappa}(\delta_{ij} - \kappa M_{ij})$$

where

$$M_{ij} \equiv (1 + \hat{e}_{\mu}\gamma_{\mu})U_{ij}$$

and $\hat{e}_{\mu}$ is the unit 4-vector in the direction of the link and with the *hopping parameter*

$$\kappa = \frac{1}{8 + 2ma} \tag{28}$$

Upon introducing source terms $(\rho, \bar{\rho})$ and integrating out the fermion fields, eq(24) becomes

$$\begin{aligned} Z(\rho, \bar{\rho}) &= \int (dU)\ det\ K\ \exp\left(\sum_{ij} \bar{\rho}_i K_{ij}^{-1} \rho_j\right)\ e^{-S_G(U)} \\ &= \int (dU)\ \exp\left(\sum_{ij} \bar{\rho}_i K_{ij}^{-1} \rho_j\right)\ e^{-S_G(U)} \end{aligned} \tag{29}$$

where the *Quenched approximation* ($det\ K = 1$; that is, no closed internal quark loops) was used in the last step.

Then, the 4-point function eq(22) can be written using eq(29)

$$\begin{aligned} G(x_0, x_1, x_2, x_3) &= \frac{1}{Z} \int \left(dU d\bar{\psi} d\psi\right) T\left(\bar{\psi}_0 \psi_0 \bar{\psi}_1 \psi_1 \bar{\psi}_2 \psi_2 \bar{\psi}_3 \psi_3\right)\ e^{-S(\psi, \bar{\psi}, \rho, \bar{\rho}, U)} \\ &= \frac{1}{Z(\rho, \bar{\rho})} \frac{\partial Z(\rho, \bar{\rho})}{\partial \rho_0 \cdots \partial \rho_3 \partial \bar{\rho}_0 \cdots \partial \bar{\rho}_3}\bigg|_{\rho=0} \\ &= \int (dU) \left(K_{01}^{-1} \cdots K_{30}^{-1} + \text{permutations}\right) e^{-S_G} \end{aligned} \tag{30}$$

By an iteration, the inverse matrix K^{-1} identically becomes

$$K_{ij}^{-1} = \kappa\left(\delta_{ij} + K_{ik}^{-1} M_{kj}\right) = \kappa\left(\sum_{l=0}^{\infty} \kappa^l M^l\right)_{ij} \tag{31}$$

Thus, K^{-1} will include the product of $(1 \pm \gamma_\mu)\, U$. One, then, finds the important result that eq(30) becomes

$$\begin{aligned} G(x_0, x_1, x_2, x_3) &\propto \sum_C \kappa^m \int (dU)\; Tr\; (U \cdots U)_C \;\; \mathrm{e}^{-S_G} \\ &= \sum_C \kappa^m \; \langle P \;\; \mathrm{e}^{ig \oint_C dx^\mu A_\mu} \rangle_{gluon} \end{aligned} \tag{32}$$

where m is the perimeter p of the loop C in lattice units, A_μ is the gauge field, and P stands for *path ordered product*. The summation runs over all the loops connecting the 4 points. The quantity in brackets $\langle \cdots \rangle$ is the expectation value of the *Wilson Loop* over the *gluon field*.

The behavior of the *Wilson Loop* expectation value for two extreme values of coupling can be analytically evaluated.

When the coupling is strong, for any fixed size loop C

$$\langle P \;\; \mathrm{e}^{ig \oint_C dx^\mu A_\mu} \rangle_{gluon} = \int (dU)\, \mathrm{e}^{ig \oint_C dx^\mu A_\mu} \;\; \mathrm{e}^{-S_G} \tag{33}$$

can be expanded in a series in terms of $1/g^2$. Since the link variable U is a group element, the integration over U is a group integration and the contribution for the lowest order in $1/g^2$ is obtained by bringing down $U_\Box$'s (*plaquettes*) from S_G to fill the inside of the loop (the *strong coupling expansion*). This results in an area dependence

$$\langle P \;\; \mathrm{e}^{ig \oint_C dx^\mu A_\mu} \rangle_{gluon} = \left(\frac{1}{g^2}\right)^{\mathcal{A}/a^2} \tag{34}$$

where $\mathcal{A}$ is the minimal area defined by the loop C and a is the lattice spacing. Any terms with bigger area than $\mathcal{A}$ are higher order in $1/g^2$ and are thereby suppressed.

As a toy example, if the loop is a rectangular with the dimensions of R and T in space and time as in Fig.25, the static potential between q and $\bar{q}$ is related to the Wilson loop via

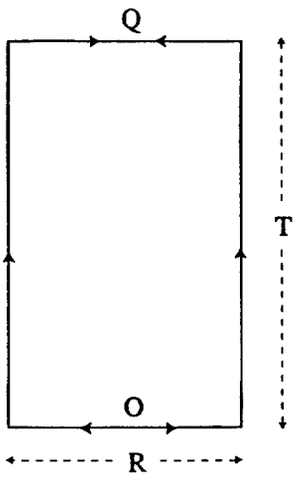

Fig. 25. The static potential can be related to the *Wilson loop* integration when the quark and anti-quark are infinitely heavy. $q\bar{q}$ are created at O and annihilated at Q after an elapsed time T.

$$\begin{aligned} V &= -\lim_{T\to\infty}\frac{1}{T}\log\langle P\ \mathrm{e}^{ig\oint_{\square}dx^{\mu}A_{\mu}}\rangle_{gluon} \\ &= -\lim_{T\to\infty}\frac{1}{T}\log\ \mathrm{e}^{-\kappa RT} \\ &= \kappa R \end{aligned} \tag{35}$$

So, when the coupling is strong, the *Wilson Loop* expectation value results in an area law (eq.(34)) and a linear potential (eq.(35)).

When the coupling is weak, the expectation value of the rectangular *Wilson Loop* with the dimensions of R and T can be calculated in perturbation theory in terms of lattice spacing[23,24]

$$\langle P\ \mathrm{e}^{ig\oint dx^{\mu}A_{\mu}}\rangle_{gluon} = \exp\left(-\frac{CT}{4\pi R}\left(g^2+\frac{22}{16\pi^2}g^4\log\frac{R}{a}\right)\right) \tag{36}$$

up to the order of g^4 where C is a group theoretical factor. The static potential between $q\bar{q}$ in Fig.25 can be extracted again using the first part of eq(35)

$$\begin{aligned} V &= -\lim_{T\to\infty}\frac{1}{T}\log\langle P\ \mathrm{e}^{ig\oint_{\square}dx^{\mu}A_{\mu}}\rangle_{gluon} \\ &= \frac{CT}{4\pi R}\left(g^2+\frac{22}{16\pi^2}g^4\log\frac{R}{a}\right) \end{aligned} \tag{37}$$

which is just a *Coulomb* potential with a higher order correction.

In order to maintain the relevant physics to be the same in a given physical volume while varying the lattice spacing which is an artificial quantity, the

lattice spacing a and the bare coupling g must be related via a *renormalization equation*[6,25]. For a small lattice spacing, the relation is

$$g^2(a) = -\frac{16\pi^2}{\left(11 - \frac{2}{3}N_f\right)\log\ \Lambda^2 a^2} \tag{38}$$

where Λ is a *renormalization constant.* Thus, the *continuum limit* is realized in the weak coupling regime. Eq(38) is not much different from the expression for the *running coupling constant* obtained in perturbative QCD, since a *lattice spacing* is another form of regularization. Λ in eq(38) is expected to be different from that of perturbative QCD, since different renormalization schemes will result in different renormalization constants in general.

Now, when the coupling gets weak (and therefore the lattice spacing gets small), the perimeter dependence still persists, in the form of $e^{-\mu P/a}$, since it represents the dependence of the fermion's internal energy while (as we have seen above) the area dependence collapses to give *Coulomb's law.* So, for weak coupling (the early perturbative region) the exponent diverges as $a \to 0$ and dominates the Green's function in this limit. The energy of the initial $q\bar{q}$ is so large that their coupling to gluons can be considered to be small. Thus this perimeter dominance overwhelmly chooses the light-cone as its trajectory in order to minimize the perimeter. Thus, this eliminates all other terms in eq(32) except a term with a loop Π which goes through the light-cone as in Fig.24, i.e.,

$$\begin{aligned} G(x_0, x_1, x_2, x_3) &\propto \sum_C \kappa^m \int (dU)\ Tr\ (U \cdots U)_C\ e^{-S_G} \\ &\simeq \kappa^m\ \langle P\ e^{ig\oint_\Pi dx^\mu A_\mu} \rangle_{gluon} \end{aligned} \tag{39}$$

Next, once the initial $q\bar{q}$ are separated far away from each other defining a *loop* Π, the coupling rapidly becomes strong, leading toward the hadronization process. The expectation value of the Wilson Loop over the gluon field in eq(39) should be evaluated considering that the coupling is a mixture of weak (near the edge of the primary $q\bar{q}$) and strong (in the middle) over the configuration Π in Fig.24. But the expectation value of the Wilson loop over the gluon field evaluated over the weak coupling region is essentially *common* to all events with different hadronic final states; hence the expectation value over the gluon field in eq(39) can be evaluated as if the coupling is strong in all regions of configuration Π in Fig.24 using the *strong coupling expansion* explained above. [Note that the expectation value of the Wilson loop evaluated over the weak coupling region can be considered as a *weak coupling correction* to the expectation value of the Wilson loop evaluated using strong coupling throughout the configuration Π. Further, since this *correction* factor is essentially *common*

to all hadronic final states (in 1+1 dimensions, it is exact), it therefore cancels in comparing the *relative* weights of the *Event Weight Function* for different final states or when using the *fragmentation function* eq(13).]

This yields an area dependence (from eq(34))

$$\left(g^2\right)^{-\mathcal{A}/a^2}$$

Thus, finally, one finds the important result in Euclidean space-time with lattice spacing a:

$$G\left(x_0, x_1, x_2, x_3\right) = \kappa^{p/a}\left(g^2\right)^{-\mathcal{A}/a^2} \tag{40}$$

where $\mathcal{A}$ is the minimal area enclosed by the loop Π, p is its perimeter, and a is lattice spacing.

The above procedure is, in fact, a dual expansion in terms of $1/(4+ma)$ (a *hopping parameter*) which gives a multiplication of successive link variables (the perimeter dependence) and a coupling constant g which gives a rule for tiling the surface with *plaquettes* (the area dependence). So, one can see there is always a competition between area dependence and perimeter dependence. One may compare the situation to making a *bubble ring* which is made by connecting the given 4-points (multiplication of the link variable along the classical quark paths) and then filling the bubble ring with the bubble which will produce its minimal surface determined by the bubble ring (gauge field integration or tiling with plaquettes).

This suggested structure not only supports the *Event Weight Function*, but also suggests an interesting possibility concerning the baryon production mechanism. The situation in Fig.26(b) depicts a *popcorn* mechanism whereas the situation in Fig.26(a) involves no *popcorn*. There have been numerous models to describe the popcorn mechanism[26]. Since three quark-antiquark pairs created out of the color-field are necessary in the situation in Fig.26(b) and the first pair (which has a different color from the initial quark and antiquark pair) has to *live long enough* to have two additional quark-antiquark pairs created in order to make the color-singlet baryon, meson, and anti-baryon, it has been suggested that diagrams such as Fig.26(b) will be suppressed via a *Heisenberg uncertainty* type of argument.

However, the perimeter dependence (above) of lattice QCD suggests Fig.26(b) is suppressed by having an additional perimeter distance (linear in mass of the popcorn meson) compared to a non-popcorn diagram in Fig.26(a). This seems to be a more fundamental and natural way to describe the suppression of the popcorn mechanism than the above Heisenberg type argument.

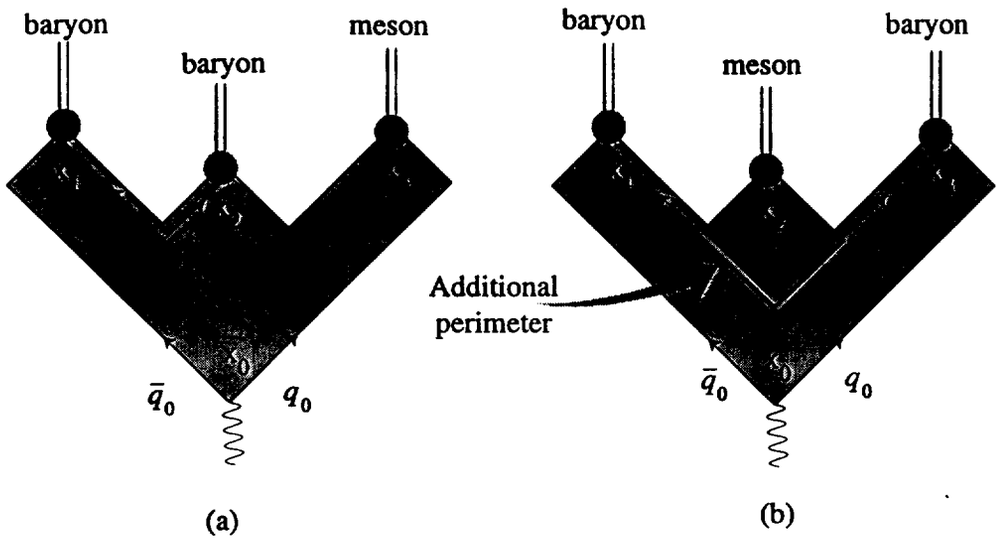

Fig. 26. Baryon, antibaryon and a meson are produced in two different situations. (a) depicts a situation where baryon and antibaryon are created adjacent while (b) depicts a situation where a meson is created between baryon and antibaryon, thus diluting the baryon-antibaryon correlation.

In summary, the application of Euclidean Lattice QCD to the high energy e^+e^- annihilation into hadrons, which is a unique situation where the relevant coupling smoothly varies from the very weak to the very strong: (a) gives an *area law* for the strong coupled region; (b) gives a *perimeter law* for the whole diagram, which, for massless quarks, leads to the dominant path being simply the light-cone trajectories; (c) suggests a popcorn suppression $\exp(-\eta \cdot m_{\text{popcorn-meson}})$ in baryon-antibaryon production through the perimeter law; and (d) provides a beginning point for understanding the relation between the early weak-coupled region and the later strong-coupled region in a consistent manner. However, to be useful, one must assume that the above phenomena extrapolate to the *continuum* limit ($a \to 0$) and into Minkowskian space-time.

8.3 Approximate Minkowskian calculation using effective QCD lagrangians – the worldline approach

The fermionic part of the QCD Lagrangian causes complications in calculations due to its anti-commuting nature. Among the recent trends[27] to avoid such difficulties is the technique of calculating the effective Lagrangian by treating a second quantized field theoretic object as a first quantized object (a world-line formalism). Typically this transcription results in a coordinate integration instead of a field and simplifies the Feynman path integration significantly. Since this effective Lagrangian (presumably) has a coupling of the fermion to the background gauge field and to the pseudo-scalar and vector

meson fields, one can, in principle, calculate an *n-point Green's function* at least for mesons. A possible recipe to do this may be first to get rid of the coordinate dependence (in a Feynman path integral) by integrating out the fermion coordinates along the classical quark paths (giving a *perimeter dependence*) using the couplings of the fermion (quark) to the scalar mesons or vector mesons. (Note; this will determine the size of the *knitting factor* discussed previously.) Then, the background gauge field integration will look just like the Wilson loop integration over the loop determined by the classical paths of the quarks

$$\langle e^{ig\oint dx^\mu A_\mu(x)} \rangle \tag{41}$$

where A_μ is a gauge field and the brackets $\langle\ \rangle$ means the average over the gauge field. When the high energy initial quark and anti-quark are separated by a large distance creating a large loop, then eq(41) is a very familiar and well known quantity which gives an area dependence for a large loop in *Lattice Gauge Theory*. By an analytic continuation from Euclidean space to Minkowski space, the lattice QCD result can be borrowed appropriately.

Thus, this sort of approach provides the prospect of estimating the sizes of the *spatial knitting factors* (and ultimately possibly the suppression factors for producing a virtual $q\bar{q}$ pairs from the colorfield, if any).

8.4 Summary of relations to QCD

Common to all the previous discussions are two results: the Green's function has (i) a perimeter dependence due to the fermion (primary $q\bar{q}$) self energy and (ii) an area dependence due to the gluon self interaction inside the boundary defined by the primary $q\bar{q}$. Also, as was pointed out, the similarity between the results of the classical string picture and Euclidean lattice QCD is fundamentally intriguing.

Overall, using these QCD-based techniques with the UCLA *Event Weight Function* as a *target* seems to open up many possibilities for calculations leading toward understanding the effects of QCD in the *hadronization process*.

9 Summary and Future Work

The hadronization process is a very interesting challenge from a QCD viewpoint in that (a) it is a fundamental QCD process, (b) it can be studied experimentally extensively in a detailed clean fashion in e^+e^- interactions and with

particularly simple fundamental probes in the form of flavored meson rates and distributions, and (c) it is a transition, as the initial quark and antiquark rapidly separate, from an original high-virtuality state where perturbative calculations can be performed to a very soft low-virtuality non-perturbative regime, traditionally the domain of lattice work and strong-coupling expansion calculations.

We have shown and discussed the steps in an emerging conceptual and calculational path from QCD to successful predictions of e^+e^- annihilation rates and distributions into hadrons, the simplest arena in which to study quark-colorfield behavior. Central to this path is construction of an *Event Weight Function* which, for our stringent UCLA assumptions, depends only on a QCD-motivated space-time area law, approximate longitudinal phasespace, and factors to knit quarks into hadronic wave functions (Clebsch-Gordon coefficients for flavor and spin, and a universal *'knitting'* factor for spatial wave functions).

Our approach is particularly successful in predicting data on light-quark meson production, thereby contributing to our understanding of this simplest manifestation of colorfield behavior. It also forms a foundation for further understanding of more sophisticated colorfield behavior – e.g., baryon formation, P_T effects, spin-spin correlations, etc – as larger samples of more detailed data become available in the future.

The *Event Weight Function* – a simple phenomenological model – also performs the valuable role of a *'target'* for physicists interested in various QCD theoretic approaches to hadronization – e.g., Euclidean-space lattice work, relativistic string modeling, approximate Minkowski-space calculations using new emerging techniques such as world-line formalism – to use as possible verification of their work.

The following outlines in its simplest form this path from QCD to successful prediction of light-quark meson data comparisons.

(A) Perform a strong-coupled expansion in $1/g^2$ for QCD at large distances ($\geq 0.2 \sim 0.5\ fm$). On a Euclidean lattice with spacing 'a' this leads to a space-time area law $e^{-b'\mathcal{A}}$ as a factor to be included in the probability of a particular event (i.e., a particular set of final state hadrons) occurring.

(B) Presume the spacetime area law holds (i) for the entire space-time area of the event (the correction due to the weak-coupled area is essentially the same for all hadronic final states and cancels when building the fragmenation function), (ii) in the real world with a Minkowskiian metric, and (iii) for the continuum lattice limit $a \to 0$. [The fact that our modeling works so well provides support for these assumptions.]

(C) Construct an *Event Weight Function* incorporating this space-time area law. Also include kinematics, approximate longitudinal phasespace, a uni-

versal spatial knitting factor, and Clebsch-Gordon coefficients. [No suppression of virtual $u\bar{u}$, $d\bar{d}$, or $s\bar{s}$ pairs created in the colorfield; all spatial knitting factors are the same.]

(D) Derive a Fragmentation Function for outside-in one-hadron-at-a-time iterative implementation from the *Event Weight Function*. This essentially yields the Lund Symmetric Fragmentation Function with
- a factor of $\exp(-bm_h^2/z)$, from the *Event Weight Function* area law, which provides a suppression in the formation of heavy hadrons arising simply from their mass.
- a universal normalization for all hadrons of $NC^2/(4\pi)^2$ where N is the universal spatial knitting factor and C^2 is the Clebsch-Gordon coefficient squared for flavor and spin.

(E) Use JETSET's recipes for parton showers and to allow the fragmentation function implementation to move past a gluon-induced kink in the colortube. Also, use JETSET's decay table to decay the hadrons produced directly from the colorstring into the daughter particles observed in the detectors.

(F) It simply works quite well for light-quark mesons. Using only the two parameters 'a' and 'b' natural to the model (with no ad hoc parameters), it predicts the light-quark meson rates and distributions at E_{CM} of 10, 29, and 91 GeV with no significant deviations. It works encouragingly well for baryon production and P_T effects.

Work to be done in the future includes:

(1) Accumulation of large flavor-identified data samples such that accurate two- and three-particle distributions can be studied in order to understand baryon formation, P_T effects, spin-spin correlations, etc. on the same level as the present understanding of meson formation. This will require $\approx 10^8$ events with good efficiency and particle identification, such as can be obtained from the continuum events of a high-luminosity B factory.

(2) More highly developed phenomenological Monte Carlo modeling, in particular of phenomena such as popcorn production and local P_T compensation, in order to help interpret the data on these phenomena. A simulation approach which allowed direct implementation of the *Event Weight Function* (rather than the intermediate step of deriving a fragmentation function) would be a significant step forward.

(3) Further phenomenological studies of heavy-quark hadron production and of orbitally excited states such as B^{**}, etc.

(4) Continued lattice work to understand the shape and possible decay of the colorfield between a quark and antiquark.

(5) As QCD calculational techniques continue to improve, attempts to derive the Event Weight Function structure (or modifications of it) and then to predict the parameter values within this structure, in particular (a)

the vertex suppression factors, which our UCLA model assumes are all approximately 1.0 for $u\bar{u}$, $d\bar{d}$, $s\bar{s}$ and 0.0 for $c\bar{c}$ and $b\bar{b}$, and (b) the knitting factors, which UCLA assumes are all approximately equal and for which probability unitarity of the *integrated/summed* fragmentation function leads to a value around $1/(75MeV)^{-2} \simeq (2.7fm)^2$.

(6) Attempts to calculate and/or understand, either from a QCD-basis or from other physical mechanisms, the values of the 'natural' constants 'a' and 'b'; e.g., using spin-and-spectator-quark counting arguments from deep inelastic crossing symmetry to estimate 'a' values for mesons and baryons.

(7) Attempt to develop the 'Initial-to-Final-State Global' approach (UCLA Stage III) described in Appendix B.2 in which the parton shower is treated as an unobserved intermediate state and an area law type of approach is applied to the entire transverse momentum (combining P_T from gluons and P_T from the finite colorfield width) of a set of specified final state hadrons.

For those interested in working with our model, the program and manual can be found at *www.physics.ucla.edu/~chuns*.

Acknowledgement

We are deeply indebted to members of the Lund group - Bo Andersson, Hans-Uno Bengtsson, Gösta Gustafson, Gunnar Ingleman, Torbjörn Sjöstrand - for many important and illuminating conversations in the development of this ansatz. We gratefully acknowledge stimulating and useful discussions with Zwi Bern, Siegfried Bethke, Dick Blankenbecler, Stan Brodsky, Phil Burrows, Mike Cornwall, Brent Corbin, Glen Cowan, Alessandro deAngelis, Eric D'Hoker, Tom Gottschalk, Werner Hofmann, J.K.Kim, Duncan Morris, Roberto Pecci, Ina Sarcevic, Terry Tomboulis, Douglas Toussaint and Brian Webber. We especially want to thank Rick Berg (who compiled the 'world average' data used at 10 GeV and 29 GeV), Sahak Khacheryan (who suggested the heavy quark modification leading to z_{eff}), James Yentang Oyang (who participated extensively in several phases of the work), and Hiroaki Yamamoto (who presented many illuminating challenges to the ansatz). This work was supported by the US Department of Energy, Division of High Energy Physics, under grant number DE-FG03-91ER40662.

A Comparison of Lund Approach and UCLA Approach

In order to simplify the description of the comparison of the Lund and UCLA

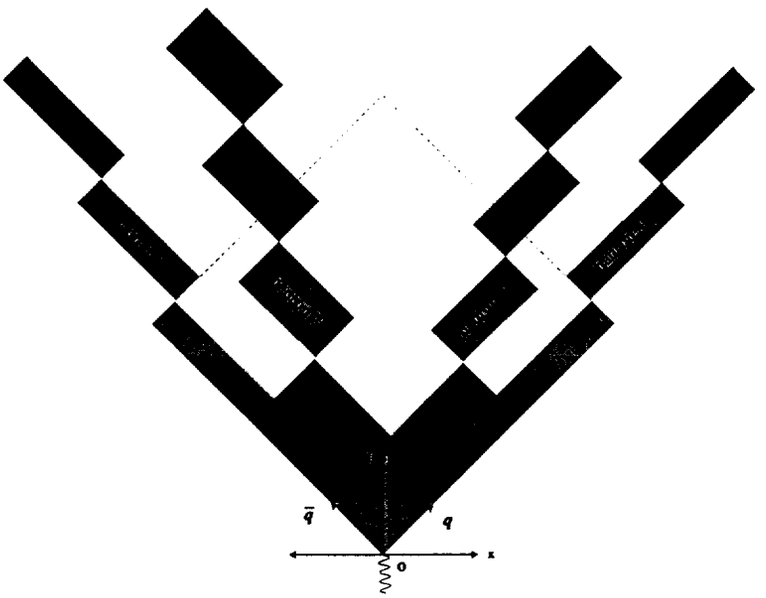

Fig. A.1. The primary $q\bar{q}$ created by the virtual photon at the origin stretch the string as they recede from each other. As the string stretches it breaks into smaller pieces (hadrons) and these smaller pieces propagate in space-time in a 'yo-yo' mode.

approaches to flavor and longitudinal momentum selection for hadrons, we restrict ourselves to a 1+1 dimension situation. Fig.A.1 displays an event for such a situation. In Appendix B.1.4, we compare the P_T techniques in 1+3 dimensions.

A.1 LUND Approach

The Lund group's approach is imbedded within an *outside-in* iterative implementation using a fragmentation function at each step to select the next hadron. Historically, they originally (≈1980) used a flat fragmentation function $f(z) = 1.0$ and employed suppression factors, following in the *Feyman-Field* tradition, of *'s/u'* to suppress strange virtual quark-antiquark production, *'vector/all'* to suppress vector meson production, and *'qq/q'* to suppress baryon production (followed by other baryon parameters to control 'extra strangeness suppression', spin 1 diquark suppression, 'popcorn' mesons, etc).

The physics rationale for *'s/u'*[3] was that constituent strange quarks ($\approx$ 150 MeV) were considerably more massive that up and down quarks ($\approx$ 2 $\sim$5 MeV) and therefore, via a WKB sort of argument, it was more difficult for the s and $\bar{s}$ of a virtual $q\bar{q}$ pair created from the colorfield to tunnel out through the potential energy barrier created by their mass in order to become 'free, on-the-mass-shell' particles. Any such actual calculation was very approximate and so

a parameter was introduced, whose value was found to be ≈ 0.3 from various data comparisons, to phenomenologically describe this situation. Thus, this provided a rationale for strange hadron production being suppressed relative to non-strange production.

The rationale for *'vector/all'*[3], with some plausible arguments, was that the spatial wave function for a vector meson was harder for a $q\bar{q}$ pair to couple into than was the wave function of a pseudoscalar meson. The *'vector/all'* parameter combined a suppression for this effect with the natural final state spin-counting which favored vector production by a factor of 3. Thus, if there was no 'spatial wave function suppression', *'vector/all'* would be 0.75. Comparisons with data yielded *'vector/all'* values of ≈ 0.45 for light quarks, ≈ 0.5 for strange quarks, and $\approx 0.60 \sim 0.65$ for charmed and bottom quarks. That is, 'spatial wave function suppressions factors' of ≈ 0.27, ≈ 0.33, and $\approx 0.53 \sim 0.62$ respectively.

The original rationale for *'qq/q'* was similar to that for *'s/u'*, namely that, to form a baryon, a diquark-antidiquark pair had to tunnel through a potential barrier, thus creating the need for a suppression factor. Experimental values of *'qq/q'* ranged from ≈ 0.06 at 10 GeV E_{CM} up to ≈ 0.10 at 91 GeV E_{CM}.

Operationally, there was a problem with many of the possible forms being used for fragmentation functions around 1980. Namely, if the *outside-in* iteration in the Monte Carlo implementation was always performed from the quark side, one would obtain statistically different results than if the implementation was always from the antiquark side. This, for example, led implementors to randomly select the side from which the next iteration would be performed.

In $\sim$ 1983, the Lund group discovered a very powerful theorem[2]: namely, that if *'Left-Right Symmetry'* (that is, the same statistical results from the quark and antiquark sides) were demanded, then the fragmentation function had to be of the form

$$f(z) = N\frac{(1-z)^a}{z}\ \mathrm{e}^{-bm_h^2/z}$$

Henceforth, they used this *'Lund Symmetric Fragmentation Function'* (LSFF) in all their treatments and discussions.

Note that the LSFF has built into it a 'natural' suppression dependent on the *final state hadron's mass*. However, the 'recipe' which Lund used, following their historical development, avoided this. Namely, the Lund recipe (restricted to mesons, for simplicity) in 1+1 dimensions is:

1) Use *'s/u'* and *'vector/all'* to select the hadron flavor. Thus, for example, a $u\bar{d}$ flavor combination will be designated as a π^+ or a ρ^+, a $u\bar{s}$ as a k^+ or

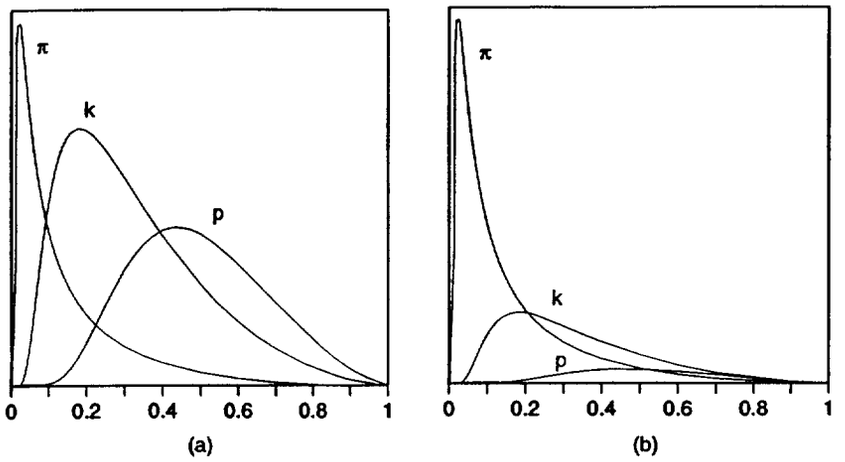

Fig. A.2. (a) Lund uses the *LSFF* to pick the z value only after determining the hadron's mass and P_T through external parameters, i.e., for each flavor, the probability integral under the curve is 1.0. (b) UCLA uses the *LSFF* as a hadron production density so that the suppression for a heavy particle arises through the *LSFF* with the same normalization factor for N for each flavor.

a k^{*+}, etc. There, however, remains an ambiguity for neutral mesons. For example, a $u\bar{u}$ pseudoscalar combination can be within a π^0 (135 MeV), an η (547 MeV) or an η' (958 MeV). In such a case, the Clebsch-Gordon couplings of the flavor combination into the meson flavor state function were used (with no regard to the hadron mass created).

2) Now that the hadron's identity (and therefore mass) had been selected, this was inputted to the LSFF in order to select the value of z for the hadron. Thus the LSFF was used to select the momentum of the hadron, but the 'natural' suppression from the final state hadron mass built into the LSFF by the factor $\exp(-b\ m_h^2/z)$ was not used (see Fig.A.2 for comparison). Instead, the suppression of heavier hadron production was controlled by the *'s/u'* and *'vector/all'* parameters.

Armed with all this machinery, the Lund approach predicts flavored hadronic production rates and distributions rather well.

In retrospect, there are three areas of potential concern with this approach: (i) In the WKB-type tunneling argument used to suppress virtual $s\bar{s}$ (and diquark-antidiquark) creation relative to $u\bar{u}$ and $d\bar{d}$ creation in the colorfield, the quark and antiquark after the tunneling are nowhere near free, contrary to the typical assumptions of the WKB approximation. Rather, they 'immediately' evolve into final state hadrons on essentially the same time or Q^2 scale, hadrons toward which QCD 'knows' it must evolve. (ii) Because of the historical order of development of the Lund modeling (s/u, etc. came before the LSFF), the 'natural' suppression within the LSFF from the final state hadronic mass is not used. (iii) There is roughly a parameter (reasonably well

motivated by plausible physics arguments) for each flavor degree of freedom. Recently, three more (physically motivated) parameters have been added to JETSET in order to improve agreement with data: a parameter of ≈ 0.65 to suppress η meson production; another of ≈ 0.27 to suppress η' production; and a third of ≈ 0.5 to suppress leading baryon production. A fourth possible concern is raised in Appendix B.1.4 where the Lundian recipe for picking P_T is discussed.

A.2 UCLA Approach

In our approach, we begin with an Event Weight Function which incorporates a QCD-motivated area-law dependence for the event. In our modeling, we assume no suppression for virtual $s\bar{s}$ production, even though the Event Weight Function structure could allow such a suppression (where the Lund approach would incorporate such a suppression with a value of ≈ 0.3) and no suppression for coupling a $q\bar{q}$ pair into a vector spatial wave function rather than into a pseudoscalar one (where, again, the Event Weight Function could allow such a suppression and the Lund approach would incorporate values ranging from ≈ 0.3 to 0.6).

From this Event Weight Function, we derive a fragmentation function for outside-in iterative one-hadron-at-a-time implementation. The result is the LSFF (with a finite energy correction), where we naturally incorporate the factor $\exp(-b\ m_h^2/z)$ providing suppression from the hadronic mass and where the relative normalization between various hadrons involves only Clebsch-Gordon coefficients with no additional suppressions from virtual quark-antiquark creation or from coupling into a vector spatial wave function.

This works quite well for predicting meson rates and distributions. The extension to the more complicated situation of baryons works encouragingly well, but with the need for a *popcorn* parameter, motivated by QCD perimeter law arguments in the present implementation.

B Treatments of Transverse Momentum

It appears that transverse momentum effects can be described fairly accurately by various different modeling approaches. This result, fortunate for those interested in simulating data, also means that it is hard to arrive at a fundamental understanding of the phenomenon.

We here describe three possible approaches: Two of them – the Lund approach

and the current UCLA approach – are based on implementation by JETSET, the Lund Monte Carlo program developed by T. Sjöstrand, and have been demonstrated to predict data rather accurately. The third is a speculation on our part which follows more closely from our initial-to-final-state approach, might lead to a more fundamental connection to QCD, but is currently under development and untested.

B.1 JETSET-based models

In this type of approach, followed successfully both in Sjöstrand's JETSET implementation and in our approach which uses a modified version of JETSET, the treatment of P_T in an event develops through a series of stages, each of which is either calculable (at least approximately) or model-able.

First, the primary $q\bar{q}$ pair created at high virtuality by the virtual photon (see Fig.2) initiate a parton shower of (virtual) gluon emission, which is calculated down to some cutoff parameter around 1 GeV at which point the shower evolution is terminated. The matrix element for the first two ('strongest') gluon emissions can be calculated exactly using perturbative QCD. A leading log approach can simulate a many-gluon shower, but is weak on the initial gluon's emitted. The most successful JETSET parton shower description uses a recipe of the leading log approach, but weights the initial emissions to agree with the matrix element calculation. It also introduces angular ordering of the emitted gluons as an approximate treatment for the coherence effects amongst gluon emissions as they become softer with longer wavelengths and overlapping effects.

The result of this parton shower, then, is a set of quarks and gluons (virtual, not on the mass shell) of defined momentum. It is visualized that a colorstring (actually, a colortube with a finite width of $\approx$ 0.6 fm) then connects these partons, running from the primary quark on one end through the various gluons to the primary antiquark on the other end. This colorstring, is straight in between partons, but is kinked at each gluon in the shower.

Second, in a fragmentation function iterative outside-in implementation it is necessary to pick a z-value (determining the longitudinal momentum along the string) for each successive hadron. This process must be allowed to move past a gluon-induced kink in the string. JETSET incorporates a sensible recipe for this process.

Thus, the remainder of the hadronization description is reduced to the simpler problem of the treatment of the evolution of a straight piece of colortube of finite width into observed final state hadrons. As the reader will note, we have used this simplification extensively.

Third, it is presumed that the finite width of the colortube leads to a finite spread in momentum effects transverse to the colortube due to the Heisenberg uncertainty principle, likely described (at least approximately) by a Gaussian distribution. (See Appendix F.)

Fourth, many of the final state hadrons directly produced from the colorstring in the process described above are, in fact, unstable; they are not directly detected, but rather the daughter products of their decays are finally observed in our detectors. These decay processes can also contribute to the transverse momentum of the final observed daughter particles.

Thus, the final total transverse momentum of an observed particle has three contributing sources in these JETSET-based approaches: (a) the kinkedness of the string as it is distorted by the momentum of the gluons in the parton shower, (b) the 'Heisenberg P_T' from the finite width of the colortube, and (c) the effects of the decays of the primary hadrons created.

The original JETSET approach and the current UCLA approach, implemented by a modified version of JETSET, share the above effects in common. However, they use very different (but comparably successful) descriptions of transverse momentum associated with the finite width of the colortube and of local correlations as successive particles are produced in the implementation chain of the Monte Carlo program.

B.1.1 Lund JETSET approach

The Lundian approach to the finite width of the color-tube focuses on the stage of virtual quark-antiquark pair production from the colorfield (a virtual stage very close in virtuality or time to the final state hadrons, which in some sense are the eigenstates toward which QCD is progressing). This approach presumes that the transverse momentum of the virtual quark is governed by a Gaussian distribution of form $\exp(-P_T^2/\sigma_q^2)$ where σ_q is an adjustable parameter related to the finite width of the colortube and is typically found to be $\approx$ 350 $\sim$ 400 MeV/c. The transverse momentum of the virtual partner antiquark is presumed to be equal and opposite to that of the virtual quark, which creates a local P_T correlation between the hadrons which are ultimately produced. The transverse momentum of a meson is then determined from the transverse momentum of the quark and antiquark (from another next-in-rank virtual pair) which are combined to form the meson.

This treatment of P_T from the finite colortube width, combined with the JETSET parton shower, the recipe for moving past a string-kink, and the hadronic decay tables used in JETSET has been quite successful in predicting topological event distributions such as sphericity, thrust, etc and also of transverse momentum distributions, both in and out of the 'event plane' determined for

example by the sphericity eigenvector approach, at center of mass energies ranging from 10 GeV to 91 GeV.

B.1.2 Current JETSET-based UCLA approach

Our current UCLA approach (within the framework of JETSET implementation and using much of the machinery of JETSET) focuses its treatment of transverse momentum associated with the finite colortube width directly on the final state hadrons produced, rather than on the intermediate stage of virtual quark-antiquark production. We should, perhaps, emphasize a paradox in our view of our current approach: It is quite adequately successful in predicting topological and transverse momentum distributions; it has reasonably attractive physical motivations; but we are not overwhelmed by its virtues and, in fact, regard it somewhat simply as a fairly reasonable mechanism which works within our framework to predict topological and transverse effects accurately enough that we can focus our present investigation on meson production without any significant biases introduced from the transverse momentum sector of the analysis. We presume that we will return to the transverse momentum sector in the future with better modeling tools and improved data with which to work.

Since our modeling focuses on the hadrons produces, we presume in our treatment that (subject to corrections from local correlations to be described below) the hadronic mass in our 1+1 dimensional description should simply be replaced by the transverse mass in 1+3 dimensions where $m_T^2 = m^2 + P_T^2$. Thus, without local correlations, our event weight function and fragmentation function would simply have the factor $\exp(-b(m^2 + P_T^2)/z)$, relative to the local string direction for each hadron. (Recall that in this JETSET-based approach, the problem has been reduced to a treatment relative to a straight piece of colorstring.)

It is quite interesting to note, as we develop below, that the structure of our Event Weight Function dW_f (see eq(2) of Section 2) in which we incorporate a form $\exp(-\chi P_T^2)$ for each hadron and a QCD-inspired area law of $\exp(-b'\mathcal{A}_{plane})$ for the event as a whole (relative to a straight string in 1+3 dimensions) can be deduced from a 'kinked area law approach'.

Thus, referring to Fig.3, where the event in 1+3 dimensions is originated by a straight piece of string, but where each of the hadrons acquires momentum transverse to the string because of the finite width of the string, we can write the Event Weight Function as

$$dW_f = (\text{phase space}) \cdot \mathrm{e}^{-b'\mathcal{A}_{\text{World-Surface}}}$$

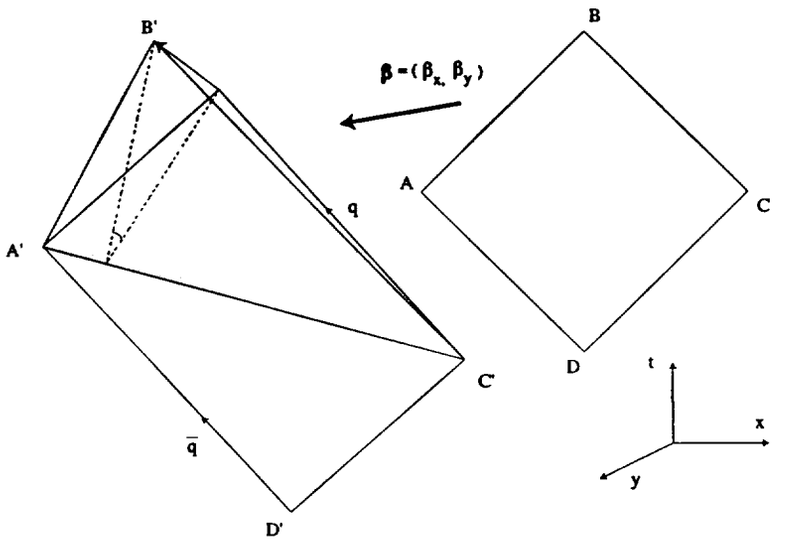

Fig. B.1. The three points A'B'C' corresponding the hadron with energy-momenum (E,P) can be calculated from the points ABC in the hadron's rest frame by making a proper Lorentz transformation.

where $\mathcal{A}_{\text{World-Surface}}$ is the 'kinked area' as shown in Fig.3. If the hadrons are produced with P_T's, the area of world-surface will be increased compared to 1+1 dimensional (planar) case. This world-surface will be one with minimal area defined by the quark and anti-quark lines (light cones). One way to approximate this bent surface is to consider two triangles as in Fig.B.1. By performing a proper Lorentz transformation from the hadron's rest frame where the hadron's momentum is *zero* to the frame where the hadron has transverse-momentum P_T and using straightforward but lengthy algebra, the area of the triangle A'B'C' is found to be

$$\mathcal{A}_{A'B'C'} = \frac{m^2}{2\kappa^2}\sqrt{\frac{m^2+2P_T^2}{m^2}} \simeq \frac{1}{2\kappa^2}\left(m^2+P_T^2\right)$$

when P_T of the hadron is small. Here κ is the string tension as usual. This means,

$$\mathcal{A}_{\text{world-surface}} \simeq \mathcal{A}_{plane} + \sum_i \frac{\chi_i}{b'} P_{T_i}^2$$

This then leads to our Event Weight Function as originally delineated in Section 2 eq(2).

It seems physically or intuitively attractive to allow the possibility of local transverse momentum correlations amongst the hadrons produced. We currently incorporate a treatment which is adapted to the *outside-in* iterative

implementation of JETSET. However, this current treatment of ours is so dependent on the outside-in implementation structure that it seems somewhat artificial in terms of an event-as-a-whole approach. But, comparisons with data indicate that some such structure is needed and that this approach does, in fact, work quite reasonably.

The derivation (suggested to us by Gösta Gustafson of the Lund group)[28] is displayed in Appendix C. The result is that a hadron's distribution in either P_x or P_y which is 'naturally' (without local correlations)

$$\exp(-P_T^2/\sigma^2)$$

becomes

$$\exp\left(-\frac{1}{\sigma^2}\frac{n}{n-1}\left(P_T-\frac{\phi}{n}\right)^2\right)$$

where, after some steps in the *outside-in* interative implementation, ϕ is the unbalanced P_T (in either P_x or P_y) accumulated over the previous steps and n is the number of following hadrons over which this accumulated ϕ is to be compensated statistically in equal amounts.

We find that $n = 2$, the most local correlation possible in this framework, yields results in agreement with data.

B.1.3 Pros and Cons of JETSET-type P_T treatments

The attractive features of these JETSET-based approaches to transverse momentum effects are:

1) The modeling proceeds step-by-step through the various stages presumed for the overall hadronization process.
2) The parton shower can be approximately calculated.
3) Local correlations, which certainly are a distinct possibility, can be built in and, in fact, seen to be necessary.
4) Good agreement with data can be achieved.

The less attractive features are:

5) The parton shower is an unobserved intermediate state which spans a transition from a perturbative high-virtuality regime to a non-perturbative low-q^2 regime. It does not end in free final state partons, but rather with a cut-off parameter which leads into the hadronization stage. Further, the parton

shower's use of the Altarelli-Parisi splitting function is a probability description rather than an amplitude description. It therefore does not naturally treat interference effects, though the JETSET use of angular ordering in the gluon emission partially compensates for this. Thus, it's 'calculation' ends up being somewhat of an approximate recipe, rather than a pure calculation.

6) It requires a recipe to move past a gluon-induced kink in the string.
7) It requires recipes to get P_T relative to the string and to incorporate local correlations.

B.1.4 Effect of P_T treatment on longitudinal structure

A dramatic example that the specific way in which an idea is implemented can affect the results in subtle, and perhaps unexpected, ways is evidenced in the effects on longitudinal momenta from the ways that P_T is handled in the Lundian and UCLA recipes.

The UCLA approach is simply to treat the LSFF as an hadronic production density. Thus the distribution in z can be simply obtained by integrating $f(z, P_T^2, m^2)$ over P_T^2 with the interesting result that the factor $1/z$ in $f(z, P_T^2, m^2)$ is canceled:

$$f(z, m^2) \propto (1-z)^a \ \mathrm{e}^{-b\ m_h^2/z}$$

The Lund approach is more complex: In 1+3 dimensions, before the LSFF is used to pick the z-value for a hadron, the value of P_T (quark) is picked from a distribution $\exp(-P_T^2/\sigma_q^2)$ at the same stage in the implementation that the flavor of the hadron is picked (see Appendix A for the 1+1 dimension flavor selection treatment). These values of both m_{hadron} and $P_{T\mathrm{hadron}}$ are then inputted into the LSFF to select z. Approximately, this maintains the $(1/z)$ factor in $f(z)$.

Thus, for a given value of *'a'* and *'b'*, the Lund distribution falls more rapidly with increasing z than does its counterpart in the UCLA approach. Therefore, when fitting to a given flavored momentum distribution, the $(1-z)^a$ factor in the LSFF implies that a larger value of *'a'* will be found to fit the distribution shape with the UCLA approach than with the Lund recipe.

Turned around, this helps to resolve an old question: 'If Lund JETSET 7.4 with *'a'* values around $0.4 \sim 0.5$ fit the momentum distributions of various hadrons at high x_p rather well, then how can UCLA, with values of *'a'* around $1.6 \sim 2.0$, also fit these data reasonably well ?' The answer, approximately, is the following:

Comparing the fragmentation functions for various flavors at $x_p = 0.9$ with

the fragmentation functions peak values at lower x_p, one finds that the factor of $(1-z)^a$ has dropped approximately a factor of ten more for the UCLA model ($a = 1.65$) than for the Lund model ($a \simeq 0.4$). However, the different treatments of P_T, in particular the $1/z$ factor not present in the distribution in z for the UCLA model), increases the UCLA model at $x_p = 0.90$ by a factor of $2 \sim 3$. The difference in *'b'* values of the best-fits, further increases the UCLA model at $x_p = 0.90$ by $10 \sim 15\%$. Thus, the net drop for the UCLA model is about a factor of $3 \sim 4$ larger than that for Lund in comparing the fragmentation functions at $x_p = 0.90$ with those at the peak heights. Comparing at $x_p = 0.95$, one finds a further drop in the UCLA fragmentation function, relative to that for Lund, of a factor of $2.0 \sim 2.5$.

Thus, one might expect that the high x_p behavior of the data might provide a sensitive probe to choose between the *'a'* values obtained in these two approaches (even despite the fact that the different P_T recipes ameliorates against this). However, this important comparison is somewhat obscured by two factors: (1) Most of the hadrons observed at low x_p are decay products rather than hadrons produced directly from the decay of the colorfield. Thus the models will be tuned to these large decay product populations. (2) The quality of the data measurements at high x_p deteriorate very rapidly. For a typical flavored distribution, the highest x_p value with fairly accurate data is $\approx 0.7 \sim 0.8$. There are weak suggestions in the comparisons, both in the flavored data at $x_p \simeq 0.7 \sim 0.8$ and in the overall N_{charged} data at $x_p \simeq 0.90 \sim 0.95$ (see Fig.9, 13~16), that the UCLA predictions might be dropping below the data.

B.2 An initial-to-final-state global approach

If we extend our philosophy of insisting on a total transition from the initial state of the q_0 and $\bar{q}_0$ directly created by the virtual photon to the final state hadrons created from the colorfield (including the parton shower as an unobserved intermediate state), then an alternate possible approach suggests itself.

In this approach, all one knows presumably is the flavors and three-momenta of the final state hadrons. One also presumes that QCD, a very strong interaction at distances greater than a few tenths of a fm, is responsible for evolution into hadrons. QCD has a form which allows the beginning of a parton shower to be calculated (though it quickly loses accuracy and does not lead to free final particles). But in the later stages of the event where QCD's coupling is very strong, it is very hard to avoid the conclusion that a space-time area law will be valid.

Let us now visualize some sort of kinked area in 1+3 dimensions spanning to the final state hadrons whose flavor and momentum have been specified. This is rather like the treatment in the current UCLA approach depicted in Fig.3 and discussed in Appendix B.1.2, but with one large difference: In our current approach of Fig.3 and Appendix B.1.2, the kinked area law approach is invoked relative to a straight piece of string *after* the parton shower and the recipe to move past kinks. In this new approach our kinked area law approach *includes* everything intermediate together, that is, the parton shower as well as P_T due to the finite width of the string (intrinsic P_T) in the JETSET-based approaches. It is clear that this sort of approach will at least qualitatively prefer jetty events, as it should. That is, a 'two-jet-like' event will have a smaller total area than a 'three jet-like' event, etc. As a matter of fact, since the world-surface in this case is a thin curved 2-dimensional surface (very similar to the string), qualitatively, one can expect most all the properties of the string. This approach is provocative to the conventional viewpoint of hadronization models including not only string models[3,8] but also parton cluster models[29].

The attractive features of such an approach are:

1) It is faithful to the proper initial-to-final state approach of quantum mechanics
2) It avoids many of the 'artificial' intermediate stages of the JETSET-based approaches such as a parton shower, as well as suppressions associated with creating virtual $q\bar{q}$ pairs from the colorfield.
3) It identifies the source of a hadron's P_T (before its decay into stable daughter particles) as a bent surface. Thus, this scheme doesn't know whether a hadron's P_T came from hard gluon emission or intrinsic P_T due to the finite size of the string.
4) It draws on the powerful space-time area law type of approach indicated by almost any strong coupled interaction such as QCD at distances greater than a few tenths of a fermi.
5) It at least qualitatively will give most of the properties of the string such as jettiness that are proven to be valid phenomenologically.

Since this scheme relates the perturbative region directly with the non-perturbative region, it may have to predict the running coupling constant α_s of perturbative QCD. Whether this scheme can be developed to be consistent with perturbative QCD is currently beyond our scope. For the time being, we are using the current JETSET-based approach of our modeling, but we recognize that the extensions of the lessons we have learned from our present approach lead in the direction of this new approach to transverse momentum.

C Transverse Momentum Correlation

Another important aspect of the transverse momentum considerations is that one has to implement its overall conservation, since it has been orphaned in the course of a longitudinal formulation of the system. To incorporate this, let's start from a simple example: When two independent Gaussian distributions

$$d\mathcal{P}_1 = \exp\left(-\frac{P_1^2}{\sigma_1^2}\right) dP_1$$

and

$$d\mathcal{P}_2 = \exp\left(-\frac{P_2^2}{\sigma_2^2}\right) dP_2$$

convolute into a distribution via a constraint

$$P_1 + P_2 = Q$$

the resulting distribution is

$$\begin{aligned}
\frac{d\mathcal{P}}{dQ} &= \int dP_1 dP_2 \exp\left(-\frac{P_1^2}{\sigma_1^2} - \frac{P_2^2}{\sigma_2^2}\right) \delta(P_1 + P_2 - Q) \\
&= \int dP_1 \exp\left(-\frac{P_1^2}{\sigma_1^2} - \frac{(Q - P_1)^2}{\sigma_2^2}\right) \\
&= \int dP_1 \exp\left(-P_1^2\left(\frac{1}{\sigma_1^2} + \frac{1}{\sigma_2^2}\right) + \frac{2QP_1}{\sigma_2^2} - \frac{Q^2}{\sigma_2^2}\right) \\
&= \int dP_1 \exp\left[-\left\{\left(\frac{1}{\sigma_1^2} + \frac{1}{\sigma_2^2}\right) P_1 - \frac{Q}{\sigma_2^2\left(\frac{1}{\sigma_1^2} + \frac{1}{\sigma_2^2}\right)}\right\}^2\right] \\
&\quad \times \exp\left(\frac{Q^2}{\sigma_2^4\left(\frac{1}{\sigma_1^2} + \frac{1}{\sigma_2^2}\right)}\right) \exp\left(-\frac{Q^2}{\sigma_2^2}\right) \\
&= \int dP_1 \exp\left(-(aP_1 - b)^2\right) \exp\left(-\frac{Q^2}{\sigma_1^2 + \sigma_2^2}\right) \\
&\propto \exp\left(-\frac{Q^2}{\sigma_1^2 + \sigma_2^2}\right)
\end{aligned}$$

where $(aP_1 - b)^2$ completes the square of P_1 and is integrated out. The above example can be extended to a system of n variables

$$d\mathcal{P} = \exp\left(-\frac{P_i^2}{\sigma_i^2}\right) dP_i \qquad (i = 1, n)$$

whose constraint is

$$\sum_{i=1}^{n} P_i = Q$$

The resulting distribution is

$$\frac{d\mathcal{P}}{dQ} \propto \exp\left(-\frac{Q^2}{\sum_{i=1}^{n} \sigma_i^2}\right)$$

Now, the transverse momentum probability distribution for a piece of string having n hadrons subject to a constraint

$$\phi = \sum_{i=1}^{n} P_i$$

can be written as

$$d\mathcal{P} = \prod_{i=1}^{n} dP_i \; \delta\left(\sum_{i=1}^{n} P_i - \phi\right) \exp\left(-\frac{P_i^2}{\sigma_i^2}\right)$$

The individual momentum distribution of each hadron is affected by the constraint on the system. The effect of the constraint on the first of the n hadrons to be studied can be seen by integrating all the hadrons' momenta except the first one. By defining a new variable R as

$$R = \sum_{i=2}^{n} P_i$$

and introducing a delta function, the integrated distribution function becomes

$$d\mathcal{P} = dP_1 \, e^{-P_1^2/\sigma_1^2} \int \prod_{i=2}^{n} dP_i \, e^{-P_i^2/\sigma_i^2} \; \delta\left(\sum_{i=1}^{n} P_i - \phi\right) \int dR \, \delta\left(R - \sum_{i=2}^{n} P_i\right)$$

$$\propto dP_1 \exp\left(-\frac{P_1^2}{\sigma_1^2}\right) \int dR \; \exp\left(-\frac{R^2}{\sum_{i=2}^{n} \sigma_i^2}\right) \delta(R + P_1 - \phi)$$

$$= dP_1 \exp\left(-\frac{P_1^2}{\sigma_1^2}\right) \exp\left(-\frac{(\phi - P_1)^2}{\sum_{i=2}^{n} \sigma_i^2}\right)$$

When all the momentum distributions have the same width, this becomes

$$\begin{aligned}
\frac{d\mathcal{P}}{dP_1} &\propto \exp\left(-\frac{P_1^2}{\sigma_1^2}\right) \exp\left(-\frac{(\phi - P_1)^2}{(n-1)\sigma^2}\right) \\
&\propto \exp\left(-\frac{1}{\sigma^2}\left(\frac{n}{n-1}\right)\left(P_1 - \frac{\phi}{n}\right)^2\right) \exp\left(-\frac{\phi^2}{n\sigma^2}\right) \\
&\propto \exp\left(-\frac{1}{\sigma^2}\left(\frac{n}{n-1}\right)\left(P_1 - \frac{\phi}{n}\right)^2\right)
\end{aligned}$$

What we have shown is, in an outside-in iterative implementation, that when there is net momentum ϕ before the particular hadron in a string and all the hadrons have a Gaussian P_T distribution with the same width, if we require compensation of this net momentum over the next n hadrons, the distribution alters its form to:

$$d\mathcal{P} \propto \exp\left(-\frac{1}{\sigma^2}\left(\frac{n}{n-1}\right)\left(P - \frac{\phi}{n}\right)^2\right) dP$$

Note that the above requirement not only alters the width of the Gaussian but also shifts the centering of the distribution.

D Discussion on Amplitude vs. Probability

The *Event Weight Function* (eq.(2)) is a probabilistic weight associated with a particular final state hadron configuration and is equivalent to the square of a quantum mechanical amplitude. Hence, in principle, one has to include interference terms amongst the degenerate final states in calculating the *Event Weight Function.* There are many degenerate diagrams which correspond to the same final state. These degenerate diagrams are obtained by *rotating the final state hadrons*, by *mirror reflecting them*, and by other permutations consistent with local flavor conservation. For example, starting from a rank-ordered diagram Fig.D.1 (a.1) for a final state of four hadrons with specific flavors and momenta, Figs.D.1(a.2-4) are its rotations, Figs.D.1(b.1-4) are its mirror reflections, and Figs.D.1(c.1-4) are other possible permutations. [Note that, in some of the permuted diagrams, the flavor of the initial $q\bar{q}$ pair created by the virtual photon may be changed.] As is shown for a typical event (Fig.D.1(a.1)), the diagrams obtained by the permutations of the original rank-ordered diagram typically have much bigger area than that of the rank-ordered diagram

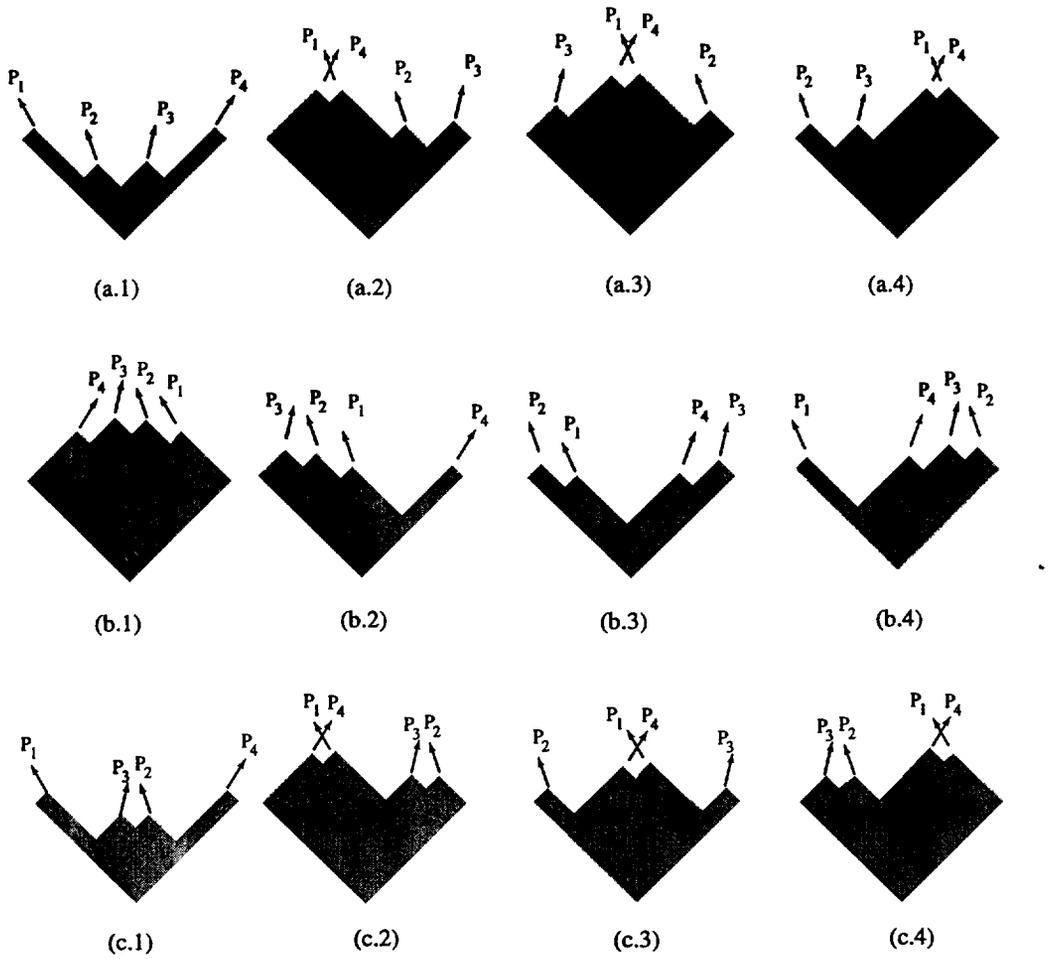

Fig. D.1. Example of diagrams corresponding to the same final hadronic state. Since all diagrams other than the rank ordered diagram (a.1) statistically have a considerably bigger area, the diagram (a.1) dominates and the interference terms are small when a probability function is obtained by squaring the amplitude.

so that their contributions to the amplitude are expected to be small. We approached the possibility of significant interference effects by permuting (in all ways consistent with local flavor conservation) a sample of Monte-Carlo generated events, presuming that all interferences were constructive in phase, and studying the area law probabilities associated with the various diagrams. Fig.D.2 displays a log-log plot to the base 10 of

$$\left(\left| \sum_{permutations} e^{-\frac{b'}{2}\mathcal{A}} \right|^2 \right)$$

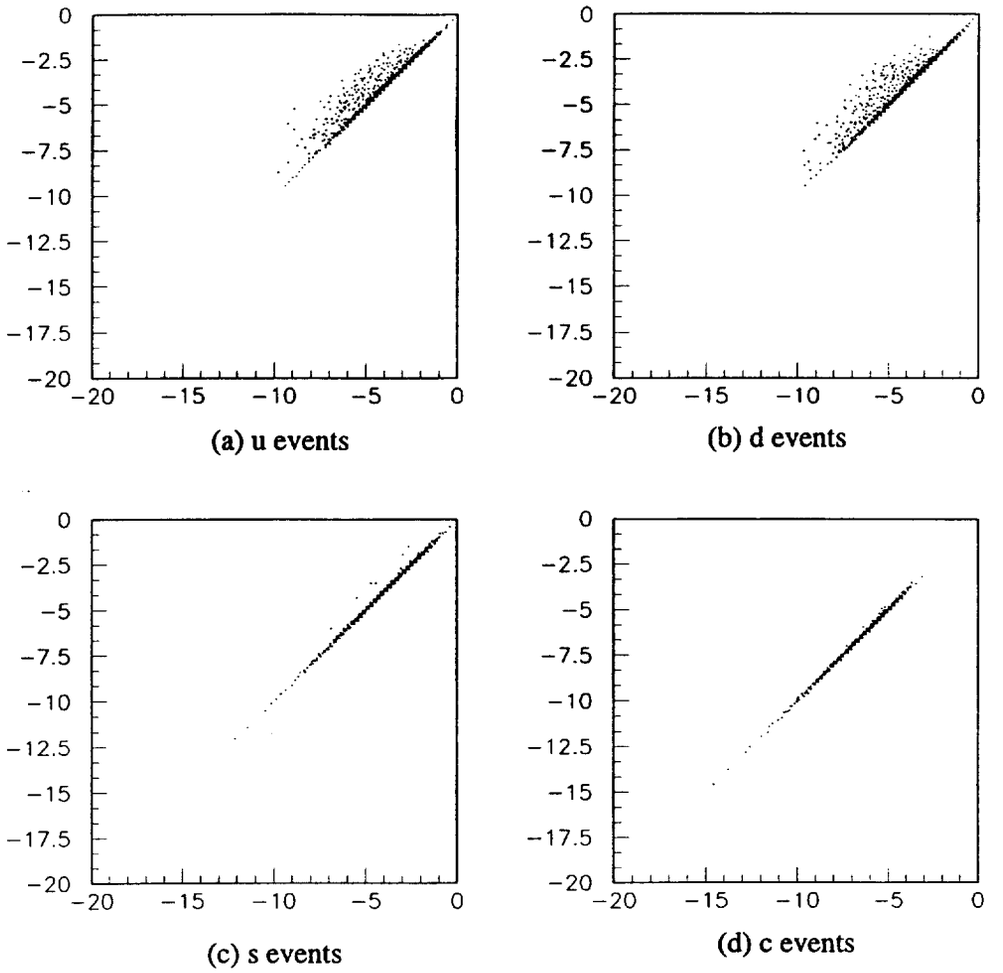

Fig. D.2. The amplitude-squared including all the diagrams leading to the same final state (vertical axis) is plotted against the amplitude squared including only the leading diagram with the minimum area in log-log (to the base 10) plots for various initial quarks. The deviations from the straight line in the light quark events indicate small contributions from the diagrams other than Fig.D.1(a.1), whereas for heavy quark events these effects are almost non-existent.

which is the total amplitude-squared of an event, plotted against

$$\left(\mid e^{-\frac{b'}{2}\mathcal{A}_{\min}} \mid^2 \right)$$

which is the amplitude squared of the leading diagram with the minimum area, using our experimental value of $b = 1.18\ GeV^{-2}$. These are displayed for different initial quark flavors, u, d, s, and c.When there are no interferences at all (that is, one diagram dominates), the points on the plots are along the diagonal line. We note that for $c\bar{c}$ and $s\bar{s}$ events, there are almost no non-leading contributions, whereas for $u\bar{u}$ and $d\bar{d}$ events there are some.

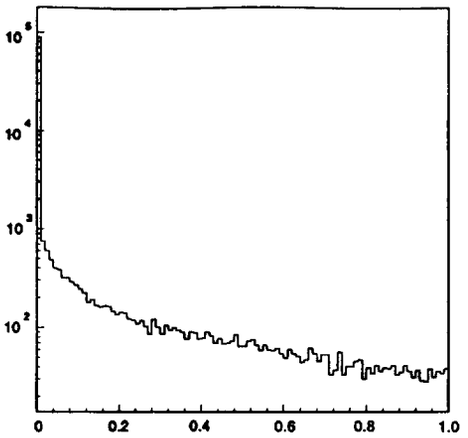

Fig. D.3. The fractional increase in probability from non-leading diagrams in events with primary $d\bar{d}$ quark pairs.

To explore this further, Fig.D.3 histograms the fractional increase in probability for final states whose dominant diagram is a $d\bar{d}$ primary quark pair, that is:

$$\frac{|\sum_i e^{-\frac{b'}{2}\mathcal{A}}|^2 - e^{-b'\mathcal{A}_{\min}}}{e^{-b'\mathcal{A}_{\min}}}$$

We find that $\approx 90\%$ of the events have $< 1\%$ increase from non-leading contributions. $\approx 5\%$ have $\geq 20\%$ increase; $\approx 2\%$ have $\geq 50\%$ increase. We draw three inferences from this:

1) For the level of our present modeling, it is a very good approximation to use probabilities (without interference) via the *Event Weight Function* dW_f, rather than to use quantum mechanical amplitudes.
2) The interference terms as in Fig.D.4 between diagrams involving different-flavored primary $q\bar{q}$ pair are quite small, since the same final hadronic state from different initial flavored $q\bar{q}$ pairs, for example $u\bar{u}$ and $d\bar{d}$, is quite rare. This supports the traditional parton model view where quarks were considered to be free, i.e.,

$$\sigma^{\text{total}}_{e^+e^-\to\text{hadrons}} \propto \sum_q Q_q^2 \tag{D.1}$$

where Q_q is the charge of a primary quark pair flavor.
3) If experimentally, one could accurately determine the flavor and momentum of *all final state hadrons* produced *directly* from the colortube, then with high reliability one could reconstruct the flavor of the primary $q\bar{q}$ pair. Unfortunately, in practice this attractive possibility is diluted both by imperfect detection equipment and by the fact that many of the observed particles are actually daughters of the hadrons produced directly from the

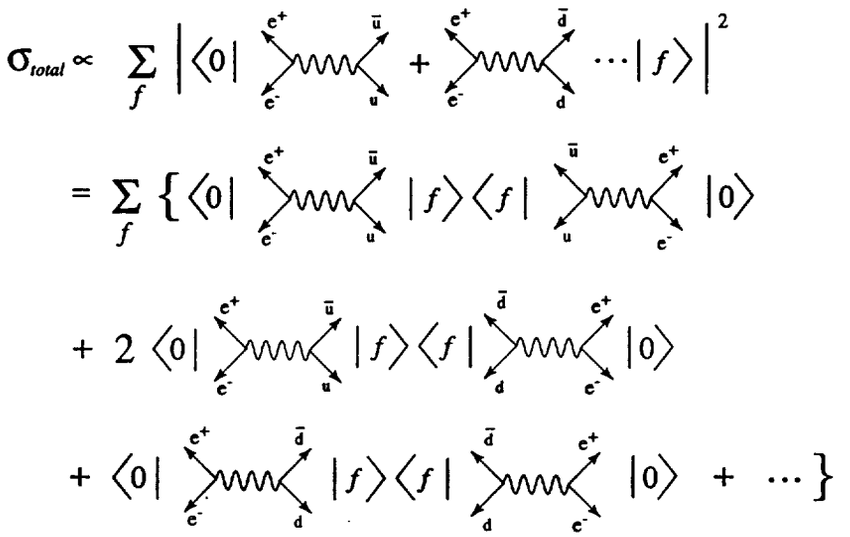

Fig. D.4. The graphical representation of the total cross section of e^+e^- →hadrons for a final state which is reachable via either $u\bar{u}$ or $d\bar{d}$ primary pairs. In principle, there are interferences possible in the square of the amplitude amongst terms from different flavor primary $q\bar{q}$ pairs that result in the same final state f. But our systematic study shows that such interference effects are quite small.

colorstring.

E Detailed Derivation of the Fragmentation Function from the *Event Weight Function*

We discuss (E.1) the derivation of the *fragmentation function* from the *Event Weight Function* in detail, (E.2) the *Lemma* for g(S), and (E.3) the *Eigenvalue Problem* for d_{ij} which arises from the unitarity equation for dP_1.

E.1 From the Event Weight Function to the fragmentation function

The Event Weight Function eq(2) for an unkinked relativistic string is:

$$dW_f{}^{q_0\bar{q}_0} = \frac{N_1 C_1^2}{(2\pi)^3} dE_1 dP_{z_1} dP_{x_1} dP_{y_1} \delta\left(E_1^2 - P_1^2 - m_1^2\right) \mathrm{e}^{-\chi\left(P_{x_1}^2 + P_{y_1}^2\right)} \nu_{12} \times \ldots$$
$$\times \nu_{n-1,n} \frac{N_n C_n^2}{(2\pi)^3} dE_n dP_{z_n} dP_{x_n} dP_{y_n} \delta\left(E_n^2 - P_n^2 - m_n^2\right) \mathrm{e}^{-\chi\left(P_{x_n}^2 + P_{y_n}^2\right)}$$

$$\times(2\pi)^4\delta\left(\mathbf{E}-\sum_i E_i\right)\delta\left(\mathbf{P}_z-\sum_i P_{z_i}\right)\delta\left(\mathbf{P}_x-\sum_i P_{x_i}\right)\delta\left(\mathbf{P}_y-\sum_i P_{y_i}\right)$$
$$\times\, e^{-b' A_{plane}}$$

This is simplified by integrating over the (assumed to be approximately independent) azimuthal angles

$$\int_{Azimuth} dE_i dP_{z_i} dP_{x_i} dP_{y_i} = \frac{1}{2}\int dE_i dP_{z_i} dP_{T_i}^2 d\theta_i = \pi dE_i dP_{T_i}^2$$

The mass-shell condition, eq(3) becomes

$$\begin{aligned}
&\pi dE_i dP_{T_i}^2 \delta\left(E_i^2 - P_{z_i}^2 - P_{x_i}^2 - P_{y_i}^2 - m_i^2\right) \\
&= \frac{\pi}{2} d\left(E_i + P_{z_i}\right) d\left(E_i - P_{z_i}\right) dP_{T_i}^2 \delta\left[\left(E_i + P_{z_i}\right)\left(E_i - P_{z_i}\right) - \left(m_i^2 + P_{T_i}^2\right)\right] \\
&= \frac{1}{2}\frac{d\left(E_i + P_{z_i}\right)}{\left(E_i + P_{z_i}\right)} d\left(E_i - P_{z_i}\right) \delta\left[E_i - P_{z_i} - \frac{m_i^2 + P_{T_i}^2}{\left(E_i + P_{z_i}\right)}\right] dP_{T_i}^2 \\
&= \frac{\pi}{2}\frac{dz_i}{z_i} dP_{T_i}^2 \qquad \text{(E.1)}
\end{aligned}$$

with the definition (introducing light cone variables W_+, W_- as in Fig.4.)

$$z_i \equiv \frac{(E_i + P_{z_i})_h}{(E + P_z)_{q_0}} \equiv \frac{W_{+_i}}{W_+} = \frac{l_1}{l_0}$$

That is, z_i is the fraction of the initial quark's energy plus longitudinal momentum which the hadron carries.

The longitudinal part of the delta function eq(4) can be rewritten as

$$\begin{aligned}
&\delta\left(\mathbf{E} - \sum_{i=1}^n E_i\right)\delta\left(\mathbf{P}_z - \sum_{i=1}^n P_{z_i}\right) = \delta\left(W_+ - \sum_{i=1}^n W_{+_i}\right)\delta\left(W_- - \sum_{i=1}^n W_{-_i}\right) \\
&= \delta\left(1 - \sum_{i=1}^n z_i\right)\delta\left(W_+ W_- - \sum_{i=1}^n W_+ W_{-_i}\right) \\
&= \delta\left(1 - \sum_{i=1}^n z_i\right)\delta\left(S_\parallel - \sum_{i=1}^n \frac{m_{T_i}^2}{z_i}\right) \\
&= \delta\left(1 - \sum_i z_i\right)\delta\left(S_\parallel - \sum_{i=1}^n \frac{m_i^2}{z_i} + \sum_{i=1}^n \frac{P_{T_i}^2}{z_i}\right)
\end{aligned}$$

with

$$S_\parallel \equiv W_+ W_- = S \quad \text{and} \quad W_{+_i} W_{-_i} = m_{T_i}^2 = m_i^2 + P_{T_i}^2$$

where bold face represent the *total* quantity as before. Then, eq(2) for the *Event Weight Function* becomes:

$$
\begin{aligned}
dW_f^{q_0\bar{q}_0}(S) &= \frac{N_1 C_1^2}{(4\pi)^2}\frac{dz_1}{z_1}\,\mathrm{e}^{-\chi P_{T_1}^2}\,dP_{T_1}^2\;\nu_{12}\times\ldots \\
&\times\nu_{n-1,n}\;\frac{N_n C_n^2}{(4\pi)^2}\frac{dz_n}{z_n}\,\mathrm{e}^{-\chi P_{T_n}^2}\,dP_{T_n}^2\cdot(2\pi)^4\delta\left(1-\sum_{i=1}^{n}z_i\right) \\
&\times\delta\left(S-\sum_{i=1}^{n}\frac{m_{T_i}^2}{z_i}\right)\delta\left(\mathbf{P}_x-\sum_{i=1}^{n}P_{x_i}\right)\delta\left(\mathbf{P}_y-\sum_{i=1}^{n}P_{y_i}\right)\;\mathrm{e}^{-b'\mathcal{A}_{plane}}
\end{aligned}
$$

Next, construct a partial weight *integrated/summed* over all possible flavors, multiplicities, and momenta of all particles except the first (outer-most) hadron:

$$
\begin{aligned}
dW_1 = \frac{N_1 C_1^2}{(4\pi)^2}\mathrm{e}^{-bm_1^2/z_1}\frac{dz_1}{z_1}\,\mathrm{e}^{-\chi P_{T_1}^2}\,dP_{T_1}^2\;\nu_{12}\sum_f\!\!\!\!\!\!\int\;\frac{N_2 C_2^2}{(4\pi)^2}\frac{dz_2}{z_2}\,\mathrm{e}^{-\chi P_{T_2}^2}\,dP_{T_2}^2\;\nu_{23}\times\ldots \\
\times\nu_{n-1,n}\;\frac{N_n C_n^2}{(4\pi)^2}\frac{dz_n}{z_n}\,\mathrm{e}^{-\chi P_{T_n}^2}\,dP_{T_n}^2\cdot(2\pi)^4\delta\left(1-z_1-\sum_{i=2}^{n}z_i\right) \\
\times\delta\left(S-\frac{m_{T_1}^2}{z_1}-\sum_{i=2}^{n}\frac{m_{T_i}^2}{z_i}\right)\delta\left(\mathbf{P}_x-P_{x_1}-\sum_{i=2}^{n}P_{x_i}\right) \\
\times\delta\left(\mathbf{P}_y-P_{y_1}-\sum_{i=2}^{n}P_{y_i}\right)\;\mathrm{e}^{-b'\tilde{\mathcal{A}}_{plane}} \qquad \text{(E.2)}
\end{aligned}
$$

where m_1^2/z is the area associated with the outermost hadron and $\tilde{\mathcal{A}}$ is the area left over after the outermost hadron is produced as defined in Fig.5. Using the identity $\delta(ax)=\frac{1}{|a|}\delta(x)$, eq.(E.2) becomes

$$
\begin{aligned}
dW_1 = \frac{N_1 C_1^2}{(4\pi)^2}\mathrm{e}^{-bm_1^2/z_1}\frac{dz_1}{z_1}\,\mathrm{e}^{-\chi P_{T_1}^2}\,dP_{T_1}^2\;\nu_{12}\sum_f\!\!\!\!\!\!\int\;\frac{N_2 C_2^2}{(4\pi)^2}\frac{dz_2}{z_2}\,\mathrm{e}^{-\chi P_{T_2}^2}\,dP_{T_2}^2\;\nu_{23}\times\ldots \\
\times\nu_{n-1,n}\;\frac{N_n C_n^2}{(4\pi)^2}\frac{dz_n}{z_n}\,\mathrm{e}^{-\chi P_{T_n}^2}\,dP_{T_n}^2\cdot(2\pi)^4\delta\left(1-\sum_{i=2}^{n}\frac{z_i}{1-z_1}\right) \\
\times\delta\left(\left(S-\frac{m_{T_1}^2}{z_1}\right)(1-z_1)-\sum_{i=2}^{n}m_{T_i}^2\frac{(1-z_1)}{z_i}\right) \\
\times\delta\left(\mathbf{P}_x-P_{x_1}-\sum_{i=2}^{n}P_{x_i}\right)\delta\left(\mathbf{P}_y-P_{y_1}-\sum_{i=2}^{n}P_{y_i}\right)\;\mathrm{e}^{-b'\tilde{\mathcal{A}}_{plane}} \qquad \text{(E.3)}
\end{aligned}
$$

The latter part of the partial sum of the weight function (excluding the variables with index 1) becomes

$$\sum\!\!\!\!\!\!\int_f \frac{N_2 C_2^2}{(4\pi)^2}\frac{d\tilde{z}_2}{\tilde{z}_2}\,\mathrm{e}^{-\chi P_{T_2}^2}\,dP_{T_2}^2\,\nu_{23}\times\ldots$$
$$\times\nu_{n-1,n}\,\frac{N_n C_n^2}{(4\pi)^2}\frac{d\tilde{z}_n}{\tilde{z}_n}\,\mathrm{e}^{-\chi P_{T_n}^2}\,dP_{T_n}^2\cdot(2\pi)^4\delta\left(1-\sum_{i=2}^{n}\tilde{z}_i\right)$$
$$\times\delta\left(\tilde{S}-\sum_{i=2}^{n}\frac{m_{T_i}^2}{\tilde{z}_i}\right)\,\delta\left(\tilde{\mathbf{P}}_x-\sum_{i=2}^{n}P_{x_i}\right)\delta\left(\tilde{\mathbf{P}}_y-\sum_{i=2}^{n}P_{y_i}\right)\,\mathrm{e}^{-b'\tilde{A}_{plane}} \qquad \text{(E.4)}$$

The definitions of the scaled variables used are:

$$\tilde{z}_i=\frac{z_i}{1-z_1} \qquad \text{(E.5)}$$

which is the scaled z with respect to the remnant system,

$$\tilde{S}=\left(S-\frac{m_{T_1}^2}{z_1}\right)(1-z_1) \qquad \text{(E.6)}$$

and

$$\tilde{\mathbf{P}}_x=\mathbf{P}_x-P_{x_1}\quad\text{and}\quad\tilde{\mathbf{P}}_y=\mathbf{P}_y-P_{y_1} \qquad \text{(E.7)}$$

that is, the longitudinal E_{CM}^2 of the remnant system and the total transverse momentum after the first hadron is peeled off respectively.

Note that eq(E.4) is simply g($\tilde{S}$). This is equivalent to saying that the property of the subsystem is the same as the original system. The situation is indicated in Fig.4(a) and (b).

If we define the *Total Weight* as

$$\mathrm{g}^{q_0\bar{q}_0}(S)=\sum\!\!\!\!\!\!\int_f dW_f{}^{q_0\bar{q}_0}(S)$$

then, eq(E.4) becomes g$\left(\tilde{S}\right)$ and the partial sum dW_1 normalized by the *Total Weight* g(S) is the probability for the first hadron to have m_1^2, z_1, and ${P_{T_1}}^2$, i.e., a *fragmentation function*

$$dP_1{}^{q_0}(z_1,P_{T_1}^2,m_1^2)=\frac{N_1C_1^2}{(4\pi)^2}\,\nu_{12}\,\mathrm{e}^{-bm_1^2/z_1}\,\frac{dz_1}{z_1}\,\mathrm{e}^{-\chi P_{T_1}^2}\,dP_{T_1}^2\,\frac{\mathrm{g}^{q_1\bar{q}_0}(\tilde{S})}{\mathrm{g}^{q_0\bar{q}_0}(S)}$$

Finally, substituting in $\mathrm{g}^{q_0\bar{q}_0}(S)=d_{q_0\bar{q}_0}S^a$ and $\mathrm{g}^{q_1\bar{q}_0}(\tilde{S})=d_{q_0\bar{q}_0}\tilde{S}^a$ (See Appendix E.2 below.), the fragmentation function is

$$dP_1^{q_0}(z_1, P_{T_1}^2, m_1^2) = \frac{N_1 C_1^2}{(4\pi)^2} \nu_{12} (1-z_1)^a \left(1 - \frac{m_1^2}{S z_1}\right)^a \mathrm{e}^{-bm_1^2/z_1} \frac{dz_1}{z_1} \mathrm{e}^{-\chi P_{T_1}^2} dP_{T_1}^2 \times \frac{d_{q_1\bar{q}_0}}{d_{q_0\bar{q}_0}}$$

E.2 A Lemma for the Total Weight g(S)

Eq(11) is rewritten

$$\frac{\partial^2 P_1^{q_0}(z, P_T^2, m^2)}{\partial z \partial P_T^2} = \frac{N_1 C_1^2}{(4\pi)^2} \nu_{12} \frac{1}{z} \mathrm{e}^{-bm^2/z} \mathrm{e}^{-\chi P_T^2} \frac{\mathrm{g}^{q_1\bar{q}_0}(\tilde{S})}{\mathrm{g}^{q_0\bar{q}_0}(S)} = f\left(z, P_T^2, m^2\right)$$

Take the natural log of both sides (suppressing the flavor indices)

$$\log f\left(z, P_T^2\right) = \text{Constant} - b\frac{m^2}{z} - \log z - \chi P_T^2 + \log \mathrm{g}(\tilde{S}) - \log \mathrm{g}(S)$$

Then, differentiate with respect to S. If $f\left(z, {P_T}^2, m^2\right)$ is not a function of S when S is large enough (a scaling phenomenon),

$$\frac{S}{\mathrm{g}^{q_0\bar{q}_0}(S)} \frac{d\mathrm{g}^{q_0\bar{q}_0}(S)}{dS} = \frac{\tilde{S}}{\mathrm{g}^{q_0\bar{q}_1}\left(\tilde{S}\right)} \frac{d\mathrm{g}^{q_0\bar{q}_1}\left(\tilde{S}\right)}{d\tilde{S}}$$

since $\tilde{S} \simeq S(1-z)$ when $S \to \infty$ and

$$\frac{\partial \tilde{S}}{\partial S} = (1-z) \simeq \frac{\tilde{S}}{S}$$

In order to hold for all S and $\tilde{S}$

$$\frac{S}{\mathrm{g}^{q_0\bar{q}_0}(S)} \frac{d\mathrm{g}^{q_0\bar{q}_0}(S)}{dS} = \frac{\tilde{S}}{\mathrm{g}^{q_0\bar{q}_0}\left(\tilde{S}\right)} \frac{d\mathrm{g}^{q_0\bar{q}_0}\left(\tilde{S}\right)}{d\tilde{S}} = a$$

with a separation constant a.

Solve the differential equation

$$\frac{d\mathrm{g}^{q_0\bar{q}_0}(S)}{\mathrm{g}^{q_0\bar{q}_0}(S)} = a\frac{dS}{S}$$

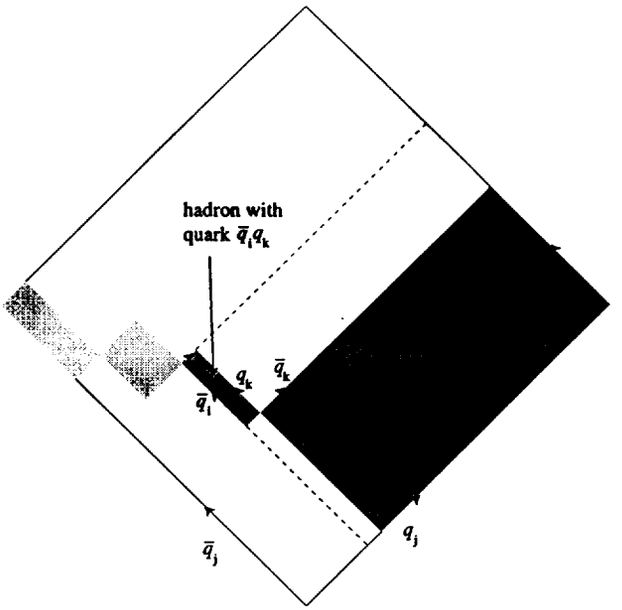

Fig. E.1. After some hadrons are peeled off from the initial system with $\bar{q}_j q_j$, a subsystem with $\bar{q}_i q_j$ is left over. The first hadron which is peeled off from the subsystem has quark content $\bar{q}_j q_k$ where a new pair $\bar{q}_k q_k$ is generated in the subsystem.

and the solution is

$$\mathrm{g}^{q_0\bar{q}_0}(S) = d_{q_0\bar{q}_0}\ S^a$$

where $d_{q_0\bar{q}_0}$ is an integration constant.

E.3 The eigenvalue problem of d_{ij}

After some hadrons are stripped off from the $\bar{q}_j$ end, a subsystem with $\bar{q}_i q_j$ is left over as in Fig.E.1. The fragmentation function for the first hadron of the subsystem is given as

$$f_{ik}\left(z, P_T^2, m^2\right) = \frac{NC_{ik}^2}{(4\pi)^2}\ \mathrm{e}^{-bm_{ik}^2/z}\,\frac{dz}{z}\ \mathrm{e}^{-\chi P_T^2}\,dP_T^2\ \frac{\mathrm{g}_{kj}(\widetilde{S})}{\mathrm{g}_{ij}(S)}$$

By integrating both sides of the above equation (where we have presumed the UCLA model all $\nu_{ij} \simeq 1.0$ and $N_i \simeq N$) over z and ${P_T}^2$, one gets an integral equation

$$\mathrm{g}_{ij}(S) = \frac{N}{(4\pi)^2}\ \sum_k C_{ik}^2 \int \frac{\mathrm{e}^{-bm_{ik}^2/z}}{z\chi}\ \mathrm{g}_{kj}\left(\widetilde{S}\right) dz \qquad \text{(E.8)}$$

where the indices represent quark flavors. Using

$$g_{ij}(S) = d_{ij}S^a$$

derived in Appendix E.2, eq(E.8) becomes

$$d_{ij} = \frac{N}{(4\pi)^2}\sum_k C_{ik}^2 \int \frac{e^{-bm_{ik}^2/z}}{z\chi}(1-z)^a \left(1-\frac{m_{ik}^2}{Sz}\right)^a dz\, d_{kj} \qquad \text{(E.9)}$$

which is an *eigenvalue problem*

$$d_{ij} = \lambda \sum_k A_{ik} d_{kj} \qquad \text{(E.10)}$$

with the definitions

$$A_{ik} \equiv C_{ik}^2 \int \frac{e^{-bm_{ik}^2/z}}{z\chi}(1-z)^a \left(1-\frac{m_{ik}^2}{Sz}\right)^a dz \qquad \text{(E.11)}$$

and

$$\lambda \equiv \frac{N}{(4\pi)^2}$$

For $\chi = 2b/z$ as used in our UCLA approach, eq(E.11) becomes

$$A_{ik} \equiv \frac{C_{ik}^2}{2b} \int e^{-bm_{ik}^2/z}(1-z)^a \left(1-\frac{m_{ik}^2}{Sz}\right)^a dz \qquad \text{(E.12)}$$

For the one flavor case in which all d_{ij} are equal, the above *eigenvalue problem* would be an unitarity equation giving a constraint among 3 parameters N, a and b. In eq(E.10), A is a 3×3 matrix without diquarks (i.e., without baryons) and a 9×9 (including 6 diquark flavors) matrix with diquarks. With the empirical values of a (1.65) and b (1.18 GeV^{-2}), one can solve eq(E.10). Its eigenvalue is

$$\lambda^{-1} \equiv \frac{(4\pi)^2}{N} = 0.80 GeV^2 \qquad \text{(E.13)}$$

for the 3×3 matrix without baryons and 0.82 for the 9×9 matrix with baryon-antibaryon pairs, but with no popcorn. We estimate this value would be $\approx 0.86 GeV^2$ with the popcorn meson inclusion. Varying either *'a'* and *'b'* by a conservative amount, i.e., $\delta a = 0.2$ and $\delta b = 0.1$, these numbers change

$\approx 12\%$. There is less than 3% variation with energy from $E_{CM} = 10GeV$ to $91GeV$. Combining all this, we find $\lambda^{-1} \simeq 0.86 \pm 0.14$, or a range of

$$0.72GeV^2 \leq \lambda^{-1} \leq 1.00GeV^2 \tag{E.14}$$

The value of the knitting factor N is, then, $N \simeq 184GeV^{-2} \simeq (74MeV)^{-2} \simeq (2.67fm)^2$ or range of

$$(2.5fm)^2 \left[= 160GeV^{-2}\right] \leq N \leq (2.9fm)^2 \left[= 220GeV^{-2}\right] \tag{E.15}$$

The eigen vectors, likewise, are

$$\frac{d_{21}}{d_{11}} \equiv \frac{d_{du}}{d_{uu}} = \frac{d_{22}}{d_{11}} \equiv \frac{d_{dd}}{d_{uu}} = 1, \;\; 0.46 \leq \frac{d_{31}}{d_{11}} \equiv \frac{d_{su}}{d_{uu}} \leq 0.49$$

$$\text{and } 0.46 \leq \frac{d_{33}}{d_{31}} \equiv \frac{d_{ss}}{d_{su}} \leq 0.49 \tag{E.16}$$

This opens up interesting questions about the structure of the weight function. For example, will the grand sum of the weight function for the system whose initial quarks are light be the same as that for the system whose initial quarks are heavy considering there is a competition between phasespace and exponential area suppression in the weight function? Eq(E.16) indicates that the *Total Weight* g(S) for a system with heavy initial quarks is smaller compared to that with light initial quarks. It is an intuitively expected answer since a system with heavy initial quarks will involve more heavy hadrons and the heavy hadrons will contribute more suppression to the *Total Weight* by taking larger areas.

F An *artist's* space-time visualization of early event structure

A semi-classical view of several phenomena involving the early structure of an event reveals a rather coherent space-time picture of hadron formation. Fig.F.1 summarizes these aspects: (1) the energy-distance relation in natural units ($1\ GeV = 5\ fm^{-1}$); (2) the region of perturbative QCD; (3) the distance from a quark or antiquark at which a virtual pair break the colortube, that is, one-half of the $q\bar{q}$ separation when a colorfield break occurs; (4) the diameter of a colortube; (5) the length associated with the spatial knitting factor; and (6) the diameter of a hadron.

1) The curve labeled '$1\ GeV = 5\ fm^{-1}$' summarizes the energy-distance relation in natural units.

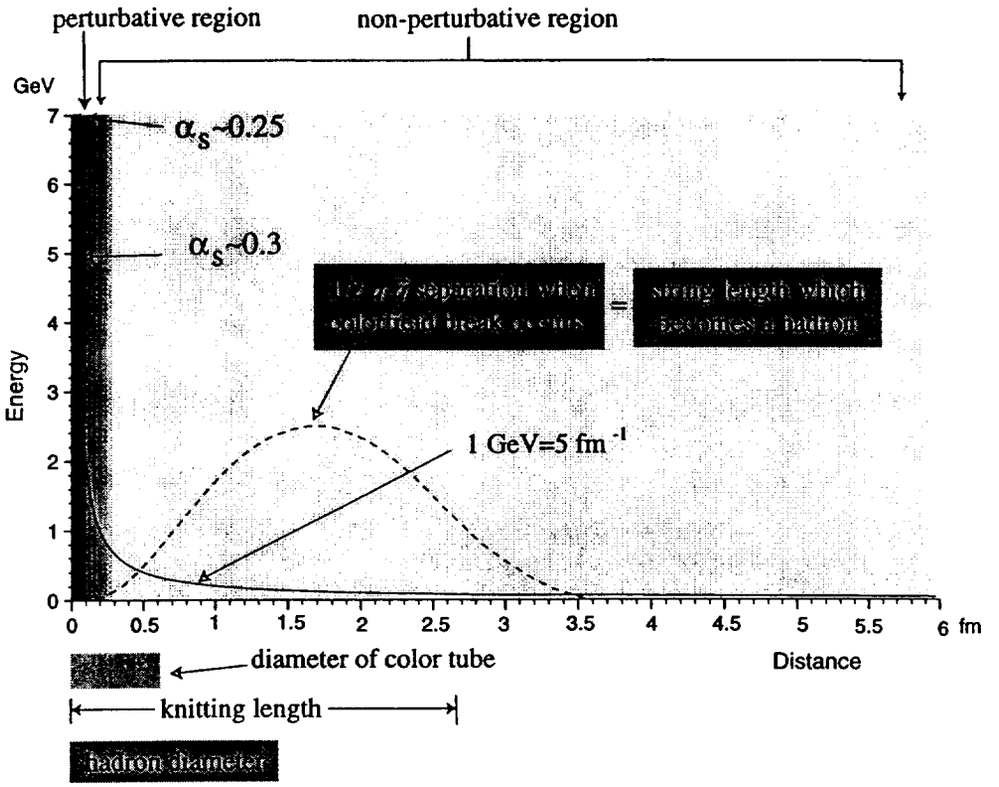

Fig. F.1. Various spatial properties related to hadron formation from a quark-colorfield-antiquark system.

2) By setting the perturbation parameter $\alpha_s \simeq 0.7$ to establish the limit of the perturbative region, where

$$\alpha_s = \frac{4\pi}{\left(11 - \frac{2}{3}N_f\right)\log\left(Q^2/\Lambda^2\right)} \tag{F.1}$$

with $\Lambda \simeq 0.35 GeV$, one finds $Q \simeq 1 GeV$; that is, when the primary quark and antiquark are separated by ≈ 0.2 fm.

3) In their paper on *Left-Right symmetry* for the fragmentation function (i.e., the requirement for the same statistical distribution whether hadrons are peeled off from the primary quark side or antiquark side[2]), the Lund group obtained the distribution of break-up points as a function of invariant time squared (Γ)

$$H(\Gamma) = C\Gamma^a \, \mathrm{e}^{-b\Gamma}$$

One finds, then, that $H(\Gamma)$ peaks at

$$\Gamma = \frac{a}{b} = 1.40 \; GeV^2$$

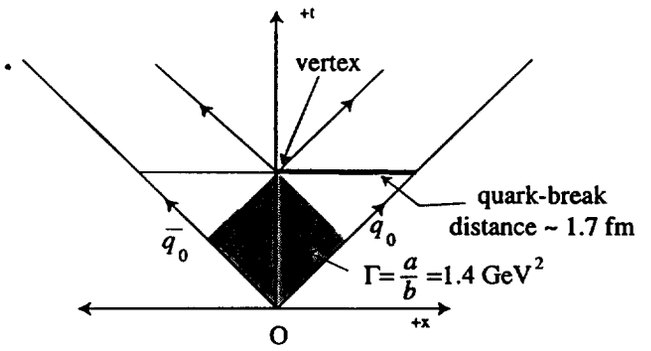

Fig. F.2. In the center of mass system, the length of string just before the first break can be calculated using the distribution $H(\Gamma)$ which peaks at $\Gamma = a/b$, where $\Gamma = \kappa^2\tau^2$, κ is the string constant, and τ is invariant time.

for our parameter values for *'a'*, *'b'*. If one views the primary $q\bar{q}$ pair in their center-of-mass system and recognizes the string tension as $\approx$ 1 GeV/fm, then for a break in the middle of the string (see Fig.F.2), the break occurs at about 1.7 fm on average from the quark (or antiquark).

4) We know that the P_T spectrum for hadrons from a straight colorstring is something like that obtained in the simple Lund description where the P_T distribution of a quark or antiquark is given by $\exp\left(-P_T^2/\sigma_q^2\right)$ with σ_q $\approx 350 \sim 400$ MeV/c. Separating the quark's P_T into x and y components and combining these with those from an antiquark, one finds the *rms* P_x component (and also P_y component) of a hadron to be equal to σ_q. Since the *Heisenberg Uncertainty Relation* is $\langle P_x\rangle_{\rm rms} \times \langle x\rangle_{\rm rms} > \frac{\hbar}{2}$, then $\langle x\rangle_{\rm rms} \simeq \langle y\rangle_{\rm rms} \simeq 0.3$ fm. When combined, this yields an *rms* radius of the colortube, also, of ≈ 0.3 fm, or an *rms* diameter of ≈ 0.6 fm.
5) The length associated with the spatial knitting factor is $\approx 2.5 \sim 3.0$ fm. (See Appendix E.3.)
6) By experimental measurement, the size of a meson is ≈ 1.2 fm diameter (and of a baryon ≈ 1.6 fm).

Thus, for the special case where the first break occurs in the middle of a colortube (where there are no Lorentz transformation effects relative to the center-of-mass system), an artist's conception of the early event space-time structure is illustrated in Fig.F.3, where 'snapshots' (with the same transverse and longitudinal scales within each snapshot) of the colorfield shape are displayed for primary quark-antiquark separations of 0, 1, 2, 3, 4, 5, 6, and 7 fm.

The quark and antiquark are, of course, created at zero separation (a). The insert (*a'*) shows that the perturbative region is over very early, at separation distances $<\approx 0.2$ fm. (For simplicity, at separation greater than this, we display an event with no string-kinking from gluon emission in this very early

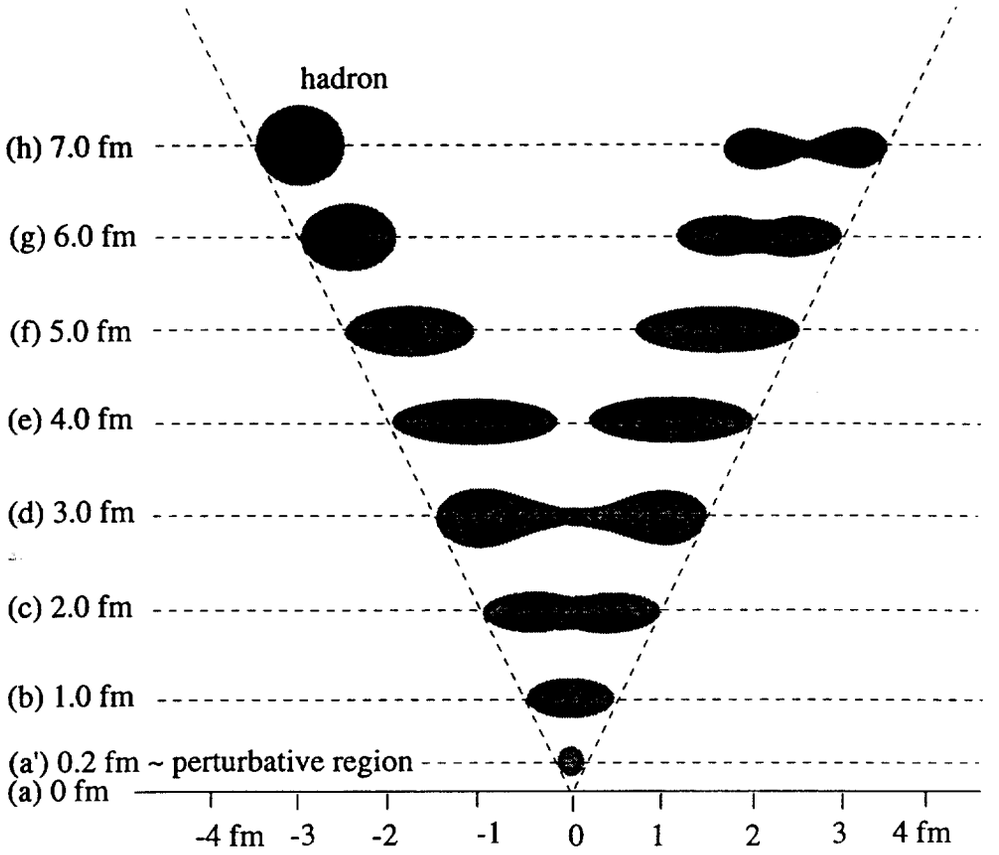

Fig. F.3. An *artist's conception* of the early stages of hadronization in $e^+e^- \rightarrow$ *hadrons*. A color-tube begins to form between the primary quark and antiquark as they recede from each other. The color-tube breaks when they are $\simeq 3 \sim 4fm$ apart. The left side is depicted becoming a hadron. The right side evolves toward further splitting.

stage.)

When the separation is 1.0 fm (b), one might guess that the colortube would have a diameter approaching its maximum. At 2.0 fm separation (c), a thinning in the center of the tube is displayed. At 3.0 fm separation (d), the colortube is typically beginning to pinch in considerably at the middle. At 4.0 fm separation between the primary quark and antiquark, the colortube is displayed as broken into two parts receding from each other, each of length $\approx$ 1.7 fm and diameter $\approx$ 0.6 fm. At high energies, each of these color-blobs will propagate, stretch, and further divide. At low energy, one or both of the blobs may turn into a hadron, rather than splitting further. In Fig.F.3, we show the left-side blob becoming a meson of diameter $\approx$ 1.2 fm and the right-side propagating toward further break-ups.

It is interesting to note from this the somewhat reassuring suggestion that a hadron, of diameter $\approx 1.2 \sim 1.6$ fm, seems to have evolved from a color-blob of comparable 3 dimensional size.

This space-time analysis also suggests a possible speculative interpretation of the spatial knitting factor, a new quantity introduced in this Report — namely, that the knitting factor is a spatial scale which controls the *'ease'* with which an extended color-blob can coalesce into a hadron. That is, if the length of the color-blob is adequately less than the knitting factor length, then the color-blob can coalesce easily; if the color-blob length is greater than the knitting factor, then it becomes increasingly difficult for such a color-blob to coalesce into a hadron.

It is interesting to note that some lattice QCD work[19] suggests a noticable decrease of the flux tube in the middle when the quark and anti-quark are separated by $\approx 0.6 \sim 0.8$ fm, which was the maximum separation in the study. Though nothing can currently be said from this about the behavior of the color flux tube at a $q\bar{q}$ separation more than about 1 fm, if future lattice study indicates that the flux tube breaks at elongation of around 1 fm, it would suggest that there may be some intrinsic contradictions between lattice QCD and our approach where the string breaks typically at $3 \sim 4$ fm of $q\bar{q}$ separation.

References

[1] C.D. Buchanan and S.-B. Chun, Phys. Rev. Lett. 59 (1987) 1997

[2] B. Andersson *et al.*, Z. Phys. **C20** (1983) 317

[3] B. Andersson *et al.*, Phys. Rep. 97 (1983) 33

[4] S.-B. Chun and C.D. Buchanan, Phys. Lett. **B308** (1993) 153

[5] K. Wilson, Phys. Rev. **D10** (1974) 2445

[6] M. Creutz, "Quarks, Gluons and Lattices", (Cambridge University Press, 1993, 2nd Edition)

[7] T. Sjöstrand, Comp. Phys. Comm. 39 (1986) 347;
M.Bengtsson and T. Sjöstrand, Comp. Phys. Comm. 43 (1987) 367;
T. Sjöstrand, Int. J. of Mod. Phys. **A3** (1988) 751

[8] T. Sjöstrand, Comp. Phys. Comm. 82 (1994) 74

[9] G.S. Bali, K. Schilling, Ch. Schichter, CERN-TH 7413/94;
The UK QCD Collaboration, Phys. Lett. **B275** (1992) 424;
R.W. Haymaker, et al, LSUHE 94-159;
Y. Peng and R.W. Haymaker, Nucl. Phys. **B34** (1994) 266

[10] E.C. Berg and C.D. Buchanan, UCLA-HEP-95-01 (Unpublished)

[11] A. De Angelis, CERN-PPE/95-135

[12] XXVIII International Conference on High Energy Physics, July, 1996, Warsaw, Poland

[13] C. Peterson, *et al.*, Phys. Rev. **D** 27 (1983) 105

[14] J.F. Gunion, Phys. Rev. **D10** (1974) 242;
S.J. Brodsky and J.F. Gunion, Phys. Rev. **D17** (1978) 848;
N.H. Fuchs and M.D. Scadron, Phys. Rev. **D20** (1979) 2421

[15] R. Blankenbecler and S.J. Brodsky, Phys. Rev. **D10** (1974) 2973

[16] Private communications with S.J. Brodsky

[17] D.C. Hom *et al.*, Phys. Rev. Lett. 36 (1976) 1236; 37 (1976) 1374

[18] F.T Dao *et al.*, Phys. Rev. Lett. 39 (1977) 1388

[19] W. Feilmair and H. Markum, Nucl. Phys. **B370** (1992) 299

[20] I. Bars, Phys. Rev. Lett. 36 (1976) 1521

[21] X. Artru and M.G. Bowler, Z. Phys. **C37** (1988) 293

[22] K. Wilson, Phys. Rep. 23 (1975) 331

[23] J.B. Kogut, "Recent Advances in Field Theory and Statistical Mechanics", Les Houches (1982)

[24] J.B. Kogut, Rev. Mod. phys. 51 (1979) 659

[25] For example see Chapter 9 of H.J. Rothe, "Lattice Gauge Theories-An Introduction", (World Scientific Publishing Co., 1992)

[26] A. Casher, H. Neuberger, and S. Nussinov, Phys. Rev. **D20** (1979) 179;
B. Andersson, et al, Phys. Script. 32 (1985) 574

[27] M.J. Strassler, Nucl. Phys. **B385** (1992) 145;
M. Mondragon, L. Nellen, M.G. Schmidt, and C. Schubert, preprint DESY 95-034HD-THEP-94-51 hep-th/9502125;
D.G. Gagne, UCLA/95/TEP/22 (unpublished)

[28] Private communication with G. Gustafson.

[29] G. Marchesini et al., Comp. Phys Comm. 67 (1992) 465;
G. Marchesini and B.R. Webber, Nucl. Phys. **B238** (1984) 1